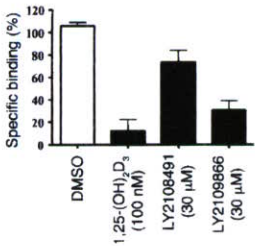

Figure 2
Binding of nonsecosteroidal VDR ligands to VDR-LBD in a classical biochemical ligand-binding assay. Inhibition of [^{3}H]-1,25-$(OH)_2D_3$ binding to VDR by cold 1,25-$(OH)_2D_3$ and its nonsecosteroidal analogs is shown. VDR ligand-binding activity was determined by using purified His-tagged VDR-LBD along with [^{3}H]-1,25-$(OH)_2D_3$ (1 nM). Concentration of each of the cold competitor ligands is shown.

nonsecosteroidal VDR ligands LY2108491 and LY2109866 (Figure 1A) were analyzed for their ability to promote RXR-VDR heterodimerization in a mammalian 2-hybrid system. A ligand-sensing assay was performed by cotransfecting SaOS-2 cells with Gal4-RXRα-LBD (LBD, ligand-binding domain) and VP16-VDR-LBD expression vectors, along with a Gal4-responsive reporter. 1,25-$(OH)_2D_3$ induced RXR-VDR heterodimerization with an EC_{50} (concentration of the ligand required to induce 50% of the maximum activity) value of 5 nM (Figure 1A). LY2108491 and LY2109866, nonsecosteroidal vitamin D analogs, promoted RXR-VDR heterodimerization with EC_{50} values of 11 nM and 13 nM, respectively (Figure 1A). Therefore, LY2108491 and LY2109866 exhibit similar potency to 1,25-$(OH)_2D_3$ in a ligand-sensing assay. The receptor specificity of nonsecosteroidal VDR ligands was confirmed by transfecting SaOS-2 cells with the Gal4-DNA-binding domain chimeras of various nuclear receptor–LBD constructs, along with a Gal4-responsive luciferase reporter. LY2108491 and LY2109866 induced the expression of the Gal4-dependent reporter only through Gal4-VDR-LBD and not through Gal4–thyroid

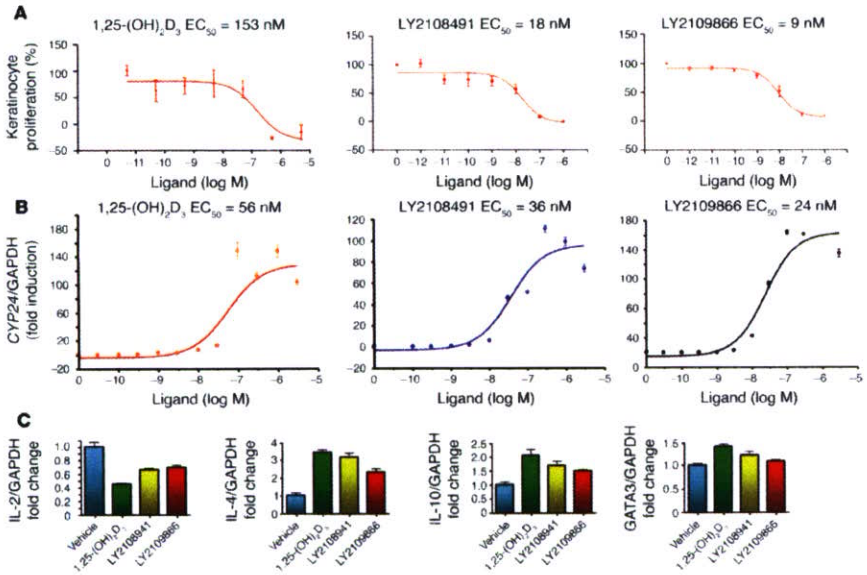

Figure 3
Nonsecosteroidal VDR ligands are potent agonists in keratinocytes and PBMCs. (**A**) LY2108491 and LY2109866 are potent inhibitors of keratinocyte proliferation. KerTr cells plated in 96-well plates were dosed with various concentrations of 1,25-$(OH)_2D_3$, LY2108491, or LY2109866 for 72 hours at 37°C before BrdU incorporation into DNA was analyzed as a measure of cell proliferation. Results (mean ± SEM) of experiments performed in triplicate are shown. (**B**) Nonsecosteroidal VDR ligands are potent inducers of *CYP24* gene expression in keratinocytes. TaqMan quantitative RT-PCR (Q-PCR) was performed on total RNA prepared from KerTr cells treated with various concentrations of 1,25-$(OH)_2D_3$, LY2108491, or LY2109866 for 24 hours. Levels of GAPDH mRNA were measured in all the samples, and the results were normalized and presented as fold induction (± SEM) compared with normalized *CYP24* levels in vehicle-treated cells. (**C**) Nonsecosteroidal VDR ligands are efficacious in TPA- and PHA-activated PBMCs. Primary cells isolated from donors were stimulated with TPA (100 ng/ml) and PHA (25 μl/ml) and treated with vehicle or 100 nM each of 1,25-$(OH)_2D_3$, LY2108491, or LY2109866 for 24 hours. TaqMan Q-PCR was performed on RNA obtained from vehicle-treated or VDR ligand–treated samples, using primer pairs and probes for IL-2, IL-4, IL-10, GATA3, and GAPDH. The amount of IL-2, IL-4, IL-10, and GATA3 transcripts relative to GAPDH transcripts is shown as mean ± SEM of quadruplicate experiments.

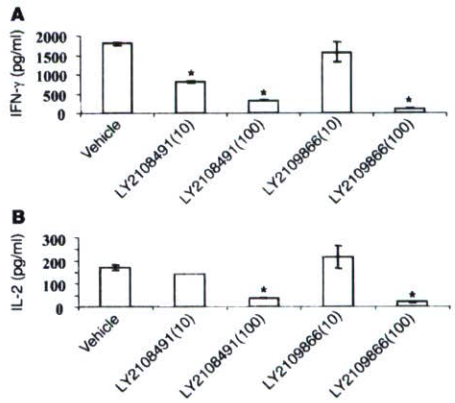

Figure 4
LY2108491 and LY2109866 decrease Th1 cytokine response in vivo. Immunized mice were treated with LY2108491 (10 and 100 μg/kg), LY2109866 (10 and 100 μg/kg), or vehicle for 10 days. Splenocytes were stimulated ex vivo with 10 μg/ml MOG_{35-55} peptide. Supernatants were collected 72 hours after stimulation, and IFN-γ (**A**) and IL-2 (**B**) levels were determined by Luminex. The values shown represent the mean of triplicate determinations, and error bars represent SEM. *$P < 0.05$.

hormone receptor α (Gal4-TRα), Gal4-TRβ, Gal4–retinoic acid receptor α (Gal4-RARα), Gal4-RARβ, Gal4-RARγ, Gal4-PPARα, Gal4-PPARδ, Gal4-PPARγ, Gal4-RXRα, Gal4–RAR-related orphan receptor α (Gal4-RORα), or Gal4-liver receptor homolog 1 (Gal4-LRH1) LBDs (data not shown). However, LY2108491 but not LY2109866 also induced the expression of a Gal4-responsive reporter through Gal4–pregnane X receptor expression vector. LY2108491, LY2109866, and the positive control rifampicin, each at a concentration of 200 nM, induced the expression of the Gal4-responsive reporter in Huh7 cells by 22-, 1-, and 5-fold, respectively. Moreover, in a biochemical cofactor recruitment assay, LY2108491 and LY2109866 induced the recruitment of steroid receptor coactivator 1 (SRC-1) to purified VDR-LBD protein but not to TRα, TRβ, estrogen receptor α (ERα), LXRα, liver X receptor β (LXRβ), RXRα, and LRH1 LBD proteins (data not shown). These results demonstrate the receptor specificity of these nonsecosteroidal ligands.

To determine whether LY2108491 and LY2109866 also induce VDRE-dependent gene expression, we used ROS17/2.8 rat osteosarcoma cells that were permanently transfected with a rat osteocalcin promoter luciferase reporter, osteocalcin-LUC (OCN-LUC) (23). 1,25-$(OH)_2D_3$ induced rat OCN-LUC gene expression with an EC_{50} value of 0.11 nM (Figure 1B). LY2108491 and LY2109866 induced the expression of the osteocalcin VDRE-based luciferase reporter with EC_{50} values of 26 nM and 2.5 nM, respectively (Figure 1B). Therefore, LY2108491 and LY2109866 are nonsecosteroidal VDR agonists.

In an in vitro ligand-binding assay, LY2108491 and LY2109866 were less potent than 1,25-$(OH)_2D_3$. Unlabeled 1,25-$(OH)_2D_3$ (100 nM) competed with [^{3}H]-1,25-$(OH)_2D_3$ for binding to baculovirus-expressed human VDR-LBD whereas LY2108491 and LY2109866 were less efficacious even at a concentration of 30 μM in the competition assay (Figure 2). This observation was true for almost all the nonsecosteroidal VDR ligands synthesized. Therefore, VDR-dependent cell-based assays were more sensitive than the in vitro VDR equilibrium ligand-binding assay in identifying nonsecosteroidal VDR ligands. A plausible explanation for the failure of nonsecosteroidal ligands of this class to compete in ligand-binding assays might be the fast on-rate and slow off-rate of the high-affinity ligand 1,25-$(OH)_2D_3$. Similarly, biphenyl class of nonsecosteroidal VDR ligands also did not efficiently compete with [^{3}H]-1,25-$(OH)_2D_3$ when the VDR binding assays were performed under equilibrium conditions (24). Further, crystal structure of LY2108491-complexed VDR-LBD revealed that the VDR ligand bound in the same space that is normally occupied by 1,25-$(OH)_2D_3$ (data not shown).

LY2108491 and LY2109866 are potent agonists in keratinocytes. 1,25-$(OH)_2D_3$ and synthetic vitamin D analogs inhibit the proliferation of keratinocytes and induce their differentiation (25). To compare the potencies of LY2108491 and LY2109866 with that of 1,25-$(OH)_2D_3$ in inhibiting the proliferation of cultured keratinocytes, human immortalized transformed keratinocyte (KerTr) cells were treated with the VDR ligands for 4 days, and cell proliferation was quantitated by BrdU incorporation into the DNA. 1,25-$(OH)_2D_3$ inhibited the proliferation of KerTr cells with an IC_{50} value of 150 nM (Figure 3A). However, LY2108491 and LY2109866 were more potent than 1,25-$(OH)_2D_3$ in inhibiting the proliferation of KerTr cells and showed IC_{50} values of 18 nM and 9 nM, respectively (Figure 3A). Therefore, LY2108491 and LY2109866 appear to be better agonists than the secosteroidal analog 1,25-$(OH)_2D_3$ in inhibiting the growth of proliferating keratinocytes. We also compared the activities of 1,25-$(OH)_2D_3$, LY2108491 and

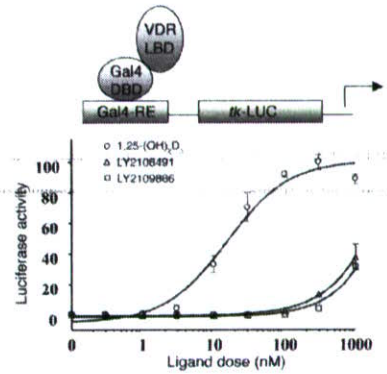

Figure 5
LY2108491 and LY2109866 are less potent in inducing VDR-dependent gene expression in intestinal cells. Luciferase activity (± SEM) of Caco-2 cells transfected with Gal4-VDR-LBD in a mammalian 1-hybrid setting in the presence of vehicle or various concentrations of 1,25-$(OH)_2D_3$, LY2108491, or LY2109866 are shown. Results are in arbitrary light units obtained from experiments performed in triplicate.

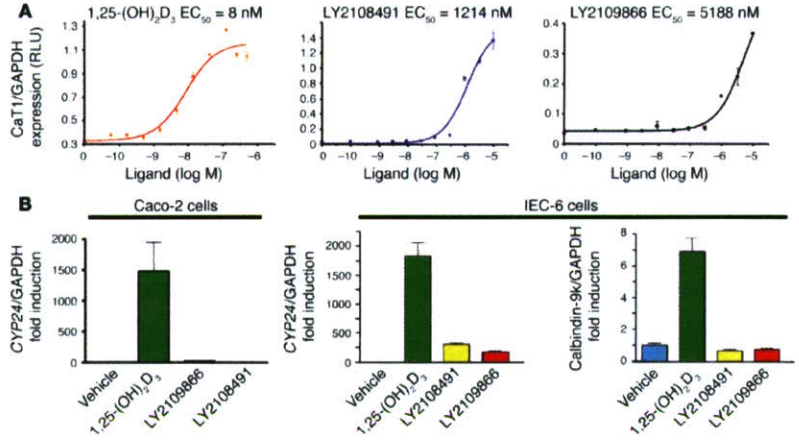

Figure 6
LY2108491 and LY2109866 are less potent and efficacious in inducing the expression of vitamin D–responsive genes in intestinal cells. (**A**) Nonsecosteroidal VDR ligands show weak potencies in inducing the expression of endogenous CaT1 genes in differentiated Caco-2 cells. TaqMan Q-PCR was performed on total RNA prepared from differentiated Caco-2 cells treated with various concentrations of 1,25-$(OH)_2D_3$, LY2108491, or LY2109866 for 24 hours. Levels of GAPDH mRNA were measured in all the samples, and the results were normalized and presented (± SEM) as RLU after normalization with the GAPDH transcript levels. (**B**) LY2108491 and LY2109866 are poor inducers of endogenous vitamin D–responsive genes in intestinal cells. TaqMan Q-PCR was performed on total RNA prepared from differentiated Caco-2 or rat duodenal IEC-6 cells treated with vehicle or 100 nM each of 1,25-$(OH)_2D_3$, LY2108491, or LY2109866 for 24 hours. The amount of *CYP24* and calbindin-9k transcripts relative to GAPDH transcripts is shown as mean ± SEM of quadruplicate experiments.

LY2109866 in inducing the expression of an endogenous VDRE-dependent gene, *CYP24* (24-hydroxylase) in immortalized keratinocytes. 1,25-$(OH)_2D_3$, LY2108491, and LY2109866 induced the expression of the endogenous *CYP24* gene with EC_{50} values of 56, 36, and 24 nM, respectively (Figure 3B). Thus, nonsecosteroidal VDR ligands are as potent as 1,25-$(OH)_2D_3$ in inducing the expression of *CYP24* gene in human keratinocytes.

LY2108491 and LY2109866 are efficacious agonists in PBMCs. Apart from keratinocyte hyperproliferation, the second hallmark of psoriasis pathology involves T cells. Psoriasis is considered to be a Th1-mediated disease since the lesions show an increased expression of proinflammatory cytokines (IL-2 and IFN-γ) and decreased expression of Th2 antiinflammatory cytokines IL-4 and IL-10 (26). 1,25-$(OH)_2D_3$ affects the Th1-Th2 balance, and it has been shown to augment Th2 cell development, which is accompanied by decreased IL-2 and increased production of IL-4 and IL-10 cytokines in vitro and in vivo (27, 28). Further, 1,25-$(OH)_2D_3$ also augments the expression of GATA-binding protein 3 (GATA3) (27), a master regulator of Th2 differentiation (29). As expected, 1,25-$(OH)_2D_3$ reduced IL-2 and induced IL-4, IL-10, and GATA3 expression in phytohemagglutinin/12-O-tetradecanoyl phorbol-13-acetate–activated (PHA/TPA-activated) PBMCs (Figure 3C). LY2108491 and LY2109866 also inhibited IL-2 and induced IL-4, IL-10, and GATA3 expression (Figure 3C). Fold changes in the expression levels of IL and GATA3 genes were statistically significant ($P < 0.05$) when compared with the vehicle treatment. The only exception was GATA3 expression, which followed the trend but did not exhibit statistical significance between LY2109866 and vehicle treatments. Interestingly, LY2108491 and 1,25-$(OH)_2D_3$ did not display significantly different efficacies in enhancing T cell–mediated expression of IL-4 and GATA3 (Figure 3C). Therefore, LY2108491 and LY2109866 are efficacious VDR agonists in T cells.

Nonsecosteroidal VDR ligands also showed inhibition of Th1 response in a T cell recall model in vivo. Compared with the vehicle-treated mice, splenocytes obtained from LY2108491- and LY2109866-treated animals produced significantly less IFN-γ in response to myelin oligodendrocyte glycoprotein (MOG_{35-55}) stimulation (Figure 4A). Both VDR ligands showed a dose-responsive inhibition of IFN-γ production, and LY2108491 was more potent in inhibition of IFN-γ elaboration than LY2109866. Both LY2108491 and LY2109866 also significantly inhibited IL-2 in response to MOG_{35-55} stimulation (Figure 4B).

LY2108491 and LY2109866 are cell context–dependent VDRMs. Although LY2108491 and LY2109866 were at least as potent as 1,25-$(OH)_2D_3$ in inducing RXR-VDR heterodimerization in SaOS-2 osteosarcoma cells and in inducing the expression of the endogenous VDRE-dependent gene *CYP24* in keratinocytes, they were more potent than the secosteroidal analog in inhibiting the proliferation of keratinocytes. However, LY2108491 and LY2109866 were less potent than 1,25-$(OH)_2D_3$ in inducing the transactivation of a Gal4-luciferase reporter with the Gal4-VDR-LBD expression vector in a mammalian 1-hybrid assay in Caco-2 human intestinal cells. The EC_{50} values for 1,25-$(OH)_2D_3$, LY2109481, and LY2109866 were 14, greater than 1000, and greater than 1000 nM, respectively, in Caco-2 cells (Figure 5). Of note, even at 1000 nM concentration, LY2108491 and LY2109866 were 60% less efficacious than 1,25-$(OH)_2D_3$ (Figure 5).

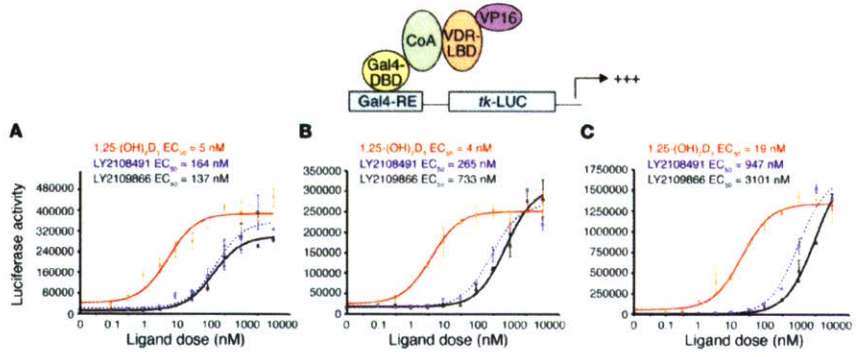

Figure 7
Nonsecosteroidal VDRMs are less potent than 1,25-$(OH)_2D_3$ in recruiting p160 family members to VDR. Luciferase activity (± SEM) of Caco-2 cells transfected with Gal4–SRC-1 (**A**), Gal4-TIF2 (**B**), or Gal4-AIB1 (**C**) and VP16-VDR-LBD in a mammalian 2-hybrid setting in the presence of vehicle or various concentrations of 1,25-$(OH)_2D_3$, LY2108491, or LY2109866 is shown. Luciferase activity is shown as arbitrary light units obtained from experiments performed in triplicate.

These results indicate the cell type selectivity of LY2108491 and LY2109866 since these compounds were less potent than 1,25-$(OH)_2D_3$ in Caco-2 cells.

We next examined the expression of an endogenous vitamin D–responsive gene, CaT1, in differentiated Caco-2 cells. CaT1, whose expression is obligatory for 1,25-$(OH)_2D_3$–mediated calcium absorption from the gut, is a vitamin D–responsive gene in vitro and in vivo, and its expression is drastically reduced in VDR-knockout animals (19, 30). Although Caco-2 cells are colon cancer cells, upon density-dependent differentiation (6–14 days of culture), they differentiate into small intestinal-like cells that express many of the markers of small intestinal luminal cells, including CaT1, which is normally expressed in duodenal cells (30). Upon differentiation, these cells also acquire the molecular machinery required for vitamin D–dependent transepithelial calcium transport (apical to basolateral membrane) analogous to that of enterocytes (31). 1,25-$(OH)_2D_3$ (EC_{50} = 8 nM) was a potent inducer of CaT1 mRNA in differentiated Caco-2 cells (Figure 6A). In contrast, LY2108491 (EC_{50} = 1214 nM) and LY2109866 (EC_{50} = 5188 nM) showed very low potency in inducing the expression of the endogenous CaT1 gene in differentiated Caco-2 cells (Figure 6A). LY2108491 and LY2109866 were also significantly less efficacious than 1,25-$(OH)_2D_3$ in inducing *CYP24* expression in Caco-2 cells. 1,25-$(OH)_2D_3$ (100 nM) induced *CYP24* gene expression by approximately 1,500-fold whereas LY2108491 and LY2109866 (100 nM each) failed to increase *CYP24* in differentiated Caco-2 cells (Figure 6B). We also compared LY2108491 and LY2109866 with 1,25-$(OH)_2D_3$ for their effect on the expression of 2 VDRE-dependent genes, namely *CYP24* and calbindin-9k in IEC-6 (rat duodenal crypt cell line) cells. Treatment of IEC-6 cells with 1,25-$(OH)_2D_3$ (100 nM) for 24 hours resulted in a robust induction of *CYP24* and calbindin-9k gene expression (Figure 6B). In contrast, LY2108491 and LY2109866 were significantly less efficacious than 1,25-$(OH)_2D_3$ in inducing the expression of endogenous *CYP24* in these cells (Figure 6B). 1,25-$(OH)_2D_3$ induced calbindin-9k expression by 7-fold after 24 hours of treatment (Figure 6B). However, both LY2108491 and LY2109866 failed to induce calbindin-9k gene expression in IEC-6 cells (Figure 6B). All of these observations further support the notion that LY2108491 and LY2109866 are cell context–dependent VDRMs.

VDR-cofactor interaction. It has been suggested that selective nuclear receptor modulators induce novel conformational changes within the LBD that lead to selective cofactor recruitment.

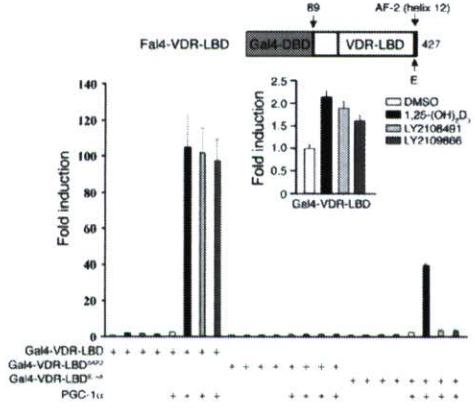

Figure 8
Differential interaction of PGC-1α–receptor interaction with VDR ligands. Luciferase activity (± SEM) of HEK 293 cells transfected with Gal4-VDR-LBD, Gal4-VDR-LBD$^{\Delta AF-2}$, or Gal4-VDR-LBD^{E420A} with or without PGC-1α expression vector in the presence of vehicle or 1 μM each of 1,25-$(OH)_2D_3$, LY2108491, or LY2109866 is shown. Luciferase activity is shown as arbitrary light units obtained from experiments performed in triplicate.

Table 1
Nonsecosteroidal VDRMs exhibit better therapeutic indices than 1,25-$(OH)_2D_3$

VDR ligand	Hypercalcemia TMED (nmol/100 μl/4 cm²)	Epidermal proliferation TMED (nmol/100 μl/4 cm²)	TI
1,25-$(OH)_2D_3$	<1	3	<0.3
LY2108491	>729	9	>81
LY2109866	>243	9	>27

TMEDs of 1,25-$(OH)_2D_3$, LY2108491, and LY2109866 required for epidermal proliferation and hypercalcemia after topical application on the backs of hairless mice are presented. A comparison of the therapeutic indices of the VDR ligands is also shown.

Ligand-selective cofactor recruitment may underlie the novel pharmacological properties of the modulators. In order to investigate this, nonsecosteroidal VDR ligands were also compared with 1,25-$(OH)_2D_3$ for their effect on the interaction of VDR with SRC/p160 coactivator family of proteins. The recruitment of SRC-1, SRC-2 (TIF2, transcription intermediary factor 2), and SRC-3 (AIB1, amplified in breast cancer 1) to VDR was monitored by a mammalian 2-hybrid system after transfection of Caco-2 cells with VP16-VDR-LBD, Gal4 DNA-binding domain chimeras of 1 of the cofactor expression vectors (Gal4-SRC-1, Gal4-TIF2, or Gal4-AIB1) and a Gal4 reporter luciferase plasmid. 1,25-$(OH)_2D_3$ was equipotent in inducing the interaction of VDR with SRC-1, TIF2, and AIB1 with EC_{50} values of 5, 4, and 19 nM, respectively, for VDR-SRC-1, VDR-TIF2, and VDR-AIB1 interactions (Figure 7, A–C). However, LY2108491 and LY2109866 were less potent than 1,25-$(OH)_2D_3$ in inducing VDR-cofactor interactions. LY2108491 augmented VDR-SRC-1, VDR-TIF2, and VDR-AIB1 interactions with EC_{50} values of 164, 265, and 947 nM, respectively (Figure 7, A–C). For LY2109866, the EC_{50} values for VDR-SRC-1, VDR-TIF2, and VDR-AIB1 interactions were 137, 733, and 3101 nM (Figure 7, A–C). In particular, LY2108491 and LY2109866 were considerably less potent in inducing VDR-TIF2 and VDR-AIB1 interactions when compared with 1,25-$(OH)_2D_3$. These results also indicate differential cofactor recruitment by LY2108491 and LY2109866 since they were 6- and 23-fold, respectively, more potent in recruiting SRC-1 than AIB1 to VDR. The attenuated ability of LY2108491 and LY2109866 in recruiting coactivator proteins (particularly AIB1) to VDR may suggest that these nonsecosteroidal VDRMs induce distinct conformations within the LBD that may explain the cell-context dependent activity of these ligands.

To demonstrate further that the occupancy of VDR-LBD by the secosteroidal and nonsecosteroidal ligands indeed induces differential conformations with pharmacological significance, we used peroxisome proliferative activated receptor γ, coactivator 1α (PGC-1α) coactivator to augment Gal4-VDR-LBD–dependent transactivation of a Gal4-responsive reporter in a mammalian 1-hybrid assay. Treatment of Gal4-VDR-LBD–transfected cells with 1 μM 1,25-$(OH)_2D_3$, LY2108491, or LY2109866 resulted in a 2-fold increase in the expression of the Gal4-responsive luciferase reporter in HEK 293 cells (Figure 8). Overexpression of PGC-1α resulted in a 50-fold enhancement of transcriptional activity of the reporter in the presence of 1,25-$(OH)_2D_3$, LY2108491, or LY2109866 (Figure 8). As expected, deletion of helix 12 (Gal4-VDR-LBD$^{\Delta AF\text{-}2}$) abolished the transcriptional activity in response to both the ligands and also to overexpression of PGC-1α. Previous studies have demonstrated the "charge clamp" glutamic acid residue in helix 12 (E420) as playing an important role in ligand-dependent VDR-mediated transcription and coactivator interaction. Further, mutation studies have shown that the VDR E420 does not play any role in either ligand binding or heterodimerization with RXR (32). It has previously been demonstrated that the requirement of the charge clamp residue of PPARγ and TRβ for their coactivation by PGC-1α is determined by the identity of the ligand (33, 34). Therefore, to ascertain whether this charge clamp E420 residue of VDR played any role in the ability of VDR ligands to differentially influence the interaction of VDR with PGC-1α, we mutated the glutamic acid to alanine and performed cotransfection assays utilizing the E420A mutant receptor in the presence of 1,25-$(OH)_2D_3$, LY2108491, or LY2109866. VDR ligands did not show any activation of the Gal4-reponsive reporter through the Gal4-VDR-LBD^{E420A} expression vector (Figure 8). Interestingly, overexpression of PGC-1α with the E420A mutant receptor resulted in a 15-fold enhancement of the transcriptional activity in the presence of 1,25-$(OH)_2D_3$ but only a 1.5-fold enhancement in the presence of either LY2108491 or LY2109866 (Figure 8). These results suggest that the nonsecosteroidal VDRMs are capable of inducing different VDR and/or RXR-VDR conformation than that engendered by the occupancy of the VDR-LBD with 1,25-$(OH)_2D_3$.

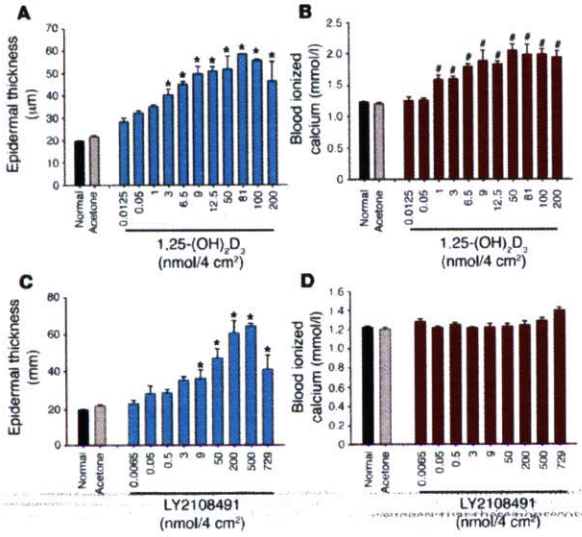

Figure 9
VDRMs are less calcemic in vivo and show efficacy in a surrogate animal model of psoriasis. **(A)** Histological evaluation of hairless mouse skin after topical treatment with 1,25-$(OH)_2D_3$ at indicated doses. **(B)** Effect of various concentrations of topical 1,25-$(OH)_2D_3$ treatment on blood ionized calcium levels in hairless mice. **(C)** Histological evaluation of hairless mouse skin after topical treatment with LY2108491 at indicated doses. **(D)** Effect of various concentrations of topical LY2108491 treatment on blood ionized calcium levels in hairless mice. Error bars represent SEM of the mean. *$P < 0.05$. #Hypercalcemia above the normal blood ionized calcium level of 1.34 mM.

LY2108491 and LY2109866 show better therapeutic indices than calcitriol in vivo. Topical calcitriol is used in clinic for the treatment of psoriasis (35). In order to compare the therapeutic indices of LY2108491 and LY2109866 with that of calcitriol in vivo, a hairless mouse model of epidermal proliferation after topical application of VDR ligands was used. This epidermal proliferation mouse model is regarded as a surrogate in vivo preclinical model of psoriasis since compounds (VDR ligands [calcitriol and calcipotriol] and retinoids [etretinate, acitretin, isotretinoin and tazarotene]) that inhibit keratinocyte proliferation in psoriatic lesions, in fact, induce epidermal proliferation when applied topically in normal skin (36, 37). This apparent paradox is also shared by psoralen and UV A as well as UV B therapies that are also therapeutically effective in psoriasis (36). In this model, serum ionized calcium was also measured at 24 hours after the dosing, and the animals were sacrificed 72 hours after dosing to collect skin for histological evaluation of epidermal proliferation. The TI is the ratio between the threshold minimum effective dose (TMED) that does not result in hypercalcemia and the TMED that results in keratinocyte proliferation (an increase of 1 keratinocyte layer thickness in the epidermis) (Table 1). TMEDs for hypercalcemia and epidermal proliferation, respectively, are thus the measures of the potencies of VDR ligands for side effects and efficacy. Calcitriol [1,25-$(OH)_2D_3$] showed an epidermal response with a TMED of 3 nmol/100 μl/4 cm², and in the same animal it produced hypercalcemia when applied topically at a dose of 1 nmol but not at 0.05 nmol/100 μl/4 cm² (Figure 9, A and B, and Table 1). Therefore, the TI of calcitriol in this in vivo model was less than 0.3 since the noncalcemic dose would be less than 1 nmol/100 μl/4 cm². Like calcitriol, LY2108491 also stimulated keratinocyte proliferation and thus increased epidermal thickness in vivo in hairless mice (Figure 9, C and D). However, the TI for LY2108491 was found to be greater than 81 (Table 1) since its TMED for epidermal proliferation was 9 nmol/100 μl/4 cm² and its TMED for hypercalcemia was greater than 729 nmol/100 μl/4 cm² (Figure 9, C and D, and Table 1). Note that even at a dose of 729 nmol, it did not raise ionized blood calcium above the normal levels. Similarly, the TI for LY2109866 was more than 27 since its noncalcemic dose was more than 243 nmol/100 μl/4 cm² and its TMED for epidermal proliferation was 9 nmol/100 μl/4 cm² (Table 1). Therefore, LY2108491 and LY2109866 were greater than 270- and greater than 90-fold, respectively, better than calcitriol in terms of their TI in vivo in a topical surrogate model of psoriasis.

Nonsecosteroidal VDRMs induce epidermal proliferation in vivo through VDR signaling pathway. In order to rule out the possibility that the VDR ligands induced epidermal proliferation in vivo by acting upon other nuclear receptors present in the skin or by pathways other than nuclear vitamin D signaling, wild-type (VDR$^{+/+}$) and VDR knockout (VDR$^{-/-}$) mice were treated topically with vehicle, 1,25-$(OH)_2D_3$, LY2108491, or LY2109866 on their shaved backs (Figure 10). Topical treatment of VDR$^{+/+}$ mice with 1,25-$(OH)_2D_3$ (10 nmol/100 μl/4 cm²) or one of the VDRMs (50 nmol/100 μl/4 cm² each) for 72 hours

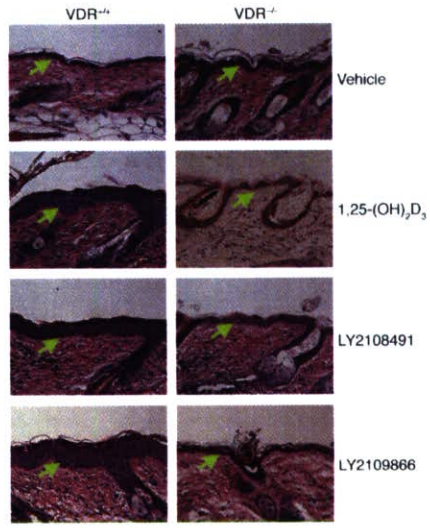

Figure 10
VDRMs do not induce epidermal proliferation in VDR-knockout mice. Histological evaluation of VDR$^{+/+}$ or VDR$^{-/-}$ mouse skin after topical treatment with vehicle, 1,25-$(OH)_2D_3$ (10 nmol), LY2108491 (50 nmol), or LY2109866 (50 nmol) is presented. Mice were sacrificed at 72 hours after dosing, and skin samples were collected. Epidermal thickness was examined by H&E staining of paraffin sections. Epidermis is shown with green arrows.

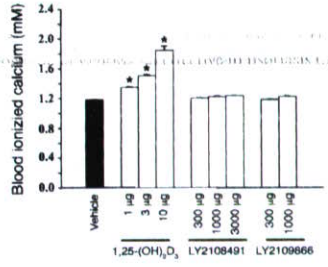

Figure 11
LY2108491 and LY2109866 are noncalcemic in vivo when administered orally in a short-term mouse model of hypercalcemia. 1,25-$(OH)_2D_3$, LY2108491, or LY2109866 were administered in sesame seed oil at indicated doses to mice by gavage for 6 consecutive days, and blood ionized calcium was measured 6 hours after the last dose. Error bars represent SEM. *$P < 0.05$.

resulted in epidermal proliferation when examined histologically by H&E staining in paraffin-embedded sections (Figure 10). However, all the VDR ligands did not show any increase in epidermal thickness when applied to the shaved backs of $VDR^{-/-}$ animals. Epidermal thickness in control vehicle-treated $VDR^{+/+}$ and $VDR^{-/-}$ animals is also presented (Figure 10).

LY2108491 and LY2109866 are less calcemic in vivo. We hypothesized that the decreased VDR-mediated transcriptional activity of LY2108491 and LY2109866 in intestinal cells and the reduced hypercalcemia liability of these VDRMs through the topical route may also translate into reduced intestinal calcium absorption and hypercalcemic action when administered orally. To examine this hypothesis, 1,25-$(OH)_2D_3$, LY2108491, and LY2109866 were analyzed for their hypercalcemia liability in vivo after oral administration. Mice were treated for 6 days with the VDR ligands, and ionized calcium was measured in the blood 6 hours after the last dosing. 1,25-$(OH)_2D_3$ resulted in statistically significant increases in blood ionized calcium levels in mice at doses as small as 1 μg/kg/day, with frank hypercalcemia observed (above the normal range) at 3 μg/kg/day (Figure 11). In contrast, LY2108491 did not result in hypercalcemia even at 3000 μg/kg/day, and LY2109866 did not result in hypercalcemia in mice at a dose of 1000 μg/kg/day (Figure 11). Therefore, LY2108491 and LY2109866 were significantly less likely (>1,000 and >300 times, respectively) to induce hypercalcemia than 1,25-$(OH)_2D_3$ in vivo through the oral route. These results confirm that LY2108491 and LY2109866 are less calcemic in vivo. Therefore, these nonsecosteroidal VDRMs may exhibit less hypercalcemia liability when administered orally and also when applied topically in a therapeutic setting.

Discussion

The clinical success of the nonsteroidal selective estrogen receptor modulators (SERMs) in reducing the estrogenic action in breast and uterus while retaining the estrogenic agonist action in bone has provided a rationale for the development of nonsteroidal nuclear receptor ligands in order to achieve tissue-selective action (21). As a result, efforts are ongoing to obtain tissue-selective modulators of estrogen, glucocorticoid, androgen, progesterone, mineralocorticoid, and PPARs for various indications (21, 22). In this manuscript, we report the first identification to our knowledge of nonsecosteroidal tissue-selective VDRMs that function as agonists in keratinocytes and PBMCs (T cells) but show extremely reduced transcriptional activity in intestinal cells. This cell context-selective action translated into reduced hypercalcemia in vivo in comparison with 1,25-$(OH)_2D_3$ when mice were treated orally or topically with the VDRMs LY2108491 and LY2109866 (Figures 9 and 11 and Table 1). Although nonsecosteroidal and nonsteroidal VDR ligands have been described (24, 38, 39), they have not been shown to act as a modulator in a cell context-dependent manner. Recently, a tissue- and cell type-selective secosteroidal VDRM (Ro-26-9228) has been described (40). However, Ro-26-9228 was less tissue-selective and showed VDR-dependent transcriptional activity in Caco-2 cells with an EC_{50} value of 120 nM (40). It showed only 17- to 27-fold better TI than 1,25-$(OH)_2D_3$ in an ovariectomized rat model of osteoporosis (40). Further, it showed a potency of 149 nM in inducing the expression of the endogenous vitamin D-responsive gene CaT1 in Caco-2 cells whereas corresponding EC_{50} values for LY2108491 and LY2109866 were 1214 and 5188 nM, respectively (data not shown).

The VDRMs LY2108491 and LY2109866 displayed many of the biological actions of 1,25-$(OH)_2D_3$. They induced RXR-VDR heterodimerization (Figure 1A); upregulated the expression of a VDRE-dependent gene, osteocalcin in osteoblasts (Figure 1B); inhibited the growth of proliferating keratinocytes (Figure 4A); and inhibited IL-2 while augmenting IL-4, IL-10, and GATA3 expression in human PBMCs (Figure 4C). They also inhibited Th1 response in a T cell recall model in vivo. However, these nonsecosteroidal VDRMs were more than 71 times less potent and 60% less efficacious than 1,25-$(OH)_2D_3$ in inducing VDR-LBD–dependent transactivation in intestinal cells (Figure 5). They were also 200 to more than 1000 times less potent than their secosteroidal counterpart in inducing the expression of CaT1, a vitamin D–responsive gene in differentiated Caco-2 cells (Figure 6A). In addition, LY2108491 and LY2109866 (100 nM) did not significantly induce the expression of another vitamin D–dependent gene, *CYP24* (Figure 6B). This cell context–dependent activity was further extended to rat IEC-6 duodenal cells, in which LY2108491 and LY2109866 (100 nM), unlike 1,25-$(OH)_2D_3$, failed to induce the expression of endogenous calbindin-9k gene (Figure 6B). Further, they were significantly less efficacious than 1,25-$(OH)_2D_3$ in enhancing the expression of endogenous *CYP24* gene in IEC-6 cells (Figure 6B). These results and the knowledge that the promoter regions of *CYP24*, calbindin-9k, and CaT1 genes contain functional VDREs (6, 19, 30) indicate a global attenuation or unresponsiveness of the VDR signaling pathway to these nonsecosteroidal VDRMs in intestinal/duodenal cells. At the same time, the vitamin D signaling pathway still responds to 1,25-$(OH)_2D_3$–complexed VDR for the expression of the above-mentioned genes in Caco-2 and IEC-6 duodenal cells (Figure 6, A and B). Our results are also in accordance with the observations that the secosteroidal VDRM, Ro-26-9228, showed weaker potency than 1,25-$(OH)_2D_3$ in inducing the expression of vitamin D–responsive genes calbindin-9k and *CYP24* in Caco-2 cells, and it did not induce the expression of vitamin D–responsive genes *CYP24*, calbindin-9k, and PMCA-1 in rat duodenum (40, 41).

Studies with VDR-null animals have indicated duodenal CaT1 to be a major mediator of 1,25-$(OH)_2D_3$–mediated calcium absorption from intestine and hypercalcemia (19). Therefore, the weak agonist activity of nonsecosteroidal VDRMs in human and rat intestinal cells predicted that these ligands might be less calcemic than 1,25-$(OH)_2D_3$ in vivo. In order to test this hypothesis, LY2108491 and LY2109866 were administered orally and topically to mice, and their effect on blood ionized calcium was examined. Both nonsecosteroidal VDRMs showed less potency in inducing hypercalcemia by either route (Figures 9 and 11 and Table 1). The reduced calcemic liability of these VDRMs prompted us to test these compounds in an in vivo surrogate model of psoriasis. The paradox in vitamin D biology is that VDR ligands inhibit the proliferation of keratinocytes in psoriatic lesions, but they also induce the proliferation of keratinocytes in normal skin (36, 37). In addition to VDR ligands, retinoids, which are also therapeutically active in psoriasis, display a similar phenotype (36). Therefore, epidermal proliferation in mouse skin has been regarded as a surrogate model of psoriasis for the identification of topically active VDR ligands. All the VDR ligands, namely calcitriol, calcipotriol, and tacalcitol, which are used in clinic for the topical treatment of psoriasis, stimulate epidermal proliferation when applied topically to mice (36, 37). In the same animal model, LY2108491 and LY2109866 exhibited a dermal effect at a dose of 9 nmol/100 μl/cm^2 dose. Interestingly, LY2108491 and LY2109866 did not raise blood calcium levels above the normal range even at the highest tested doses of 729 and 243 nmol/100 μl/cm^2, respectively (Figure 9D and Table 1). Therefore, nonsecosteroidal VDRMs show striking dissociation of biological efficacy from calcium liability in vivo. Both LY2108491 and LY2109866 showed more than 270- and more than 900-fold, respectively, better therapeutic indices than calcitriol in the surrogate model of psoriasis (Figure 9 and Table 1). The skin effect of the VDRM was mediated through VDR since the epidermal proliferation effect was not observed in VDR-null animals (Figure 10). These results also demonstrate the receptor specificity of the VDRMs described herein.

Psoriasis is characterized by hyperproliferation and abnormal differentiation of keratinocytes as well as epidermal infiltration of activated T cells (15). Therefore, an ideal therapeutic for psoriasis ought to be efficacious in both keratinocytes and immune cells for maximum clinical benefit and to satisfy the current unmet medical need. The nonsecosteroidal VDRMs also showed efficacy in skewing the balance of helper T cells from pathologic Th1 to antiinflammatory Th2 cells, as evidenced by their ability to inhibit IL-2 and augment IL-4 and IL-10 expression in PHA/TPA-activated PBMCs (Figure 3C). Both IL-4 and IL-10 possess antiinflammatory properties and can suppress T cell–mediated autoimmune processes (26, 28). Further, IL-10 promotes Th2 response by regulating Th1-Th2 balance through antigen-presenting cells (26, 28). The regulation of these cytokines assumes significance because an IL-2 diphtheria immunotoxin (42) and protein biologics for IL-4 (43) as well as IL-10 (44) have been successfully used in clinic for the treatment of plaque-type psoriasis. LY2108491 and LY2109866 also induced the expression of GATA3 (Figure 3C), a transcription factor that is obligatory for the development of Th2 cells (29).

It has been postulated that the tissue-selective activity of the nuclear receptor modulators is due to their ability to induce distinct conformational changes in the receptor, which may result in differential recruitment of cofactors required for the regulation of target gene expression. Our results indicate that LY2108491 and LY2109866 may impart different receptor conformations relative to 1,25-$(OH)_2D_3$ since they were less potent in facilitating the recruitment of cofactors to VDR in Caco-2 cells (Figure 7). It was particularly true for VDR-AIB1 interaction, where the EC_{50} values were 947 and 3101 nM, respectively, for LY2108491 and LY2109866, whereas for 1,25-$(OH)_2D_3$, the corresponding EC_{50} value was 18 nM in Caco-2 cells (Figure 7C). Further, the differential recruitment of PGC-1α to E420A mutant of the receptor by the VDR ligands (Figure 8) indicates that the nonsecosteroidal VDRMs described herein impart different conformational change to the receptor than that conferred by 1,25-$(OH)_2D_3$. Interestingly, Takeyama et al. reported the first selective interaction of VDR with cofactors, using a secosteroidal vitamin D analog, OCT (45). OCT was found to be less potent than 1,25-$(OH)_2D_3$ in inducing VDR-SRC-1 and VDR-AIB1 interactions (45). Similarly, 1,25-$(OH)_2D_3$, and not the secosteroidal VDRM, Ro-26-9228, complexed with VDR obtained from Caco-2 cells and interacted with glutathione-S-transferase–TIF2 in vitro in a glutathione-S-transferase–pulldown assay (41). These results also suggest that the binding of synthetic ligands with a spectrum of variations in their cellular activities may induce slight differences in VDR conformations in a ligand structure–dependent manner, which may result in differential recruitment of coactivators. Therefore, tissue selectivity may arise as a result of differential cofactor recruitment by VDRMs. Although cocrystallization of VDR-LBD with various synthetic ligands does not support this notion (46), it should be borne in mind that the crystallization efforts, although extremely important in understanding VDR-ligand interactions, did not involve wild-type VDR-LBD, RXR, and coactivators.

In summary, we report here the synthesis and characterization of novel nonsecosteroidal VDRMs that function in a cell and tissue context–dependent manner. Nonsteroidal modulators of estrogen receptor, tamoxifen and raloxifene, are approved drugs for the treatment of breast cancer and prevention/treatment of postmenopausal osteoporosis, respectively. Similarly, nonsteroidal modulators of androgen receptor (bicalutamide and flutamide) are approved drugs for the treatment of prostate cancer. Steroidal analogs of nuclear receptors, in general, are traditionally limited by their undesirable side effects, which in the case of VDR ligands include hypercalcemia. Our results clearly show that nonsecosteroidal VDRMs are more tissue selective in action and as a result are less calcemic in vivo. LY2108491 and LY2109866 also display superior therapeutic indices in vivo in a surrogate model of psoriasis. Therefore, these nonsecosteroidal VDRMs might have therapeutic utility in dermal indications, such as psoriasis, actinic keratosis, and skin cancers. The identification of VDRMs further extends the recurring theme of tissue-selective action in nuclear receptor biology to VDR and demonstrates that nonsecosteroidal ligands have the potential to elicit cell- and tissue-selective effects that may lead to improved therapeutic indices. Our observations, along with the molecular tools described in this manuscript, also open the potential for the discovery and identification of bone-selective, prostate-selective, or promyelocyte-selective VDRMs as future therapeutics for various indications. The structurally novel nonsecosteroidal tissue-selective VDRMs belonging to the phenylthiophene class described herein might have utility not only in the treatment of other dermal indications, but also in those that are nondermal.

Methods

Cell culture and transfections. For the RXR-VDR heterodimerization assay, SaOS-2 cells maintained in DMEM supplemented with 10% FBS were plated at 5000 cells per well in a 96-well plate. The next day, cells were transfected using 0.5 μl of FuGENE (Roche Diagnostics Corp.), 100 ng of luciferase reporter vector pFR-LUC (Stratagene), and 10 ng each of pVP16-VDR-LBD and pGal4-RXRα-LBD expression vectors per well. For the Caco-2 1-hybrid mammalian transactivation assay, Caco-2 cells, maintained in DMEM supplemented with 10% FBS, were plated at 5000 cells per well in a 96-well plate. Cells were transfected using 0.5 μl of FuGENE (Roche Diagnostics Corp.), 100 ng of luciferase reporter vector pFR-LUC (Stratagene), and 10 ng of pGal4-VDR-LBD expression vectors per well. For the VDR-cofactor interaction assays, Caco-2 cells maintained in DMEM supplemented with 10% FBS were plated at 5000 cells per well in a 96-well plate. The next day, cells were transfected using 0.5 μl of FuGENE, 100 ng of luciferase reporter vector pFR-LUC, and 10 ng each of pVP16-VDR-LBD and 1 of the Gal4-cofactor (pGal4-SRC-1, pGal4-TIF2 or pGal4-AIB1) expression vectors per well. Total DNA amount was kept constant by adding empty vector DNA as needed. Cells were treated with the ligand 24 hours after transfection, and luciferase activity was quantitated the next day using Steady-Glo luciferase detection reagent (Promega). HEK 293 cells were maintained in DMEM supplemented with 10% FBS and 1% penicillin/streptomycin. Prior to transfections, cells were plated into 96-well plates at a density of 25,000 cells per well in the medium supplemented with 10% dextran charcoal-stripped FBS. Transfections were performed using FuGENE 6 (Roche Molecular Biochemicals). Each transfection contained 25 ng of luciferase reporter plasmid and various combinations of other expression plasmids as described in the legend to Figure 8. Twenty-four hours after transfection, fresh media containing vehicle, 1,25-$(OH)_2D_3$

(100 nM), LY2108491 (1 μM), or LY2109866 (1 μM) were added. Luciferase activity was quantitated the next day using Steady-Glo luciferase detection reagent (Promega).

Rat OCN-LUC assay. The activation of osteocalcin VDRE by VDR ligands was evaluated in a rat osteoblast–like cell line (ROS17/2.8) stably expressing rat osteocalcin promoter (1.154 kb) fused with luciferase reporter gene. The development of the stably transfected ROS17/2.8 cell line (RG-15) containing OCN-LUC has been described (23). Confluent RG-15 cells maintained in DMEM/F-12 medium (3:1) containing 5% FBS and 300 μg/ml G418 at 37°C were trypsinized (0.25% trypsin) and plated into white opaque 96-well cell culture plates (25000 cells per well). After 24 hours, cells (in DMEM/F-12 medium containing 2% FBS) were treated with the indicated concentrations of the compounds. After 48 hours of treatment, the medium was removed, and cells were lysed with 50 μl of lysis buffer (from Luciferase Reporter Assay System, Roche Diagnostics Corp.) and assayed for luciferase activity, using the Luciferase Reporter Gene Assay kit from Boehringer Mannheim. Aliquots (20 μl) of cell lysates were pipetted into wells of white opaque microtiter plates (DYNEX Technologies) and placed in an automated injection MLX microtiter plate luminometer. The luciferase reaction mix (100 μl) was injected sequentially into the wells. The light signals generated in the reactions were integrated over an interval of 2 seconds, and the resulting luminescence values were used as a measure of luciferase activity (relative units).

VDR ligand binding. Determination of VDR ligand–binding activity was performed using purified baculovirus-produced His-tagged VDR-LBD protein. Assays were performed in 96-well Optiplates (PerkinElmer). Each binding reaction was performed in binding assay buffer (50 mM Tris-HCl, pH 7.5, 1.5 mM EDTA, 5 mM DTT, 300 mM KCl, and 0.01% Tween 20) using 1 μg of VDR protein and 1 nM 1,25-dihydroxy[23,24(n)-^{3}H]cholecalciferol (102 Ci/mmol) (Amersham Biosciences) with varying concentrations of competitor compounds in 150 μl total volume for 15 minutes at room temperature. After 15 minutes incubation, 50 μl of polylysine-coated yttrium silicate SPA beads (0.125 mg/50 μl in 30% glycerol/binding assay buffer) (Amersham Biosciences) was added to each binding reaction followed by shaking for 30 minutes. Nonspecific binding was determined by incubation with 1,000-fold excess of cold 1,25-$(OH)_2D_3$. Plates were read using Packard TopCount Scintillation Counter (PerkinElmer).

Keratinocyte proliferation inhibition assay. KerTr cells (human transformed skin keratinocyte, obtained from ATCC) were plated in 96-well flat-bottom plates (3000 cells per well) in 100 μl keratinocyte serum-free medium supplemented with bovine pituitary extract in the absence of EGF (Invitrogen Corp.) and incubated at 37°C for 2 days. The cells were treated with various concentrations of VDR ligands in triplicate, dissolved in 100 μl keratinocyte serum-free medium supplemented with bovine pituitary extract in the absence of EGF, and incubated at 37°C for 72 hours. BrdU (5-bromo-2′-deoxyuridine) incorporation was analyzed (Cell Proliferation ELISA kit; Roche Diagnostics Corp.), and absorbance was measured at 405 nm. Potency values (IC_{50}) values were determined as the concentration (nM) of compound that elicited a half-maximal response.

Quantitative RT-PCR assays. Human colon carcinoma, Caco-2 cells, maintained in DMEM (high glucose with 25 mM HEPES buffer; Invitrogen Corp.) supplemented with 10% FBS (Invitrogen Corp.) were plated at 5500 cells per well in a 96-well plate in a total volume of 100 μl/well. The cells were kept in the 96-well plate for 6 days to differentiate them into small intestinal cells that express the calcium transporter CaT1. On day 3 after plating, spent media were removed and replaced with fresh media (150 μl/well). On day 6, the spent media were again removed, and the cells were maintained in treatment media (180 μl/well) (DMEM [low glucose, without phenol red; Invitrogen Corp.] containing 10% charcoal-stripped FBS [HyClone]). The cells were treated with various concentrations of VDR ligands prepared in treatment media (20 μl/well).

Rat IEC-6 duodenal cells maintained in DMEM (high glucose with 25 mM HEPES buffer; Invitrogen Corp.) supplemented with 10% FBS (Invitrogen Corp.) were plated in T25 flasks. On the day of treatment with the VDR ligands, spent media were removed, and the cells were kept in treatment media (DMEM [low glucose, without phenol red; Invitrogen Corp.] containing 10% charcoal-stripped FBS [HyClone]). The cells were treated with vehicle, 1,25-$(OH)_2D_3$, LY2108491, or LY2109866 (100 nM each) prepared in treatment media.

PBMCs were isolated from normal human donors by sedimentation on Ficoll-Hypaque. Informed consent was obtained from human donors. Cells were resuspended in RPMI-1640 supplemented with charcoal-treated FBS (2%). PBMCs (25×10^6/T75 flask) were activated with PHA (10 μg/ml) and TPA (100 ng/ml). The cells were cultured in the presence of 1,25-$(OH)_2D_3$, LY2108491, or LY2109866 (100 nM each) prepared in RPMI-1640 containing 2% charcoal-treated FBS.

Twenty hours after treatment, total RNA was prepared by the RNeasy 96 method, as described by the manufacturer (QIAGEN). The RNA was reverse transcribed and amplified for various human and rat (human CaT1, *CYP24*, and GAPDH for Caco-2 cells; human IL-2, IL-4, IL-10, GATA3, and GAPDH for PBMCs; and rat *CYP24*, calbindin-9k, and GAPDH for IEC-6 cells) mRNAs by quantitative RT-PCR using the ABI PRISM 7900HT Sequence Detection System (Applied Biosystems). Optimized primer pairs and probes for human (CaT1, *CYP24*, and GAPDH) and rat (*CYP24*, calbindin-9k, and GAPDH) genes were obtained commercially (Applied Biosystems). Each 20 μl quantitative RT-PCR reaction in a 384-well TaqMan PCR plate consisted of forward and reverse primers (900 nM), TaqMan probe (200 nM), total RNA (4 μl for each well of the 96-well culture plate), and 10 μl of TaqMan Universal PCR Master Mix, (Roche Diagnostics Corp.). Reactions were incubated at 48°C for 30 minutes, followed by 10 minutes at 95°C, and subjected to 40 cycles of PCR (95°C for 15 seconds followed by 60°C for 1 minute).

Antigen-specific T cell recall assay. This study was approved by the Animal Committee of Eli Lilly and Company to ensure compliance with NIH guidelines. Female C57BL/6 mice purchased from Taconic were immunized s.c. at 2 sites on the back with 300 μg MOG_{35-55} (MEVGWYRSPFSRVVH-LYRNGK, Peptides International Inc.) emulsified in a total of 200 μl CFA (BD Diagnostics) containing 500 μg *M. tuberculosis* H37 Ra (BD Diagnostics). Immunized mice were treated with vehicle (sesame oil), LY2108491 (10 and 100 μg/kg), or LY2109866 (10 and 100 μg/kg). Ten days later, splenocytes were isolated by homogenizing spleens between frosted glass slides (Fisher Scientific International), and rbcs were removed with ACK lysing buffer (BioWhittaker Inc.). Pooled splenocytes of 5 individual mice from the same group were plated in triplicate in a 96-well round-bottom plate at 2×10^5 cells per well in 200 μl complete RPMI 1640 medium (Invitrogen Corp.) supplemented with 2 mM L-glutamine, 25 mM HEPES, 100 U/ml penicillin, 100 μg/ml streptomycin, 5.5×10^{-5} M 2-mercaptoethanol, and 5% FCS (all supplements from Invitrogen Corp.) containing 10 μg/ml MOG_{35-55} (Peptides International Inc.) or medium, and cultured at 37°C, 5% CO_2 for 72 hours. Cytokine levels produced from cultured splenocytes were analyzed with R&D Systems MAP kit (R&D Systems) (LUM000) with IL-2 (LUM402) and IFN-γ (LUM485) beads. Comparisons of cytokine levels among various groups were analyzed by ANOVA test, and *P* values of less than 0.05 were considered significant.

Vector construction. Gal4-DBD chimeras of SRC-1, TIF2, or AIB1 have been reported previously (45). Expression vectors pVP16-VDR-LBD, pGal4-RXRα-LBD, and pGal4-VDR-LBD have also been described (2). Gal4-VDR-LBD$^{\Delta AF\text{-}2}$ was constructed from Gal4-VDR-LBD (pM-VDR-LBD; encompassing amino acids 89–427 of VDR) (2) by PCR amplification and subcloned into the *Eco*RI and *Xba*I sites of the pM vector (Clontech Laboratories Inc.). Full-length VDR and VDR activation function–2 (AF-2) fused to the Gal4-DBD were constructed by PCR amplification and cloned into the pM vector between the *Eco*RI and *Xba*I sites. The E420A mutant in Gal4-VDR-LBD was generated using the QuikChange site-directed mutagenesis kit (Stratagene). The expression plasmid for PGC-1α has been described (34).

In vivo hypercalcemia assay. Female, 6- to 7-week-old DBF1 mice weighing approximately 25 g were purchased from Harlan. Mice were housed with ad libitum access to food (TD 5001 with 0.95% calcium and 0.67% phosphorus, vitamin D3, 4500 IU/kg; Harlan Teklad) and water. Compounds were given orally via gavage daily for 6 days. Dosing volume was 100 μl/mouse with 4 mice in each group. Serum ionized calcium was examined at 6 hours after last dosing using a Ciba-Corning 634 Ca^{++}/pH Analyzer (Chiron Corp.).

In vivo epidermal proliferation model. Female, 40- to 42-day-old, SKH1-hrBR (CRJ) hairless mice (Charles River Laboratories) weighing approximately 20 g were housed with ad libitum access to food (TD 5001 with 0.95% calcium and 0.67% phosphorus, vitamin D3 4500 IU/kg; Harlan Teklad) and water. Solutions for topical treatment were prepared in acetone, and a single topical application of various doses of the compounds was administered to a preset surface area of 2×2 cm^2 on the back waist area. Dosing volume was 100 μl/mouse with 4 mice in each group. Serum ionized calcium was examined at 24 hours after dosing using a Ciba-Corning 634 Ca^{++}/pH Analyzer (Chiron Corp.). Mice were sacrificed at 72 hours after dosing, and skin samples were collected. Epidermal cell height was quantitated on 8-μm thickness of H&E-stained paraffin sections using an image probe system (Image-Pro Plus version 3.0; MediaCybernetics). Special attention was paid to ensure that the sections were cut perpendicular to the skin surface.

Epidermal proliferation in VDR$^{+/+}$ and VDR$^{-/-}$ mice. VDR$^{-/-}$ mice were generated by gene targeting as described previously (47). VDR$^{+/+}$ and VDR$^{-/-}$ mice were weaned at 3 weeks of age and housed with ad libitum access to food (CE-2 with 1.03% calcium and 0.97% phosphorus; CLEA Japan Inc.) and water. Female, 40- to 42-day-old, back-shaved VDR$^{+/+}$ and VDR$^{-/-}$ mice weighing 15–20 g were used in this study. VDR$^{+/+}$ mice ($n = 3$) and VDR$^{-/-}$ mice ($n = 3$) were treated topically as described above with vehicle, 1,25-$(OH)_2D_3$ (10 nmol), LY2108491 (50 nmol), or LY2109866 (50 nmol). Mice were sacrificed at 72 hours after dosing, and skin samples were collected. Epidermal thickness was assessed using H&E-stained paraffin sections

Statistics. Statistical significance versus control was defined as $P < 0.05$ in the Dunnett's test. Compound potency for hypercalcemia and epidermal proliferation was defined as the TMED, which is the lowest dose achieving a mean response greater than a predetermined level of serum calcium or cell proliferation that is also statistically significant in the Dunnett's test. In vitro concentration-response curves were fit using the sigmoidal/variable slope fitting option in GraphPad Prism (version 4; GraphPad Software).

Acknowledgments

We thank Chahrzaad Montrose-Rafizadeh, Karen Pinette, Mariam Elizabeth, and Robert Barr for technical help.

Received for publication June 8, 2005, and accepted in revised form January 16, 2006.

Address correspondence to: Sunil Nagpal, Lilly Research Laboratories, Eli Lilly and Company, Lilly Corporate Center, Indianapolis, Indiana 46285, USA. Phone: (484) 865-5627; Fax: (484) 865-9389; E-mail: nagpals@wyeth.com.

Sunil Nagpal's present address is: Women's Health & Musculoskeletal Biology, Wyeth Research, Collegeville, Pennsylvania, USA.

Y. Ma and B. Khalifa contributed equally to this work.

1. Mangelsdorf, D.J., et al. 1995. The nuclear receptor superfamily: the second decade. *Cell.* **83**:835–839.
2. Bettoun, D.J., et al. 2003. Retinoid X receptor is a nonsilent major contributor to vitamin D receptor-mediated transcriptional activation. *Mol. Endocrinol.* **17**:2320–2328.
3. Lemon, B., and Freedman, L. 1996. Selective effects of ligands on vitamin D3 receptor- and retinoid X receptor-mediated gene activation *in vivo*. *Mol. Cell. Biol.* **16**:1006–1016.
4. Rachez, C., and Freedman, L.P. 2000. Mechanisms of gene regulation by vitamin D(3) receptor: a network of coactivator interactions. *Gene.* **246**:9–21.
5. Holick, M.F. 1995. Noncalcemic actions of 1,25-dihydroxyvitamin D3 and clinical applications. *Bone.* **17**(Suppl. 2):107S–111S.
6. Nagpal, S., Na, S., and Rathnachalam, R. 2005. Non-calcemic actions of vitamin D receptor ligands. *Endocr. Rev.* **26**:662–687.
7. Cantorna, M.T., Hayes, C., and DeLuca, H.F. 1996. 1,25-dihydroxyvitmin D3 reversibly blocks the progression of relapsing encephalomyelitis, a model of multiple sclerosis. *Proc. Natl. Acad. Sci. U. S. A.* **93**:7861–7864.
8. Cantorna, M.T., Hayes, C.E., and DeLuca, H.F. 1998. 1, 25-dihydroxycholecalciferol inhibits the progression of arthritis in murine models of human arthritis. *J. Nutr.* **128**:68–72.
9. Cantorna, M.T., Munsick, C., Bemiss, C., and Mahon, B.D. 2000. 1, 25-dihydroxycholecalciferol prevents and ameliorates symptoms of experimental murine inflammatory bowel disease. *J. Nutr.* **130**:2648–2652.
10. Bourke, J.F., et al. 1997. The effects of topical calcipotriol on systemic calcium homeostasis in patients with chronic plaque psoriasis. *J. Am. Acad. Dermatol.* **37**:929–934.
11. Langner, A., Verjans, H., Stapor, V., Mol, M., and Fraczykowska, M. 1993. Topical calcitriol in the treatment of chronic plaque psoriasis: a double-blind study. *Br. J. Dermatol.* **128**:566–571.
12. Scott, L.J., Dunn, C.J., and Goa, K.L. 2001. Calcipotriol ointment. A review of its use in the management of psoriasis. *Am. J. Clin. Dermatol.* **2**:95–120.
13. Perez, A., et al. 1996. Efficacy and safety of topical calcitriol (1,25-dihydroxyvitamin d3) for the treatment of psoriasis. *Br. J. Dermatol.* **134**:238–246.
14. Perez, A., Raab, R., Chen, T.C., Turner, A., and Holick, M.F. 1996. Safety and efficacy of oral calcitriol (1,25-dihydroxyvitamin D3) for the treatment of psoriasis. *Br. J. Dermatol.* **134**:1070–1078.
15. Lebwohl, M. 2003. Psoriasis. *Lancet.* **361**:1197–1204.
16. Kragballe, K., et al. 2004. Efficacy of once-daily treatment regimens with calcipotriol/betamethasone dipropionate ointment and calcipotriol ointment in psoriasis vulgaris. *Br. J. Dermatol.* **150**:1167–1173.
17. Lamba, S., and Lebwohl, M. 2001. Combination therapy with vitamin D analogues. *Br. J. Dermatol.* **144**(Suppl. 58):27–32.
18. Bouillon, R., Okamura, W.H., and Norman, A.W. 1995. Structure-function relationships in the vitamin D endocrine system. *Endocr. Rev.* **16**:200–257.
19. Van Cromphaut, S.J., et al. 2001. Duodenal calcium absorption in vitamin D receptor-knockout mice: functional and molecular aspects. *Proc. Natl. Acad. Sci. U. S. A.* **98**:13324–13329.
20. Bronner, F. 2003. Mechanisms of intestinal calcium absorption. *J. Cell. Biochem.* **88**:387–393.
21. Lin, X., and Huebner, V. 2000. Non-steroidal ligands for steroid hormone receptors. *Curr. Opin. Drug Disc. Develop.* **3**:383–398.
22. Smith, C.L., and O'Malley, B.W. 2004. Coregulator function: a key to understanding tissue specificity of selective receptor modulators. *Endocr. Rev.* **25**:45–71.
23. Boguslawski, G., et al. 2000. Activation of osteocalcin transcription involves interaction of protein kinase A- and protein kinase C-dependent pathways. *J. Biol. Chem.* **275**:999–1006.
24. Boehm, M.F., et al. 1999. Novel nonsecosteroidal vitamin D mimics exert VDR-modulating activities with less calcium mobilization than 1,25-dihydroxyvitamin D_3. *Chem. Biol.* **6**:265–275.
25. Bikle, D.D., Tu, C.-L., Xie, Z., and Oda, Y. 2003. Vitamin D regulated keratinocyte differentiation: role of coactivators. *J. Cell. Biochem.* **88**:290–295.
26. Asadullah, K., Volk, H.D., and Sterry, W. 2002. Novel immunotherapies for psoriasis. *Trends Immunol.* **23**:47–53.
27. Boonstra, A., et al. 1998. 1, 25-dihydroxyvitmin D3 has a direct effect on naïve CD4+ T cells to enhance the development of Th2 cells. *J. Immunol.* **167**:4974–4980.
28. Mathieu, C., and Adorini, L. 2002. The coming age of 1,25-dihydroxyvitamin D3 analogs as immunomodulatory agents. *Trends Mol. Med.* **8**:174–179.
29. Pai, S.Y., Truitt, M.L., and Ho, I.C. 2004. GATA-3 deficiency abrogates the development and maintenance of T helper type 2 cells. *Proc. Natl. Acad. Sci. U. S. A.* **101**:1993–1998.
30. Wood, R.J., Tchack, L., and Taparia, S. 2001. 1,25-Dihydroxyvitamin D3 increases the expression of the CaT1 epithelial calcium channel in the Caco-2 human intestinal cell line. *BMC Physiol.* **1**:11.
31. Giuliano, A.R., and Wood, R.J. 1991. Vitamin D-regulated calcium transport in Caco-2 cells: unique *in vitro* model. *Am. J. Physiol.* **260**:G207–G212.
32. Masuyama, H., Brownfield, C.M., St-Arnaud, R., and MacDonald, P.N. 1997. Evidence for ligand-dependent intramolecular folding of the AF-2 domain in vitamin D receptor-activated transcription and coactivator interaction. *Mol. Endocrinol.*

11:1507–1517.
33. Wu, Y., Chin, W.W., Wang, Y., and Burris, T.P. 2003. Ligand and coactivator identity determines the requirement of the charge clamp for coactivation of the peroxisome proliferator-activated receptor gamma. *J. Biol. Chem.* **278**:8637–8644.
34. Wu, Y., Delerive, P., Chin, W.W., and Burris, T.P. 2002. Requirement of helix 1 and the AF-2 domain of the thyroid hormone receptor for coactivation by PGC-1. *J. Biol. Chem.* **277**:8898–8905.
35. Camarasa, J.M., Ortonne, J.P., and Dubertret, L. 2003. Calcitriol shows greater persistence of treatment effect than betamethasone dipropionate in topical psoriasis therapy. *J. Dermatolog. Treat.* **14**:8–13.
36. Gniadecki, R., and Serup, J. 1995. Stimulation of epidermal proliferation in mice with 1-alpha, 25-dihydroxyvitamin D3 and receptor-active 20-epi analogues of 1-alpha, 25-dihydroxyvitamin D3. *Biochem. Pharmacol.* **49**:621–624.
37. Lutzow-Holm, C., De Angelis, P., and Clausen, O.P. 1996. Calcitriol and its analog KH 1060 induce similar changes in keratinocyte cell cycle progression after topical application to mouse skin. A bromodeoxyuridine pulse-chase flow cytometric study. *J. Investig. Dermatol. Symp. Proc.* **1**:54–59.
38. Verstuyf, A., et al. 1998. The biological activity of non-steroidal vitamin D hormone analogs lacking both the C- and D-rings. *J. Bone Miner. Res.* **13**:549–558.
39. Verstuyf, A., et al. 2000. Biological activity of CD-ring modified 1alpha,25-dihydroxyvitamin D analogues: C-ring and five-membered D-ring analogues. *J. Bone Miner. Res.* **15**:237–252.
40. Peleg, S., Uskokovic, M., Ahene, A., Vickery, B., and Avnur, Z. 2002. Cellular and molecular events associated with the bone-protecting activity of the noncalcemic vitamin D analog Ro-26-9228 in osteopenic rats. *Endocrinology.* **143**:1625–1636.
41. Ismail, A., et al. 2004. Effect of cellular environment on the selective activation of the vitamin D receptor by 1-alpha,25-dihydroxyvitamin D3 and its analog 1-alpha-fluoro-16-ene-20-epi-23-ene-26,27-bishomo-25-hydroxyvitamin D3 (Ro-26-9228). *Mol. Endocrinol.* **18**:874–887.
42. Gottlieb, S.L., et al. 1995. Response of psoriasis to a lymphocyte-selective toxin (DAB389IL-2) suggests a primary immune, but not keratinocyte, pathogenic basis. *Nat. Med.* **1**:442–447.
43. Ghoreschi, K., et al. 2003. Interleukin-4 therapy of psoriasis induces Th2 responses and improves human autoimmune disease. *Nat. Med.* **9**:40–46.
44. Asadullah, K., et al. 1998. IL-10 is a key cytokine in psoriasis. Proof of principle by IL-10 therapy: a new therapeutic approach. *J. Clin. Invest.* **101**:783–794.
45. Takeyama, K.-I., et al. 1999. Selective interaction of vitamin D receptor with transcriptional coactivators by a vitamin D analog. *Mol. Cell. Biol.* **19**:1049–1055.
46. Tocchini-Valentini, G., Rochel, N., Wurtz, J.M., Mitschler, A., and Moras, D. 2001. Crystal structures of the vitamin D receptor complexed to superagonist 20-epi ligands. *Proc. Natl. Acad. Sci. U. S. A.* **98**:5491–5496.
47. Yoshizawa, T., et al. 1997. Mice lacking the vitamin D receptor exhibit impaired bone formation, uterine hypoplasia and growth retardation after weaning. *Nat. Genet.* **16**:391–396.

nature Vol 446|29 March 2007|doi:10.1038/nature05683

LETTERS

Dioxin receptor is a ligand-dependent E3 ubiquitin ligase

Fumiaki Ohtake[1,2], Atsushi Baba[2], Ichiro Takada[2], Maiko Okada[2], Kei Iwasaki[1], Hiromi Miki[2], Sayuri Takahashi[2,3], Alexander Kouzmenko[1,2], Keiko Nohara[4], Tomoki Chiba[5], Yoshiaki Fujii-Kuriyama[6,7] & Shigeaki Kato[1,2]

Fat-soluble ligands, including sex steroid hormones and environmental toxins, activate ligand-dependent DNA-sequence-specific transcriptional factors that transduce signals through target-gene-selective transcriptional regulation[1]. However, the mechanisms of cellular perception of fat-soluble ligand signals through other target-selective systems remain unclear. The ubiquitin–proteasome system regulates selective protein degradation, in which the E3 ubiquitin ligases determine target specificity[2–4]. Here we characterize a fat-soluble ligand-dependent ubiquitin ligase complex in human cell lines, in which dioxin receptor (AhR)[5–9] is integrated as a component of a novel cullin 4B ubiquitin ligase complex, CUL4B^{AhR}. Complex assembly and ubiquitin ligase activity of CUL4B^{AhR} *in vitro* and *in vivo* are dependent on the AhR ligand. In the CUL4B^{AhR} complex, ligand-activated AhR acts as a substrate-specific adaptor component that targets sex steroid receptors for degradation. Thus, our findings uncover a function for AhR as an atypical component of the ubiquitin ligase complex and demonstrate a non-genomic signalling pathway in which fat-soluble ligands regulate target-protein-selective degradation through a ubiquitin ligase complex.

The transcriptional regulatory system and the ubiquitin–proteasome system are two major target-selective systems that control intracellular protein levels. This target selectivity depends on the recognition of specific DNA elements by sequence-specific transcription factors[1] and the recognition of degradation substrates by E3 ubiquitin ligases[2–4]. These transcription factors and ligases serve primarily as specific adaptors that subsequently recruit transcriptional co-regulators and E2 ubiquitin-conjugating enzymes, respectively, to appropriate targets. The selective biological effects of fat-soluble ligands have been reported to be mediated by two classes of sequence-specific transcription factors, nuclear receptors[1] and arylhydrocarbon receptor (AhR) belonging to the basic helix–loop–helix (bHLH)/Per-Arnt-Sim (PAS) family[5–9].

AhR ligands modulate oestrogen and sex hormone, signalling both positively and negatively[8,10–13]. Functional impairments of male and female reproductive organs in AhR-deficient mice indicate the possible importance of AhR in sex hormone signalling[10,14]. Different AhR agonists[9], including 3-methylcholanthrene (3MC) and 2,3,7,8-tetrachlordibenzo-*p*-dioxin (TCDD), modulate oestrogen-dependent oestrogen receptor (ER)-α transactivation through the association of activated AhR/Arnt with ER-α[15]. Similarly, the transcriptional activity of nuclear androgen receptor (AR) was modulated by association with activated AhR (Supplementary Fig. S2a). However, ligand-bound AhR did not block oestrogen-induced co-activator recruitment on the oestrogen-responsive promoter (Supplementary Fig. S2b). This implies another mode of function for ligand-activated AhR beyond transcriptional regulation.

On activation of AhR by 3MC, we observed that protein levels of endogenous ER-α (in mammary tumour MCF-7 cells), ER-β (in ovarian tumour KGN cells) and AR (in prostate cancer LNCaP cells) were drastically decreased (Fig. 1a–c, and Supplementary Fig. 3a) without a change in messenger RNA levels (data not shown), irrespective of the presence of their cognate hormones. Other AhR agonists[9] (namely β-naphthoflavone (β-NF), environmental toxins such as TCDD and benzo[a]pyrene, and the endogenous metabolite indirubin) were similarly effective in protein degradation for ER-α (Fig. 1b) and ER-β/AR (data not shown), in agreement with a previous report on downregulated levels of uterine ER-α protein in rats treated with TCDD[16]. An AhR partial agonist/antagonist α-naphthoflavone (α-NF) was unable to accelerate the degradation of either AhR or ER-α (Fig. 1b, and Supplementary Fig. S3b).

AhR ligand-induced degradation (Fig. 1a–c) and functional repression (Supplementary Fig. S2c, d) of sex steroid receptors were abrogated in the presence of a proteasome inhibitor MG132. Consistently, poly-ubiquitination of ER-α was promoted by the activated AhR regardless of the presence of oestrogen (Fig. 1d, and Supplementary Fig. S3c). Pulse-chase kinetic analysis indicated that 3MC-induced degradation of ER-α was coupled to that of AhR[8,17,18] (Supplementary Fig. S3d). Moreover, the self-ubiquitination activity of the ligand-bound AhR immunocomplex was detected in an E1/E2-dependent manner (Supplementary Fig. S3e). Together with 3MC-dependent recognition of sex steroid receptors by AhR[8,12,13,15], these properties of AhR resemble those of classical adaptor components of the E3 ubiquitin ligase complexes, such as F-box proteins[3] or von Hippel–Lindau protein[19]. We therefore reasoned that activated AhR might act as an E3 ubiquitin ligase complex component.

To address this idea, AhR-containing complexes were purified from HeLa cells expressing Flag–AhR treated with 3MC or α-NF[15,20]. AhR formed large complexes in the presence of 3MC (Supplementary Fig. S4a–c). Further purification revealed five major 3MC-dependent complexes containing AhR (Fig. 1e). Complexes A and C contained well-known co-activators TRAP220/DRIP205/Med220 and p300 (ref. 1) (Supplementary Fig. S4d, e). Endogenous ER-α was detected in complexes B and C; however, ubiquitinated components were seen only in complex B (Fig. 1f, g).

Complex B was composed of the ubiquitin ligase core components cullin 4B (CUL4B)[3,21,22], damaged-DNA-binding protein 1 (DDB1)[23–27] and Rbx1 (Roc1)[3], together with subunits of the proteasomal 19S regulatory particle (19S RP), Arnt and transducin-β-like 3 (TBL3) (Fig. 1h). These components eluted with AhR in the presence of 3MC but not in the presence of α-NF (Fig. 1i, and Supplementary Fig. S4f). Neither CUL4A nor known substrate-specific adaptor components of CUL4A, such as DDB2, CSA and DET1[23,24], were present

[1]ERATO, Japan Science and Technology Agency, 4-1-8 Honcho, Kawaguchi, Saitama 332-0012, Japan. [2]Institute of Molecular and Cellular Biosciences, University of Tokyo, 1-1-1 Yayoi, Bunkyo-ku, Tokyo 113-0032, Japan. [3]Department of Urology, Faculty of Medicine, University of Tokyo, 7-3-1 Hongo, Bunkyo-ku, 113-8655, Japan. [4]National Institute for Environmental Studies, Tsukuba, Ibaraki 305-8506, Japan. [5]Graduate School of Life and Environmental Sciences, and [6]TARA Center, University of Tsukuba, 1-1-1 Tennodai Tsukuba, 305-8577, Japan. [7]SORST, Japan Science and Technology Agency, 4-1-8 Honcho, Kawaguchi, Saitama 332-0012, Japan.

in the AhR–CUL4B complex. As the cullin amino terminus binds adaptor components and the carboxy terminus interacts with an E2 enzyme-binding subunit Rbx1 (ref. 3), we performed tandem purification of the AhR–CUL4B complex with glutathione *S*-transferase (GST)-tagged CUL4B-N (N-terminal domain of CUL4B) and Flag–AhR. This led to the identification of a core complex consisting of five components: DDB1, AhR, Arnt, TBL3 and CUL4B (Fig. 1j). Together with Rbx1, this complex is denoted by $CUL4B^{AhR}$.

Immunoprecipitation of AhR together with endogenous CUL4B from MCF-7 and LNCaP cells was observed only in the presence of 3MC (Fig. 2a, b). Consistently, ligand-dependent co-localization of AhR with CUL4 was seen in MCF-7 cells (Fig. 2c). Whereas CUL4B seemed to act as a scaffold mediating DDB1–TBL3 and AhR–DDB1 interactions in $CUL4B^{AhR}$ (Fig. 2d, lane 4), ligand-activated AhR induced the assembly of complex components (Fig. 2d, lanes 1–3). DDB1 did not bridge CUL4B association with TBL3 or AhR, apparently because of the absence of the signature WDXR/DWD box[22,23–27] of either TBL3 or AhR, which is essential for DDB1 binding (Fig. 2d, lane 5, and Supplementary Fig. S5a). Consistently, specific and 3MC-dependent interaction of the conserved C-terminal acidic domain of AhR with the N-terminal region of CUL4B, but not with DDB1, was observed in a GST pulldown assay (Supplementary Figs S5b and S6). Because a constitutively active AhR mutant (AhRΔPASB)[9] interacted with CUL4B in the absence of ligand (Supplementary Fig. S5b), ligand-dependent structural alteration presumably induces AhR–CUL4B interaction. An AhR mutant lacking the CUL4B-binding acidic domain (AhRΔacid; Supplementary Fig. S6a) was indeed unable to promote ER-α ubiquitination *in vivo*, although the mutant retained 3MC-dependent transactivation function (Supplementary Fig. S5c). This indicates that the ubiquitin ligase function of AhR is independent of its transactivation function.

With two separately prepared components of recombinant AhR and CUL4B/DDB1/Rbx1 purified from *Spodoptera frugiperda* (Sf9) cells (Supplementary Fig. S7a), complex assembly *in vitro* was also dependent on 3MC (Fig. 2e). Furthermore, by *in vitro* ubiquitination assay (Supplementary Fig. S7b), the E3 ubiquitin ligase activity of $CUL4B^{AhR}$ for ER-α was dependent on 3MC but not on 17β-oestradiol (E_2) (Fig. 2f). These data indicate that both the complex assembly and the ubiquitin ligase activity of $CUL4B^{AhR}$ may be dependent on AhR agonists.

We then examined whether the recognition of sex steroid receptors for 3MC-dependent ubiquitination is indeed mediated by AhR. Co-immunoprecipitation analyses indicated that ligand-activated AhR was required for the recruitment of ER-α (Fig. 2a, d) or AR (Fig. 2b, and data not shown) to $CUL4B^{AhR}$. TBL3 and DDB1 did not seem essential for ER-α recruitment but stabilized the association of ER-α with $CUL4B^{AhR}$ (Fig. 2d). Moreover, knockdown of $CUL4B^{AhR}$ components (Supplementary Fig. S8) impaired the 3MC-induced ubiquitination and degradation of ER-α (Fig. 3a–d, and Supplementary Fig. S9a, b) and AR (Fig. 3e, Supplementary Fig. S9c and data not shown), and abolished the AhR-ligand-induced repression of ER-α transactivation (Supplementary Fig. S10a). Recognition of ER-α by activated AhR was retained, but ubiquitination of AhR-bound ER-α was abrogated, by knockdown of the other $CUL4B^{AhR}$ components (Fig. 3d). An ER-α AA/B mutant[15] that lacks interaction with AhR, and an ER-α K7R mutant in which seven lysine residues had been replaced with arginine (Supplementary Fig. S6b), were resistant to AhR-dependent ubiquitination and transrepression (Fig. 3f, and Supplementary Fig. S10b). Taken together, these data suggest that ligand-activated AhR functions as a substrate-specific adaptor component of $CUL4B^{AhR}$. AhR is therefore a unique and atypical substrate-specific component of a cullin-based E3 complex, because AhR bears no known interaction motif with cullin complexes yet associates directly with CUL4B. Ubiquitination of ER-α-associated AhR was similarly abolished by the knockdown, and the overall ubiquitination and degradation of AhR[8,17,18] were partly affected (Supplementary Fig. S11a, b). This implies the existence of $CUL4B^{AhR}$-dependent (self-ubiquitination[3]) and $CUL4B^{AhR}$-independent pathways for AhR degradation.

Human ER-α (hER-α) degradation is reportedly accelerated by the binding of E_2 (ref. 1) or the phosphorylation of Ser 118 (ref. 28), whereas a partial antagonist, tamoxifen, has been shown to stabilize ER-α[1]. Nevertheless, 3MC-activated AhR efficiently induced the ubiquitination and subsequent degradation of tamoxifen-bound ER-α and ER-α-S118A mutant (Fig. 3f). Reciprocally, AhR was dispensable for E_2-dependent ER-α degradation (Supplementary Fig. S11c). These results indicate that the $CUL4B^{AhR}$ system may act independently of innate protein degradation system(s) for ER-α. XAP2/ARA9/AIP[7,8,17], a chaperone that modulates the stability of unliganded AhR, seemed unlikely to mediate the accelerated degradation of ER-α by activated AhR (Supplementary Fig. S11d).

Last, we addressed the physiological significance of $CUL4B^{AhR}$ for sex hormone signalling in intact animals. Injection with either 3MC (Fig. 4a) or β-NF (Fig. 4c) did not affect the expression of ER-α or AR mRNA (data not shown) but caused a decrease in protein levels of uterine ER-α in ovariectomized female wild-type mice and of prostate AR in castrated male wild-type mice (Fig. 4b) regardless of their treatment with cognate sex hormones. However, AhR deficiency ($AhR^{-/-}$ mice)[9,14] abolished such effects of AhR ligands but did not affect the modulation of stability of sex steroid receptors by their respective hormones (Fig. 4a, b). As a result of reduced sex steroid receptor levels after pretreatment with 3MC, E_2-dependent induction of c-*fos* in the uterus[15] and dihydrotestosterone (DHT)-dependent induction of *Probasin* in the prostate[10] were severely impaired (Fig. 4a, b). Cellular proliferation and gene induction in response to sex hormones in primary cultured epithelial cells from normal mouse uterus and prostate were consistently suppressed by 3MC (Supplementary Fig. S12a, b) and β-NF (Supplementary Fig. S12c), but no effect was detected in $AhR^{-/-}$ cells (Supplementary Fig. S12a, b). The significance of $CUL4B^{AhR}$ complex components in the AhR-mediated suppression of sex hormone effects

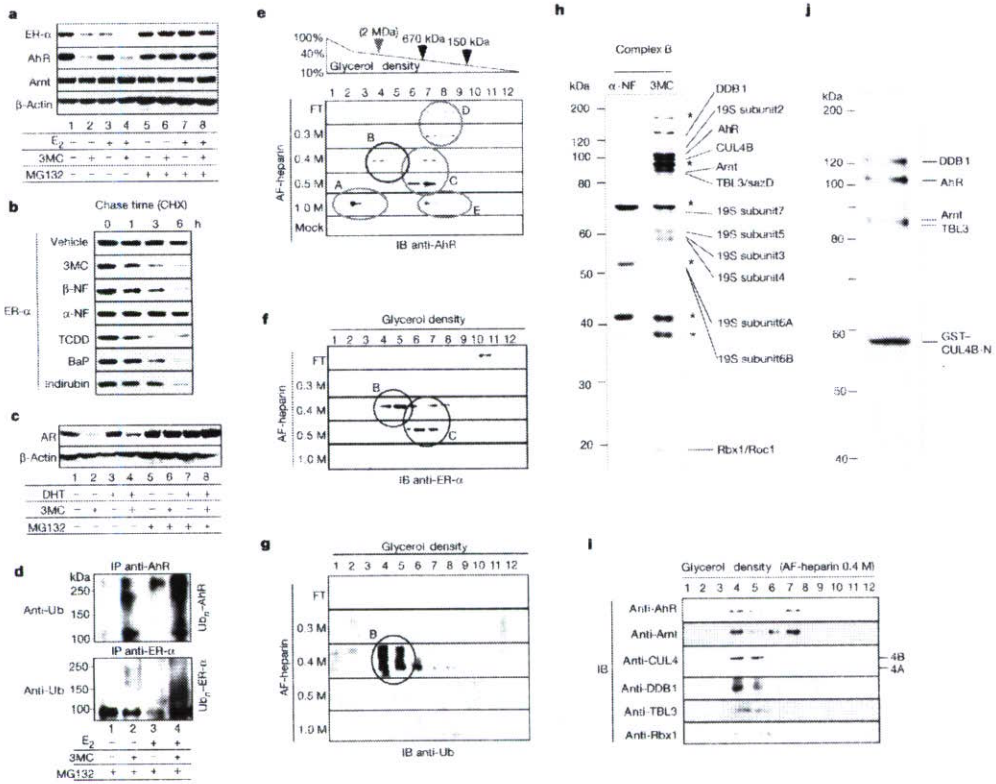

Figure 1 | Activated AhR acts as an E3 ubiquitin ligase. a–c, AhR-ligand-induced proteasomal degradation of ER-α (**a**, **b**) and AR (**c**). MCF-7 cells (**a**, **b**) and LNCaP cells (**c**) were incubated as indicated with E_2 (10 nM), DHT (10 nM) and/or 3MC (1 μM), β-NF (1 μM), benzo[a]pyrene (BaP; 100 nM), TCDD (10 nM), indirubin (10 nM) and α-NF (1 μM) in the presence or absence of MG132 (10 μM) and cycloheximide (CHX; 5 μM) for 3 h (**a**, **c**) or the indicated durations (**b**). Cell lysates were subjected to western blotting with specified antibodies. **d**, AhR-ligand-induced ubiquitination of ER-α. MCF-7 cells were incubated with the indicated ligands for 6 h. Western blots were subjected to dark exposure to detect poly-ubiquitinated forms of the receptors. IP, immunoprecipitation; Ub, ubiquitin. **e**, **f**, Biochemical separation and identification of AhR-associated complexes. Flag–AhR-associated proteins in the presence of 3MC or α-NF from HeLa cells stably expressing Flag–AhR were first fractionated by glycerol-density-gradient centrifugation (top, fractions 1–12), and then separated by Toyopearl AF-heparin column chromatography with the indicated KCl concentrations (FT, 1.0 M KCl). Samples from the 3MC-treated cells were resolved into five distinct complexes. IB, immunoblotting. **g**, Components of an AhR-associated complex are highly ubiquitinated. Western blots with anti-ubiquitin antibody. **h**, Identification of AhR-associated CUL4B ubiquitin ligase complex components. Components from complex B in **e** (fractions 4 and 5 from the glycerol-density-gradient centrifugation, eluted from an AF-heparin column at 0.4 M KCl) were resolved by SDS–PAGE, silver-stained and identified by matrix-assisted laser desorption ionization–time-of-flight MS analysis. **i**, Co-elution of the complex B components as a large complex. **j**, Association of activated AhR with the CUL4B complex. The $CUL4B^{AhR}$ complex from Flag–AhR-expressing HeLa cells treated with 3MC was affinity purified with GST-tagged N-terminal domain of CUL4B followed by anti-Flag antibody column fractionation.

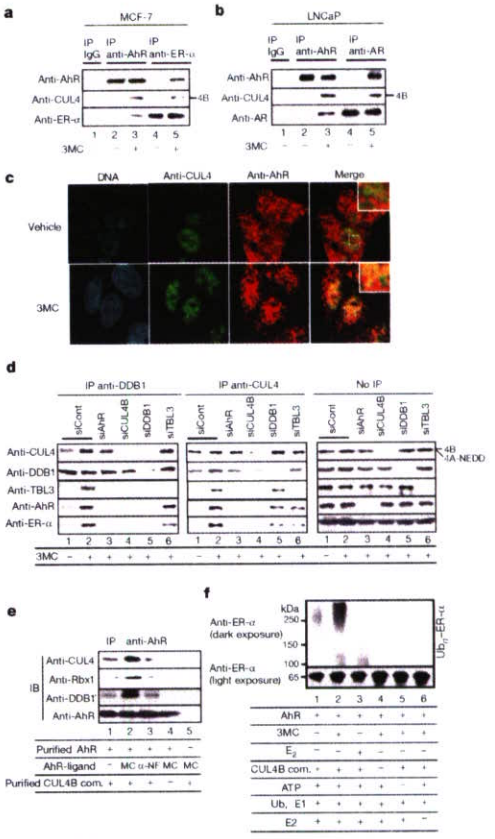

Figure 2 | AhR ligand-dependent assembly and ubiquitin ligase activity of $CUL4B^{AhR}$. a, **b**, 3MC-dependent association of endogenous CUL4B and AhR with ER-α and AR. Co-immunoprecipitation analyses from MCF-7 (**a**) and LNCaP (**b**) cells incubated with ligand and MG132 for 2 h. IP, immunoprecipitation. **c**, 3MC-dependent co-localization of AhR with CUL4. MCF-7 cells incubated with 3MC and MG132 for 2 h were immunostained with the indicated antibodies. **d**, Formation of the $CUL4B^{AhR}$ complex. MCF-7 cells were transfected with specified short interfering RNAs (siRNAs) for 48 h, treated with 3MC and MG132 for 2 h, and immunoprecipitated with the indicated antibodies. **e**, Assembly of the CUL4B complex components with AhR is dependent on 3MC *in vitro*. Immunoprecipitation with anti-AhR antibodies of the indicated recombinant CUL4B complex components (CUL4B com.) was observed only in the presence of 3MC. IB, immunoblotting. **f**, $CUL4B^{AhR}$ ubiquitinates ER-α *in vitro*. ER-α protein was incubated with and without recombinant $CUL4B^{AhR}$ E3 complex components, ubiquitin (Ub), ATP, E1 and E2 enzymes as indicated, then subjected to western blotting.

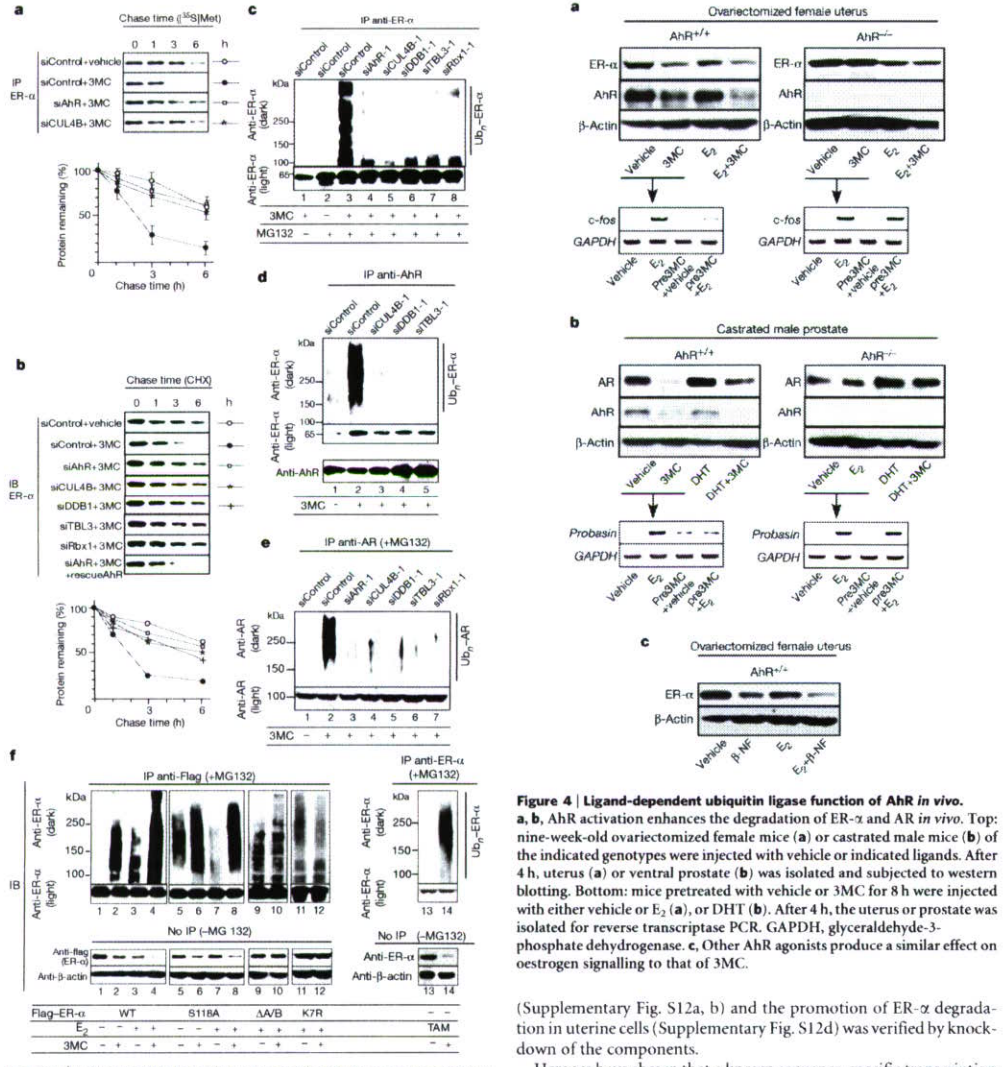

Figure 3 | Activated AhR is a substrate-specific adaptor component of the CUL4B^{AhR} complex. **a**–**c**, Components of CUL4B^{AhR} are required for 3MC-dependent ubiquitination and degradation of ER-α. MCF-7 cells were transfected with indicated siRNAs for 48 h, then used in pulse-chase analysis as in Supplementary Fig. S3d (**a**), in cycloheximide (CHX) chasing (**b**) and in the *in vivo* ubiquitination assay with ligand incubation for 6 h (**c**). All values are shown as means ± s.d. ($n = 3$) (**a**) or as means ($n = 3$) (**b**). The knockdown efficiency in the same lysates was confirmed in Supplementary Fig. S9a. IB, immunoblotting; IP, immunoprecipitation. **d**, AhR is the substrate-specific adaptor in the targeting of ER-α by CUL4B^{AhR}. MCF-7 cells transfected with the indicated siRNAs were lysed in TNE buffer and immunoprecipitated with anti-AhR antibody in the presence of MG132. Ubiquitination of the ER-α co-immunoprecipitated with AhR was detected by western blotting. **e**, LNCaP cells were subjected to the same analysis as in **a**–**c**. **f**, AhR-ligand-induced ER-α ubiquitination requires intact lysine residues and is independent of oestrogen binding or S118 phosphorylation of hER-α. Intact MCF-7 cells (right) or cells transfected with Flag–hER-α, AhR and their derivatives (left) were treated with the indicated ligands in the presence (top) or absence (bottom) of MG132 for 6 h, then subjected to western blotting. TAM, tamoxifen; WT, wild type.

Figure 4 | Ligand-dependent ubiquitin ligase function of AhR *in vivo*. **a**, **b**, AhR activation enhances the degradation of ER-α and AR *in vivo*. Top: nine-week-old ovariectomized female mice (**a**) or castrated male mice (**b**) of the indicated genotypes were injected with vehicle or indicated ligands. After 4 h, uterus (**a**) or ventral prostate (**b**) was isolated and subjected to western blotting. Bottom: mice pretreated with vehicle or 3MC for 8 h were injected with either vehicle or E_2 (**a**), or DHT (**b**). After 4 h, the uterus or prostate was isolated for reverse transcriptase PCR. GAPDH, glyceraldehyde-3-phosphate dehydrogenase. **c**, Other AhR agonists produce a similar effect on oestrogen signalling to that of 3MC.

(Supplementary Fig. S12a, b) and the promotion of ER-α degradation in uterine cells (Supplementary Fig. S12d) was verified by knockdown of the components.

Here we have shown that a known sequence-specific transcription factor AhR acts as a ligand-dependent CUL4B-based E3 ubiquitin ligase for selectively targeting sex steroid receptors to bring about accelerated protein degradation. The transcription and ubiquitination functions of AhR seem to be responsible for a distinct set of biological events caused by endogenous and exogenous AhR ligands. In ubiquitin ligase complexes, substrate recognition by known substrate-specific components is generally evoked by substrate modifications[2–4]. However, the recognition and subsequent ubiquitination of sex steroid receptors by AhR requires dioxin-type compounds as ligands but does not require the phosphorylation or ligand binding of sex steroid receptors. We have therefore shown that fat-soluble ligands directly control the function of a ubiquitin ligase complex for targeted protein destruction in animals (see Supplementary Fig. S1). In plants, auxin was recently found to control protein destruction through the auxin receptor SCF^{TIR1} (refs 29, 30). However, whereas SCF^{TIR1} is regulated by ligand-dependent substrate recognition by TIR1, CUL4B^{AhR} is primarily regulated by the assembly of a ligand-dependent complex as well as substrate recognition. Considered together, ubiquitin-ligase-based perception mechanisms of fat-soluble ligands may be diverse in different species. It is possible that other nuclear receptors and binding proteins for fat-soluble ligands also serve as key components of ubiquitin ligases to mediate a non-genomic pathway of fat-soluble ligands to regulate target-protein-selective destruction.

METHODS

More detailed descriptions of all materials and methods are supplied in the Supplementary Information.

Biochemical purification and separation of AhR-associated complexes. The nuclear extracts preparation, anti-Flag affinity purification and mass spectrometry were performed as described previously[15,20]. For purification of the core CUL4B^{AhR} complex, the nuclear extracts were first bound to the GST–CUL4B-N (amino acid residues 1–318) columns before being loaded on anti-Flag columns[20].

***In vitro* ubiquitination assay.** The *in vitro* ubiquitination assay was performed as described previously[21]. Purified Flag–AhR (0.2 μg) was incubated either with 3MC (10 μM) or vehicle (dimethylsulphoxide) for 30 min at 25 °C, then mixed with Flag–CUL4B/DDB1/Rbx1 complex (0.2 μg), and after further incubation for 30 min at 25 °C the substrate, ER-α (Calbiochem), was added.

Plasmids, antibodies, immunoprecipitation, *in vivo* ubiquitination, pulse-chasing, ligand responses in mice, and RNA-mediated interference experiments. Detailed methods used in this study can be found in the Supplementary Information.

Received 13 December 2006; accepted 16 February 2007.

1. McKenna, N. J. & O'Malley, B. W. Combinatorial control of gene expression by nuclear receptors and coregulators. *Cell* **108**, 465–474 (2002).
2. Hershko, A. & Ciechanover, A. The ubiquitin system. *Annu. Rev. Biochem.* **67**, 425–479 (1998).
3. Deshaies, R. J. SCF and Cullin/Ring H2-based ubiquitin ligases. *Annu. Rev. Cell Dev. Biol.* **15**, 435–467 (1999).
4. Harper, J. W. A phosphorylation-driven ubiquitination switch for cell-cycle control. *Trends Cell Biol.* **12**, 104–107 (2002).
5. Poellinger, L. Mechanistic aspects—the dioxin (aryl hydrocarbon) receptor. *Food Addit. Contam.* **17**, 261–266 (2000).
6. Hankinson, O. The aryl hydrocarbon receptor complex. *Annu. Rev. Pharmacol. Toxicol.* **35**, 307–340 (1995).
7. Swanson, H. I. & Bradfield, C. A. The AH-receptor: genetics, structure and function. *Pharmacogenetics* **3**, 213–230 (1993).
8. Carlson, D. B. & Perdew, G. H. A dynamic role for the Ah receptor in cell signaling? Insights from a diverse group of Ah receptor interacting proteins. *J. Biochem. Mol. Toxicol.* **16**, 317–325 (2002).
9. Mimura, J. & Fujii-Kuriyama, Y. Functional role of AhR in the expression of toxic effects by TCDD. *Biochim. Biophys. Acta* **1619**, 263–268 (2003).
10. Lin, T. M. *et al.* Effects of aryl hydrocarbon receptor null mutation and in utero and lactational 2,3,7,8-tetrachlorodibenzo-*p*-dioxin exposure on prostate and seminal vesicle development in C57BL/6 mice. *Toxicol. Sci.* **68**, 479–487 (2002).
11. Brunnberg, S. *et al.* The basic helix-loop-helix-PAS protein ARNT functions as a potent coactivator of estrogen receptor-dependent transcription. *Proc. Natl Acad. Sci. USA* **100**, 6517–6522 (2003).
12. Matthews, J., Wihlen, B., Thomsen, J. & Gustafsson, J. A. Aryl hydrocarbon receptor-mediated transcription: ligand-dependent recruitment of estrogen receptor α to 2,3,7,8-tetrachlorodibenzo-*p*-dioxin-responsive promoters. *Mol. Cell. Biol.* **25**, 5317–5328 (2005).
13. Beischlag, T. V. & Perdew, G. H. ER α-AHR-ARNT protein–protein interactions mediate estradiol-dependent transrepression of dioxin-inducible gene transcription. *J. Biol. Chem.* **280**, 21607–21611 (2005).
14. Baba, T. *et al.* Intrinsic function of the aryl hydrocarbon (dioxin) receptor as a key factor in female reproduction. *Mol. Cell. Biol.* **25**, 10040–10051 (2005).
15. Ohtake, F. *et al.* Modulation of oestrogen receptor signalling by association with the activated dioxin receptor. *Nature* **423**, 545–550 (2003).
16. Romkes, M., Piskorska-Pliszczynska, J. & Safe, S. Effects of 2,3,7,8-tetrachlorodibenzo-*p*-dioxin on hepatic and uterine estrogen receptor levels in rats. *Toxicol. Appl. Pharmacol.* **87**, 306–314 (1987).
17. Davarinos, N. A. & Pollenz, R. S. Aryl hydrocarbon receptor imported into the nucleus following ligand binding is rapidly degraded via the cytosplasmic proteasome following nuclear export. *J. Biol. Chem.* **274**, 28708–28715 (1999).
18. Roberts, B. J. & Whitelaw, M. L. Degradation of the basic helix-loop-helix/Per-ARNT-Sim homology domain dioxin receptor via the ubiquitin/proteasome pathway. *J. Biol. Chem.* **274**, 36351–36356 (1999).
19. Maxwell, P. H. *et al.* The tumour suppressor protein VHL targets hypoxia-inducible factors for oxygen-dependent proteolysis. *Nature* **399**, 271–275 (1999).
20. Kitagawa, H. *et al.* The chromatin-remodeling complex WINAC targets a nuclear receptor to promoters and is impaired in Williams syndrome. *Cell* **113**, 905–917 (2003).
21. Zhong, W., Feng, H., Santiago, F. E. & Kipreos, E. T. CUL-4 ubiquitin ligase maintains genome stability by restraining DNA-replication licensing. *Nature* **423**, 885–889 (2003).
22. Higa, L. A. *et al.* CUL4–DDB1 ubiquitin ligase interacts with multiple WD40-repeat proteins and regulates histone methylation. *Nature Cell Biol.* **8**, 1277–1283 (2006).
23. Groisman, R. *et al.* The ubiquitin ligase activity in the DDB2 and CSA complexes is differentially regulated by the COP9 signalosome in response to DNA damage. *Cell* **113**, 357–367 (2003).
24. Wertz, I. E. *et al.* Human De-etiolated-1 regulates c-Jun by assembling a CUL4A ubiquitin ligase. *Science* **303**, 1371–1374 (2004).
25. Jin, J., Arias, E. E., Chen, J., Harper, J. W. & Walter, J. C. A family of diverse Cul4-Ddb1-interacting proteins includes Cdt2, which is required for S phase destruction of the replication factor Cdt1. *Mol. Cell* **23**, 709–721 (2006).
26. Angers, S. *et al.* Molecular architecture and assembly of the DDB1–CUL4A ubiquitin ligase machinery. *Nature* **443**, 590–593 (2006).
27. He, Y. J., McCall, C. M., Hu, J., Zeng, Y. & Xiong, Y. DDB1 functions as a linker to recruit receptor WD40 proteins to CUL4–ROC1 ubiquitin ligases. *Genes Dev.* **20**, 2949–2954 (2006).
28. Valley, C. C. *et al.* Differential regulation of estrogen-inducible proteolysis and transcription by the estrogen receptor alpha N terminus. *Mol. Cell. Biol.* **25**, 5417–5428 (2005).
29. Dharmasiri, N., Dharmasiri, S. & Estelle, M. The F-box protein TIR1 is an auxin receptor. *Nature* **435**, 441–445 (2005).
30. Kepinski, S. & Leyser, O. The *Arabidopsis* F-box protein TIR1 is an auxin receptor. *Nature* **435**, 446–451 (2005).

Supplementary Information is linked to the online version of the paper at www.nature.com/nature.

Acknowledgements We thank K. Tanaka, C. K. Glass, J. Yanagisawa, Y. Gotoh and J. Mimura for comments; S. Murata, T. Matsuda, T. Suzuki and Y. Tateishi for providing materials; T. Matsumoto, M. Igarashi and S. Fujiyama for technical assistance; and H. Higuchi for manuscript preparation. This work was supported in part by the Program for Promotion of Basic Research Activities for Innovative Biosciences (PROBRAIN) and priority areas from the Ministry of Education, Culture, Sports, Science and Technology (to Y.F.-K. and S.K.).

Author Contributions F.O., T.C., Y.F.-K. and S.K. designed the experiments. F.O., A. B., M.O., K.I., H.M., S.T. and I. T. performed the experiments. F.O., A.K. and S.K. wrote the paper.

Author Information Reprints and permissions information is available at www.nature.com/reprints. The authors declare no competing financial interests. Correspondence and requests for materials should be addressed to S.K. (uskato@mail.ecc.u-tokyo.ac.jp).

Estrogen Prevents Bone Loss via Estrogen Receptor α and Induction of Fas Ligand in Osteoclasts

Takashi Nakamura,[1,2,9] Yuuki Imai,[1,3,9] Takahiro Matsumoto,[1,2] Shingo Sato,[4] Kazusane Takeuchi,[1] Katsuhide Igarashi,[5] Yoshifumi Harada,[6] Yoshiaki Azuma,[6] Andree Krust,[7] Yoko Yamamoto,[1] Hiroshi Nishina,[4] Shu Takeda,[4] Hiroshi Takayanagi,[4] Daniel Metzger,[7] Jun Kanno,[5] Kunio Takaoka,[3] T. John Martin,[8] Pierre Chambon,[7] and Shigeaki Kato[1,2,*]

[1]Institute of Molecular and Cellular Biosciences, University of Tokyo, Yayoi 1-1-1, Bunkyo-ku, Tokyo 113-0032, Japan
[2]Exploratory Research for Advanced Technology, Japan Science and Technology Agency, Honcho 4-1-8, Kawaguchi, Saitama 332-0012, Japan
[3]Department of Orthopaedic Surgery, Osaka City University Graduate School of Medicine, Asahimachi 1-4-3, Abeno-ku, Osaka, 545-8585, Japan
[4]Tokyo Medical and Dental University, Yushima 1-5-45, Bunkyo-ku, Tokyo 113-8510, Japan
[5]Division of Cellular and Molecular Toxicology, National Institute of Health Sciences, 1-18-1 Kamiyoga, Setagaya-ku, Tokyo 158-8501, Japan
[6]Teijin Institute for Biomedical Research, Asahigaoka 4-3-2, Hino, Tokyo 191-8512, Japan
[7]Institut de Génétique et de Biologie Moleculaire et Cellulaire, Departement of Physiological Genetics / Inserm, U-596 / CNRS, UMR7104 / Université Louis Pasteur, Illkirch, Strasbourg, F-67400 France
[8]St. Vincent's Institute of Medical Research, 9 Princes Street, Fitzroy VIC 3065, Australia
[9]These authors contributed equally to this work.
*Correspondence: uskato@mail.ecc.u-tokyo.ac.jp
DOI 10.1016/j.cell.2007.07.025

SUMMARY

Estrogen prevents osteoporotic bone loss by attenuating bone resorption; however, the molecular basis for this is unknown. Here, we report a critical role for the osteoclastic estrogen receptor α (ERα) in mediating estrogen-dependent bone maintenance in female mice. We selectively ablated ERα in differentiated osteoclasts ($ER\alpha^{\Delta Oc/\Delta Oc}$) and found that $ER\alpha^{\Delta Oc/\Delta Oc}$ females, but not males, exhibited trabecular bone loss, similar to the osteoporotic bone phenotype in postmenopausal women. Further, we show that estrogen induced apoptosis and upregulation of Fas ligand (FasL) expression in osteoclasts of the trabecular bones of WT but not $ER\alpha^{\Delta Oc/\Delta Oc}$ mice. The expression of ERα was also required for the induction of apoptosis by tamoxifen and estrogen in cultured osteoclasts. Our results support a model in which estrogen regulates the life span of mature osteoclasts via the induction of the Fas/FasL system, thereby providing an explanation for the osteoprotective function of estrogen as well as SERMs.

INTRODUCTION

Bone remodeling is a dynamic metabolic process. The destruction or "resorption" of pre-existing bone by mature osteoclasts is followed by the formation of new bone by osteoblasts. Osteoblasts are derived from pleiotropic mesenchymal stem cells in the bone marrow. Mature osteoclasts are multinuclear, macrophage-like cells, derived from hematopoietic stem cells also in the bone marrow. Bone resorption and deposition are tightly coupled, and their balance defines both bone mass as well as quality. The regulation of bone remodeling is complex. A number of systemic hormones and transcription factors directly regulate the proliferation and differentiation of osteoblasts and osteoclasts (Karsenty, 2006; Karsenty and Wagner, 2002; Rodan and Martin, 2000; Teitelbaum and Ross, 2003). Additionally, the indirect cellular communication among groups of bone cells is also physiologically critical for bone growth and remodeling (Martin and Sims, 2005; Mundy and Elefteriou, 2006). The molecular and genetic mechanisms governing bone cell fate have been intensively studied; however, how the life span of bone cells is determined on a molecular level remains elusive.

Estrogen is a key hormone in bone remodeling in several species. The osteoprotective action of estrogen is demonstrable in rodents and is clinically important in humans, particularly older women (Chien and Karsenty, 2005;

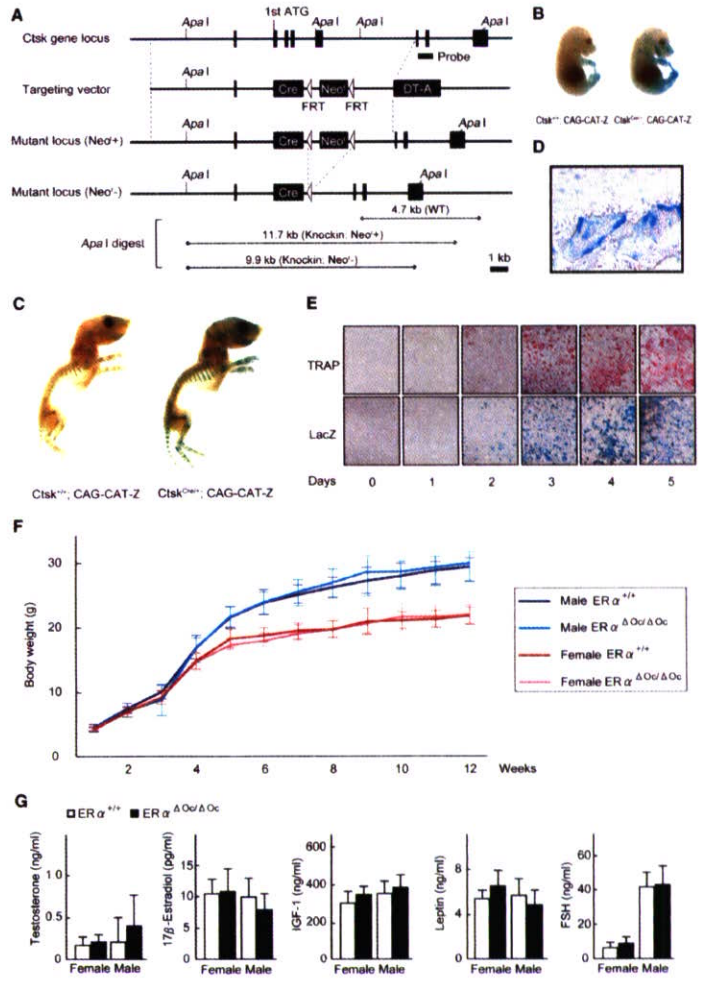

Figure 1. Generation of Knockin Mice Selectively Expressing Cre in Mature Osteoclasts

(A) Illustration of the targeting strategy for insertion of the *Cre* gene into the mouse *Cathepsin K* (*Ctsk*) gene. A targeting vector was generated to contain the *Cre* cDNA at the endogenous ATG start site, followed by a *FRT* (Flp-recombinase target)-flanked *Neo*^{r} cassette. The *DT-A* (diphtheria toxin-A) gene was also inserted to avoid random integrations.

(B and C) *Ctsk-Cre* mice were then crossed with *CAG-CAT-Z* mice. β-galactosidase activity derived from the activated *LacZ* reporter gene was monitored to test if expressed Cre excised the *loxP* sites in mature osteoclasts. LacZ expression patterns reflected the localization patterns of mature osteoclasts in the developing bone at 16.5 days post coitum embryos and in the skeletal tissues of 7-day-old pups.

(D) The LacZ expression induced by Cre-mediated excision was also seen in osteoclasts attached to trabecular bone in the lumber vertebrae of 12-week-old mice.

(E) LacZ expression was induced during osteoclastogenesis. Osteoclast-like cells that differentiated from bone-marrow macrophages following culture in the presence of M-CSF and RANKL were stained with TRAP (tartrate-resistant acid phosphatase), a mature osteoclast marker.

Delmas, 2002; Raisz, 2005; Rodan and Martin, 2000). Estrogen deficiency in postmenopausal women frequently leads to osteoporosis, the most common skeletal disorder. Similarly, ovariectomy clearly produces an osteoporotic bone phenotype in mice. Osteoporotic bone loss is the result of high bone turnover in which bone resorption outpaces bone deposition (Rodan and Martin, 2000; Teitelbaum, 2007). This imbalance in bone turnover that is induced by estrogen deficiency in women and female rodents can be ameliorated with bio-available estrogens including selective estrogen receptor modulators (SERMs) (Riggs and Hartmann, 2003).

Estrogen and SERMs primarily act by regulating gene transcription via estrogen receptors (ERα, ERβ) (Couse and Korach, 1999; Shang and Brown, 2002). ERs belong to the nuclear receptor gene superfamily and act as ligand-inducible transcriptional factors (Mangelsdorf et al., 1995). ER dimers directly or indirectly associate with specific DNA elements in the target gene promoter (Shang and Brown, 2002) and control transcription through reorganizing chromatin structure and histone modifications (Belandia and Parker, 2003). Genetic mouse models (KO mice) lacking ERα ($ER\alpha^{-/-}$) and ERβ ($ER\beta^{-/-}$) provide insights into ER function (Mueller and Korach, 2001; Windahl et al., 2002). In mice, though ERα appears to be the major receptor in most estrogen target tissues including bone (Sims et al., 2003), neither clear bone loss nor high bone turnover is detectable in ERα single or ERα/ERβ double-KO females (Syed and Khosla, 2005; Windahl et al., 2002). This unexpected maintenance of bone mass in female mutants is presumed to be due to unphysiologically elevated levels of other osteoprotective hormones, like androgens. Systemic defects in the hypothalamus caused by ER inactivation appear to impair the negative feedback system of hormone production (Syed and Khosla, 2005). This leads to an excess in estrogen precursors, notably androgens. In fact, the anabolic effects of androgens mediated by the androgen receptor (AR) are evident in female mice (Kawano et al., 2003; Sims et al., 2003). In males, estrogen is also osteoprotective, as is evident by the development of osteopenia in male patients genetically deficient in ERα (Smith et al., 1994) or aromatase activity (Simpson and Davis, 2001). Thus, irrespective of the accumulating clinical and basic research data on the osteoprotective actions of estrogen and SERMs, the molecular basis of this osteoprotection in females remains elusive.

To study the molecular interactions behind the antibone resorptive actions of estrogen in women and female animals, we genetically ablated ERα in mature osteoclasts ($ER\alpha^{\Delta Oc/\Delta Oc}$). Selective ablation of ERα in differentiated osteoclasts ($ER\alpha^{\Delta Oc/\Delta Oc}$) was accomplished by crossing a *Cathepsin K-Cre* knockin mouse with a floxed *ERα* mouse. This resulted in clear trabecular bone loss and high bone turnover associated with increased osteoclast numbers in females but not in males. In the female mutants, further bone loss following ovariectomy was not significant and recovery by estrogen was ineffective in the trabecular areas of long bones and lumbar vertebral bodies. Upregulated expression of *Fas ligand* (*FasL*) gene, and increased apoptosis in differentiated osteoclasts by estrogen was found in the intact bone of wild-type females but undetectable in $ER\alpha^{\Delta Oc/\Delta Oc}$ females. Induction of FasL and apoptosis by estrogen as well as a SERM also required ERα in cultured osteoclasts. Thus, we propose that the osteoprotective actions of estrogen and SERMs are mediated at least in part through osteoclastic ERα in trabecular bone, and the life span of mature osteoclasts is regulated through the activation of the FasL signaling.

RESULTS

Generation of Osteoclast-Specific *ERα* Gene Disruption by Knocked-In *Cre* in the *Cathepsin K* Gene

To specifically disrupt *ERα* gene in mature osteoclasts, we knocked in *Cre* into the gene locus of *Cathepsin K* ($Ctsk^{Cre/+}$) (Figures 1A, S1A, and S1B), a gene known to be expressed in differentiated osteoclastic cells arising from hematopoietic stem cells. This gene is functionally indispensable for mature osteoclasts (Saftig et al., 1998). Only one copy appears enough to support normal bone formation and bone turnover, since heterozygous mutant mice of *Cathepsin K* ($Ctsk^{+/-}$) have no obvious bone phenotype (Gowen et al., 1999; Li et al., 2006; Saftig et al., 1998) . Clear, bone-specific expression of the *Cre* transcript in the adult $Ctsk^{Cre/+}$ mice was observed in the tested tissues (Figure S1C). To confirm Cre protein expression, the $Ctsk^{Cre/+}$ mice were crossed with tester mice (*CAG-CAT-Z*). These mice were genetically engineered to express β-galactosidase by excision of the transcribed stop sequence in front of the *β-galactosidase* gene (*LacZ*) in cells expressing Cre (Sakai and Miyazaki, 1997). β-galactosidase expression visualized by LacZ staining was observed in the bones of 16.5 dpc embryos and 7-day-old pups of $Ctsk^{Cre/+}$; *CAG-CAT-Z* mice. Expression patterns were consistent with the appearance and skeletal localization of functionally mature osteoclasts (Figures 1B and 1C). Histochemical staining of LacZ in the lumbar vertebrae of 12-week-old mice was localized in multinuclear osteoclasts (Figure 1D) but not seen in osteoblasts and osteocytes (Figure S1D) and the hypothalamus (Figure S1E). Since *Cathepsin K* gene expression is evident in differentiated osteoclasts (Saftig et al., 1998), we used an in vitro culture cell system to test whether Cre expression was driven by the endogenous promoter that is induced at the time of osteoclast differentiation. Osteoclast-precursor cells derived from bone marrow were cytodifferentiated for 1 week in the presence of M-CSF (macrophage colony stimulating factor) and RANKL (receptor activator of NFκB ligand) (Koga et al., 2004). TRAP-positive osteoclasts emerged after 3 days of culture (Figure 1E). The number of TRAP-positive osteoclasts and the number of LacZ-expressing cells simultaneously increased. In the contrast, the LacZ expression was not detected in primary cultured osteoblasts derived from the calvaria (Figure S1F). In view of both our in vivo and in vitro observations, we conclude that the $Ctsk^{Cre/+}$ mouse line expresses Cre in differentiated osteoclasts. Moreover, estrogen response in bone mass control was not distinguishable in between $Ctsk^{Cre/+}$ and $Ctsk^{+/+}$ mice (Figure S2A).

We then crossed floxed *ERα* mice (Dupont et al., 2000) with $Ctsk^{Cre/+}$ mice to disrupt ERα in differentiated osteoclasts ($ER\alpha^{\Delta Oc/\Delta Oc}$). Excision of the *ERα* gene (Figure S1G) was confirmed by Southern blotting of DNA from adult female and male (data not shown) bone as well as in cultured mature osteoclasts (Figure S1H). No overt differences were observed in the growth curve, reproduction, or tissues for up to 12 weeks of age (Figure 1F) between the $Ctsk^{Cre/+}$; $ER\alpha^{+/+}$ ($ER\alpha^{+/+}$) and the $Ctsk^{Cre/+}$; $ER\alpha^{flox/flox}$ ($ER\alpha^{\Delta Oc/\Delta Oc}$) mice, with the exception of the female bones. Serum levels of sex hormones and bone remodeling regulators such as IGF-I, leptin, and follicle-stimulating hormone (Sun et al., 2006; Takeda et al., 2002) appeared unchanged in both male and female $ER\alpha^{\Delta Oc/\Delta Oc}$ mice at 12 weeks (Figure 1G).

Osteopenia Occurred in Osteoclast-Specific ERα KO Females But Not Males

The 12-week-old $ER\alpha^{\Delta Oc/\Delta Oc}$ females exhibited a clear reduction in bone mineral density (BMD) in the femurs (Figures 2A–2C) and tibiae (data not shown) when compared with $ER\alpha^{+/+}$ mice. Though cortical bone appeared unaffected, trabecular bone loss (Figure 2A) with significant reduction of trabecular bone volume (BV/TV) (Figure 2F) was clearly seen. This is similar to the osteoporotic abnormalities observed in women during natural menopause or following ovariectomy (Delmas, 2002; Tolar et al., 2004). However, unlike men deficient in aromatase or ERα activity (Simpson and Davis, 2001; Smith et al., 1994), $ER\alpha^{\Delta Oc/\Delta Oc}$ males unexpectedly exhibited no clear bone loss even in the trabecular areas (Figures 2A–2C). In $ER\alpha^{\Delta Oc/\Delta Oc}$ females, both the bone-formation rate, estimated by double-calcein labeling (Figure 2D), as well as the bone-resorption rate, estimated from TRAP-positive differentiated osteoclast numbers (Figure 2E), were increased, indicating high bone turnover. Histomorphometric analyses of $ER\alpha^{\Delta Oc/\Delta Oc}$ females supported the observation of accelerated bone resorption, as increased numbers of osteoclasts (Oc. S/BS and N. Oc/BS) were observed together with more eroded bone surface (ES/BS in Figure 2F). Bone formation was also enhanced as the rates of mineral apposition (MAR) and bone formation (BFR/BS) were both upregulated without an increase in osteoblast numbers (Ob.S/BS) (Figure 2F). Thus, considering all of these findings, it is conceivable that the increased number of differentiated osteoclasts following ERα ablation accelerates bone resorption over formation, leading to bone loss in the trabecular areas.

No Further Bone Loss Results from Estrogen Deficiency in $ER\alpha^{\Delta Oc/\Delta Oc}$ Females

To verify whether osteoclastic ERα indeed mediates osteoprotective estrogen actions, estrogen action was investigated by ovariectomy (OVX) of 12-week-old female mice. As expected, OVX in $ER\alpha^{+/+}$ females resulted in significantly reduced BMD particularly in the trabecular bone (Figures 3A and 3B) but not in the cortical bone (Figure 3C). Consistent with previous reports, (Kimble et al., 1995; Teitelbaum and Ross, 2003), estrogen deficiency following OVX upregulated the serum levels of cytokines like TNFα and IL-1α (Figure 3D). These cytokines enhance bone resorption through stimulation of osteoclastogenesis, leading to the loss of bone mass (Teitelbaum and Ross, 2003). OVX did not further reduce BMD or trabecular bone volume of the femurs of $ER\alpha^{\Delta Oc/\Delta Oc}$ females (Figure 3B) nor affect increased number of TRAP-positive osteoclasts (see lower panel in Figure 3A) despite upregulation of serum cytokines. This suggests that the expression of cytokines known to regulate bone resorption is not under the control of osteoclastic ERα.

Estrogen Treatment Failed to Rescue the Osteoporotic Bone Phenotype of $ER\alpha^{\Delta Oc/\Delta Oc}$ Mice

Estrogen treatment by estrogen pellet implantation (OVX + E2) for 2 weeks after OVX in $ER\alpha^{+/+}$ mice elicited a dramatic increase in bone mass in both the trabecular and cortical areas of the femurs (data not shown) and lumbar vertebral bodies (Figure 4A). Estrogen action during E2 treatment in female mutants ($ER\alpha^{\Delta Oc/\Delta Oc}$) was not as pronounced as in the $ER\alpha^{+/+}$ females (Figures 4A and 4B), and the increase in the trabecular portions of the distal femurs was slight (data not shown). Histomorphometric analysis of the lumbar vertebral bodies (Figure 4B) supported the idea that E2 treatment in the female mutants was not sufficient to suppress accelerated bone resorption. These in vivo findings in the $ER\alpha^{\Delta Oc/\Delta Oc}$ females suggest that in at least the trabecular areas of the long bones and lumbar vertebral bodies, the osteoprotective estrogen action is primarily mediated via osteoclastic ERα inhibiting bone resorption.

To further test this hypothesis, we investigated ERα protein expression in mature osteoclasts from trabecular bone. Few reports document osteoclastic expression of ERα protein and an estrogen response in both intact animals and in in vitro cultured osteoclasts (Bland, 2000). We therefore reasoned that ER expression ceases during differentiation into mature cells from primary cultures of osteoclast precursors, similar to that observed in other primary culture cell systems such as avian oviduct cells, in which ERα protein expression is drastically decreased during culture (Kato et al., 1989). Using highly sensitive immunohistochemistry, we investigated whether

(F) The growth curve of $ER\alpha^{\Delta Oc/\Delta Oc}$ mice was indistinguishable from that of the control mice. Data are represented as mean ± SEM.
(G) Serum hormone levels were normal in 12-week-old $ER\alpha^{\Delta Oc/\Delta Oc}$ (filled column) versus $ER\alpha^{+/+}$ (open column) mice (n = 10–11 animals per genotype). Data are represented as mean ± SEM.

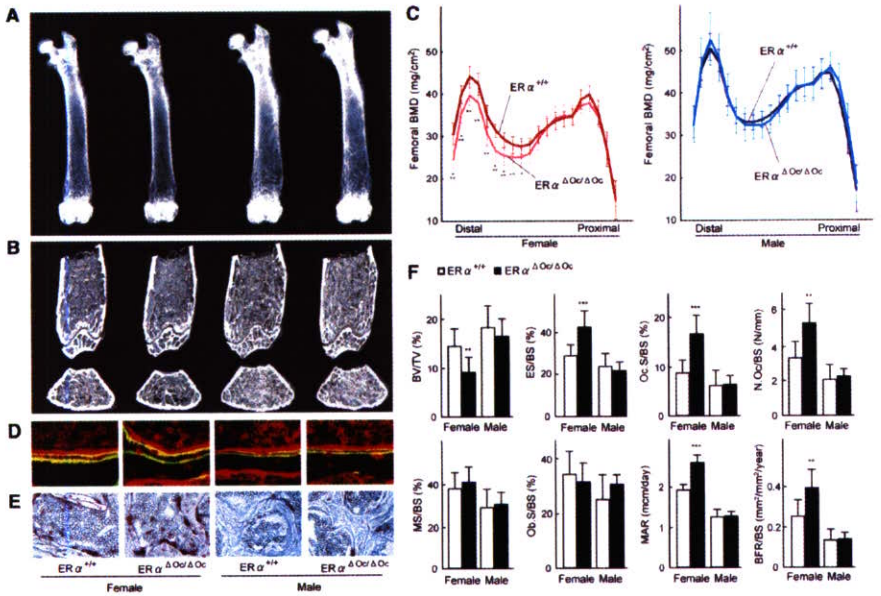

Figure 2. High Bone Turnover Osteopenia Was Observed in $ER\alpha^{\Delta Oc/\Delta Oc}$ Females But Not Males

(A) Soft X-ray images of femurs from 12-week-old $Ctsk^{Cre/+}$; $ER\alpha^{flox/flox}$ ($ER\alpha^{\Delta Oc/\Delta Oc}$) mice.

(B) Three-dimensional computed tomography images of the distal femurs and axial sections of distal metaphysis from representative 12-week-old $Ctsk^{Cre/+}$; $ER\alpha^{+/+}$ ($ER\alpha^{+/+}$) and $ER\alpha^{\Delta Oc/\Delta Oc}$ mice.

(C) BMD of each of 20 equal longitudinal divisions of femurs from 12-week-old $ER\alpha^{+/+}$ and $ER\alpha^{\Delta Oc/\Delta Oc}$ mice. (n = 10–11 animals per genotype; Student's t test, *p < 0.05; **p < 0.01; ***p < 0.001). Data are represented as mean ± SEM.

(D) Bone formation was also accelerated in $ER\alpha^{\Delta Oc/\Delta Oc}$ females when two calcein-labeled mineralized fronts visualized by fluorescent micrography were measured in the proximal tibia of 12-week-old mice.

(E) The number of TRAP-positive osteoclasts in the lumbar spine of female mice was increased by selective disruption of ERα in osteoclasts, indicating enhanced bone resorption.

(F) Bone turnover parameters as measured by dynamic bone histomorphometry after calcein labeling indicated high bone turnover in $ER\alpha^{\Delta Oc/\Delta Oc}$ females. Parameters are measured in the proximal tibia of 12-week-old $ER\alpha^{+/+}$ (open column) and $ER\alpha^{\Delta Oc/\Delta Oc}$ (filled column) mice. BV/TV: bone volume per tissue volume. ES/BS: eroded surface per bone surface. Oc.S/BS: osteoclast surface per bone surface. N.Oc/BS: osteoclast number per bone surface. MS/BS: mineralizing surface per bone surface. Ob.S/BS: osteoblast surface per bone surface. MAR: mineral apposition rate. BFR/BS: bone formation rate per bone surface (n = 10–11 animals per genotype; Student's t test, *p < 0.05; **p < 0.01; ***p < 0.001). Data are represented as mean ± SEM.

ERα protein expresses in differentiated osteoclasts in the bone tissues of femur sections from 12-week-old mice. ERα protein expression appeared abundant in osteoblasts and osteocytes of femur sections (Figure 4C) as well as hypothalamus (Figure S2B) from 12-week-old mice, in agreement with a previous report (Zaman et al., 2006). Likewise, expression levels of ERα in primary cultured osteoblasts derived from calvaria of $ER\alpha^{\Delta Oc/\Delta Oc}$ females appeared unaffected (Figure S2C). In contrast, in differentiated osteoclasts of the same femur sections, ERα expression was definitely detectable but very low in the $ER\alpha^{+/+}$ but undetectable in $ER\alpha^{\Delta Oc/\Delta Oc}$ females (Figure 4C).

Signaling by Osteoclastogenic Factors and Osteoclastogenesis Is Intact in Osteoclasts Deficient in ERα

It is possible that the osteoprotective function of osteoclastic ERα inhibits osteoclastogenesis. To address this issue, osteoclastogenesis was tested in cultured osteoclasts derived from bone-marrow cells of $ER\alpha^{\Delta Oc/\Delta Oc}$ mutants. In this cell culture system, a possible contribution of contaminated immune cells and stromal cells could be excluded, since osteoclastogenesis is only inducible by M-CSF treatment followed by M-CSF + RANKL (Koga et al., 2004).

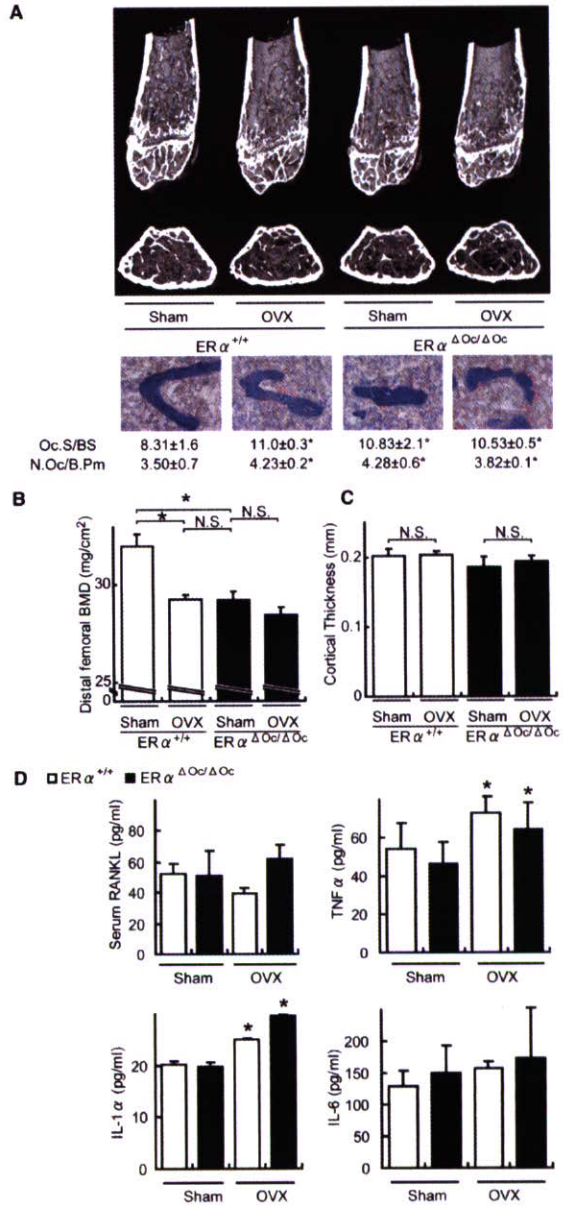

Figure 3. No Further Bone Loss of $ER\alpha^{\Delta Oc/\Delta Oc}$ Females by Ovariectomy

(A) Distal femoral micro CT analysis and lumbar vertebral bone histomorphometrical analysis of sham-operated or ovariectomized (OVX) 12-week-old $ER\alpha^{+/+}$ and $ER\alpha^{\Delta Oc/\Delta Oc}$ mice (*p < 0.05 compared to $ER\alpha^{+/+}$ sham group). Two weeks after OVX, the bone phenotype was analyzed.

(B) BMD of the distal femurs within each group are described in Figure 3A (*p < 0.05; N.S., not significant). Data are represented as mean ± SEM.

(C) Cortical thickness evaluation from micro CT analysis of femurs within each group described in Figure 3A. Data are represented as mean ± SEM.

(D) The levels of TNFα, IL-1α, and IL-6 in the bone-marrow cells culture media and serum RANKL (*p < 0.05 compared to each sham group). Data are represented as mean ± SEM.

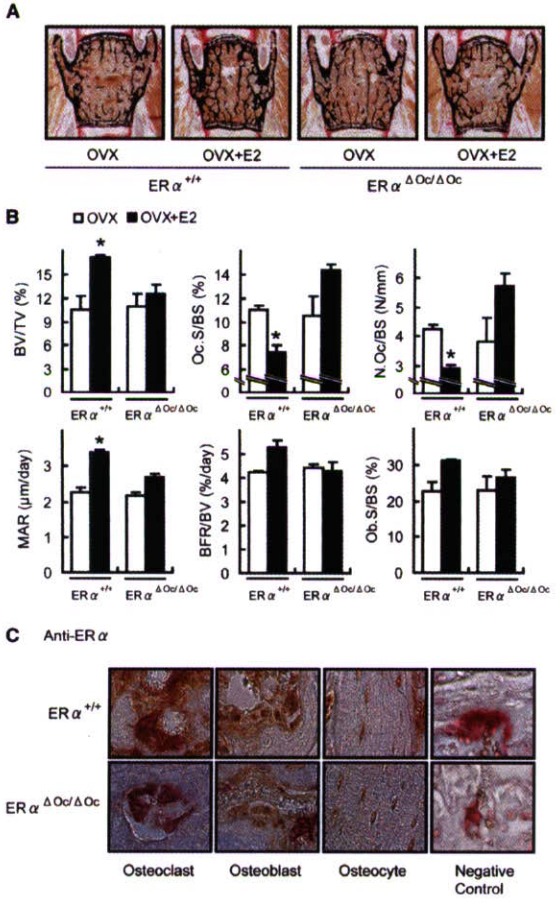

Figure 4. Estrogen treatment failed to reverse trabecular bone loss of ovariectomized $ER\alpha^{\Delta Oc/\Delta Oc}$ females

(A) von kossa staining of lumbar vertebral bodies of ovariectomized $ER\alpha^{+/+}$ and $ER\alpha^{\Delta Oc/\Delta Oc}$ mice treated with or without 17β-estradiol (0.83 μg/day) for 2 weeks (+E2) groups.

(B) Bone histomorphometrical analyses of the lumber vertebral bodies of 12-week-old ovariectomized $ER\alpha^{+/+}$ (left columns) and $ER\alpha^{\Delta Oc/\Delta Oc}$ (right columns) mice with (filled columns) or without (open columns) E2 treatment for 2 weeks (*$p < 0.05$ compared with E2-treated ovariectomized $ER\alpha^{\Delta Oc/\Delta Oc}$ mice). BV/TV: bone volume per tissue volume. ES/BS: eroded surface per bone surface. Oc.S/BS: osteoclast surface per bone surface. N.Oc/BS: osteoclast number per bone surface. MS/BS: mineralizing surface per bone surface. Ob.S/BS: osteoblast surface per bone surface. MAR: mineral apposition rate. BFR/BS: bone formation rate per bone surface. Data are represented as mean ± SEM.

(C) Immunochemical identification of ERα (brown) in TRAP-positive (red) differentiated osteoclasts. The femurs of 12 week-old mice were used for the immunodetection of ERα in bone cells. All labels were abolished when the primary antibody was preadsorbed with the immunizing peptide (negative control).

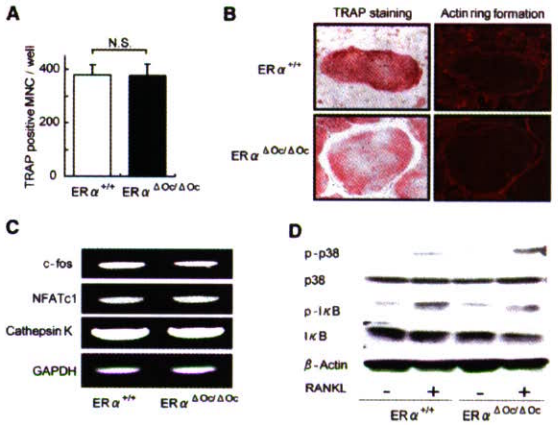

Figure 5. ERα Deficiency Did Not Affect Osteoclastogenesis

(A) TRAP-positive multinucleated cell count at 3 days after RANKL stimulation, cultured in 24-well plates (n = 6, N.S., not significant). Data are represented as mean ± SEM.

(B) TRAP staining and actin ring formation of RANKL induced primary cultured osteoclasts from bone-marrow cells of $ER\alpha^{+/+}$ and $ER\alpha^{\Delta Oc/\Delta Oc}$ mice.

(C) RT-PCR analysis of genes related to osteoclastogenesis.

(D) Western blot analysis of phosphorylated p38, JNK, and IκB of primary cultured bone-marrow cells stimulated with or without 100 ng/ml of RANKL for 15 min.

The number of TRAP-positive osteoclasts differentiated from the bone-marrow cells of $ER\alpha^{\Delta Oc/\Delta Oc}$ females was almost the same as that from $ER\alpha^{+/+}$ females (Figure 5A) and males (data not shown). The differentiated $ER\alpha^{\Delta Oc/\Delta Oc}$ osteoclasts had typical osteoclastic features, including the characteristic cell shape, TRAP-positive, multiple nuclei, and actin-ring formation, and were indistinguishable from the $ER\alpha^{+/+}$ osteoclasts (Figure 5B).

The expression levels of the prime osteoclastogenic transcription factors, *c-fos* and *NFATc1*, were unaltered by ERα deficiency in differentiated osteoclasts (Figure 5C). Furthermore, responses to RANKL in intracellular signaling, as represented by phosphorylation of p38 and IκB, were unaffected in $ER\alpha^{\Delta Oc/\Delta Oc}$ osteoclasts from females (Figure 5D) as well as males (data not shown). In light of these findings, it is unlikely that activated ERα in osteoclastic cells attenuates osteoclastogenesis.

Activation of the Fas/FasL System by Estrogen in Intact Bone Is Impaired by Osteoclastic ERα Deficiency

To examine osteoclastic ERα function in intact bone, DNA microarray analysis following real-time RT-PCR of RNA from the femurs of ovariectomized $ER\alpha^{\Delta Oc/\Delta Oc}$ females treated with or without estrogen, was performed. During the search for candidate ERα target genes in bone by DNA microarray analysis (Figure S3), we found that a number of apoptosis-related factors were regulated by estrogen in the intact bone of $ER\alpha^{+/+}$ females but dysregulated in $ER\alpha^{\Delta Oc/\Delta Oc}$ females. This observation is consistent with a previous report of estrogen-induced apoptosis of mature osteoclasts (Kameda et al., 1997). Real-time RT-PCR to validate the estrogen regulations of the candidate genes revealed that gene expression of *FasL*, an apoptotic factor, was responsive to E2 (Figure 6A). Estrogen treatment (+E2) indeed induced expression of FasL protein in bone of ovariectomized $ER\alpha^{+/+}$, but this induction was not obvious in ovariectomized $ER\alpha^{\Delta Oc/\Delta Oc}$ mice (Figures 6B and 6C). Reflecting FasL induction by estrogen, estrogen-induced apoptosis (as observed by the TUNEL assay) in TRAP-positive mature trabecular osteoclasts in the distal femurs of the $ER\alpha^{+/+}$ mice was detected, but this E2 response was abolished in the $ER\alpha^{\Delta Oc/\Delta Oc}$ mice (Figure 6D). Furthermore, in mice lacking functional FasL ($FasL^{gld/gld}$), neither enhanced bone resorption nor bone mass loss was induced by ovariectomy (Figures 6E and 6F).

Osteoclastic ERα Mediates Estrogen-Induced apoptosis by FasL

The expression level of ERα protein in differentiated osteoclasts derived from bone marrow cells was very low, but induction of *FasL* gene expression was also detectable in the cultured osteoclasts of $ER\alpha^{+/+}$ females as well as males (Figure 7A). However, this E2 response was impaired in cultured osteoclasts from $ER\alpha^{\Delta Oc/\Delta Oc}$ females (Figure 7A). It is notable that such responses are also induced by tamoxifen (Figure 7C), which is an osteoprotective SERM (Harada and Rodan, 2003). ERα overexpression augmented *FasL* gene expression in response to estrogen in cultured osteoclasts from $ER\alpha^{\Delta Oc/\Delta Oc}$ females (Figure S4A). In primary cultured calvarial osteoblasts from females as well as males (Suzawa et al., 2003), *FasL* gene induction by E2 and tamoxifen was also seen; however, it was not accompanied by increased apoptosis (data not shown). Thus, it appears that estrogen-induced apoptosis in osteoclasts is mediated by FasL expression in osteoclasts in the trabecular bone areas, presumably as well as in osteoblasts in cortical bone areas. As expected, the cell number of TUNEL-positive osteoclasts was increased by E2 in the cultured osteoclasts from $ER\alpha^{+/+}$ females, but E2-induced apoptosis was undetectable in $ER\alpha^{\Delta Oc/\Delta Oc}$ osteoclasts (Figure 7B). Consistent with FasL-induced apoptosis, *Fas* gene expression was observed (Figure 7D), but it was likely that Fas expression did not require ERα function (Figures S4B and S4C). Expression levels of *Fas* and *ERα* as well as E2 response in apoptosis appeared to fluctuate during osteoclast differentiation (Figures S4B–S4D); however, in FasL mutant ($FasL^{gld/gld}$) females, the E2-induced apoptosis was abolished (Figure S4E). These findings suggest that activated ERα in differentiated osteoclasts induces apoptosis through activating FasL/Fas signaling. This leads to suppression of bone resorption through truncating the already short life span of differentiated osteoclasts (Teitelbaum, 2006).

DISCUSSION

Selective ablation of ERα in mature osteoclasts in female mice shows that the osteoprotective effect of estrogen is mediated by osteoclastic ERα, at least in the trabecular regions of the tibiae, femur, and lumbar vertebrae of female mice. Activated ERα by estrogen as well as SERMs appears to truncate the already short life span (estimated at 2 weeks) of differentiated osteoclasts by inducing apoptosis through activation of the Fas/FasL system.

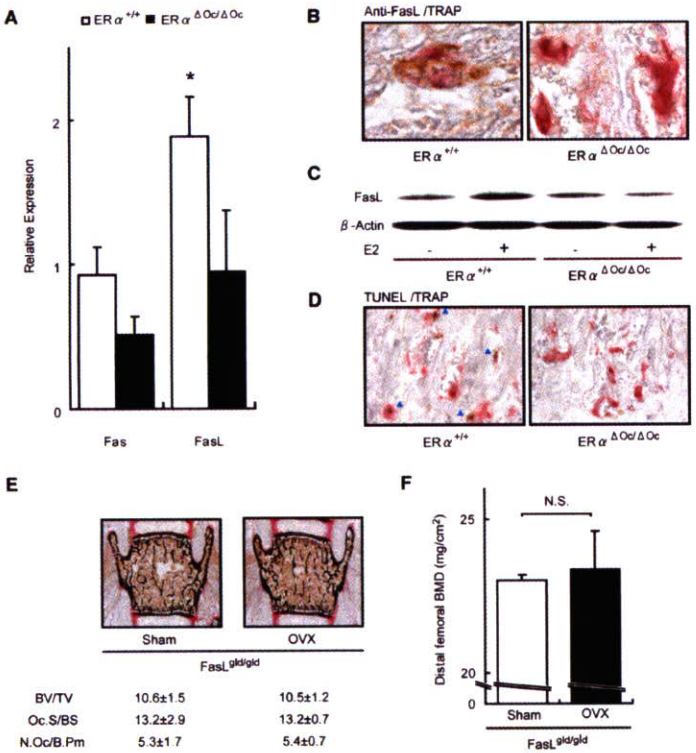

Figure 6. Activated ERα Induced Fas Ligand Expression and Apoptosis in Differentiated Osteoclasts of Intact Bone

(A) Real-time RT-PCR analysis of *Fas* and *FasL*. Expression levels in bones from E2-treated ovariectomized $ER\alpha^{+/+}$ (open column) and $ER\alpha^{\Delta Oc/\Delta Oc}$ (filled column) were compared with the ovariectomized groups of each genotype without E2 administration (*$p < 0.05$ compared to $ER\alpha^{+/+}$). Data are represented as mean ± SEM.

(B) Immunohistochemical analysis of anti-FasL with TRAP staining of the sections from the distal femurs of E2-treated ovariectomized $ER\alpha^{+/+}$ and $ER\alpha^{\Delta Oc/\Delta Oc}$ mice. Brawny stained cells are anti-FasL positive.

(C) Anti-FasL western blot analysis of proteins obtained from femurs of ovariectomized $ER\alpha^{+/+}$ and $ER\alpha^{\Delta Oc/\Delta Oc}$ mice treated with or without E2, using anti-β-actin as internal control.

(D) TUNEL staining with TRAP staining of the sections from the distal femurs of E2-treated ovariectomized $ER\alpha^{+/+}$ and $ER\alpha^{\Delta Oc/\Delta Oc}$ mice. Arrowheads indicate both TUNEL (brown)- and TRAP-positive staining cells.

(E) Bone histomorphometrical analysis of sham-operated or ovariectomized $FasL^{gld/gld}$ mice.

(F) BMD of the distal femurs of sham operated or ovariectomized $FasL^{gld/gld}$ mice. Data are represented as mean ± SEM.

This attenuates bone resorption. This idea is supported by previous observations that estrogen deficiency following menopause or ovariectomy leads to high bone turnover, particularly in the trabecular areas, as bone is rapidly lost through enhanced resorption (Delmas, 2002; Tolar et al., 2004). Thus, estrogen treatment leads to recovery from osteopenia by reducing resorption (Delmas, 2002; Rodan and Martin, 2000), partly by the induction of osteoclast cell death.

In contrast to the osteopenia seen in the $ER\alpha^{\Delta Oc/\Delta Oc}$ females, the $ER\alpha^{\Delta Oc/\Delta Oc}$ male mice unexpectedly had no bone loss. The male mice still demonstrated an ERα-mediated induction of FasL in response to estrogen with subsequent apoptosis of osteoclasts (Figure 7). Both male mice with a deficiency of aromatase that are unable to locally produce estrogen from testosterone and men with a genetic mutation in the *ERα* gene suffer from osteoporosis (Smith et al., 1994). Considering that the

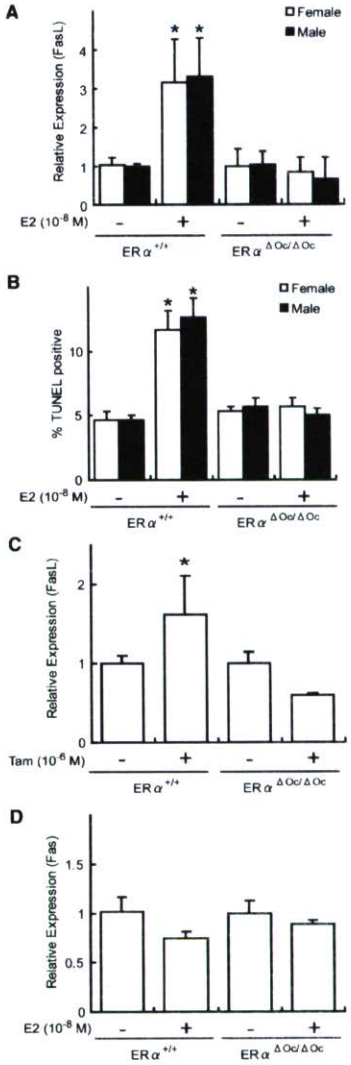

Figure 7. Estrogen-Induced *FasL* Expression and Apoptosis Required ERα in Cultured Osteoclasts

(A) Real-time RT-PCR analysis of *FasL* expression using total RNA obtained from in vitro primary cultured osteoclasts of each genotype at 3 days after RANKL stimulation, treated with or without E2 (10^{-8} M) for 4 hr (*$p < 0.05$ compared to the group treated without E2). Data are represented as mean ± SEM.

markedly elevated levels of testosterone in ERα KO females may be potent enough to maintain normal bone turnover (Syed and Khosla, 2005), it is likely that the activated AR might be functionally sufficient in male mice to compensate for the ERα deficiency in bone (Kawano et al., 2003). However, species differences in the osteoprotective action of sex steroid hormones still need to be carefully addressed.

Fas/FasL system-mediated apoptotic induction of osteoclasts by estrogen may well be a part of the mechanism for the antiresorptive action of estrogen and SERMs in trabecular bone areas (Delmas, 2002; Rodan and Martin, 2000; Simpson and Davis, 2001; Syed and Khosla, 2005; Tolar et al., 2004). Regulation of osteoclast differentiation is tightly coupled to osteoblastic function in terms of cytokine production and cell-cell contact (Karsenty and Wagner, 2002; Martin and Sims, 2005; Mundy and Elefteriou, 2006; Teitelbaum and Ross, 2003). Indeed, upregulation of osteoclastogenic cytokines by ovariectomy was unaffected in $ER\alpha^{\Delta Oc/\Delta Oc}$ females. Considering the observation that cortical bone mass is increased in ovariectomized $ER\alpha^{\Delta Oc/\Delta Oc}$ females during estrogen treatment, it is conceivable that the antiresorptive estrogen action in cortical bone is also mediated by osteoblastic ERα. In this regard, FasL induction by estrogen in osteoblasts may contribute to the osteoprotective estrogen action, and *FasL* gene induction by estrogen was in fact detected in primary cultured osteoblasts from female calvaria by us as well as another group (S. Krum and M. Brown, personal communication). Thus, similar experiments in which ERα is selectively ablated in osteoblasts are needed to define the role of ERα in these cells.

In osteoclastic cells, expression of the *FasL* gene, which leads to apoptosis, appears to be positive controlled by activated ERα. Not surprisingly, a direct binding site for ERα has been mapped in the *FasL* gene locus (S. Krum and M. Brown, personal communication). An osteoclast- and cell-differentiation stage-specific mechanism may underlie this gene induction in the *FasL* gene promoter. A recent study demonstrated that ERα recruitment to specific promoter sites of given ERα target genes was cell-type specific (Carroll et al., 2005). Thus, there is significant impetus to identify the osteoclastic factor that associates with ERα in the *FasL* gene promoter. Such identification will lead to a better understanding of the molecular basis of the osteoprotective estrogen action and provide a target against which to develop SERMs of greater effectiveness.

(B) Apoptotic cells were defined as those with TUNEL-positive nuclei among TRAP-positive multinucleated primary cultured osteoclasts treated with or without E2 (10^{-8} M) for 12 hr in 96-well plates (*$p < 0.05$ compared to the group treated without E2). Data are represented as mean ± SEM.

(C) *FasL* expression in each genotypic female osteoclastic cells treated with or without Tam (10^{-6} M) (*$p < 0.05$ compared to the group treated without Tam). Data are represented as mean ± SEM.

(D) Expression of *Fas* was measured as described in the legend of Figure 7A. Data are represented as mean ± SEM.

EXPERIMENTAL PROCEDURES

Ctsk-Cre Construction and Generation of the Knockin Mouse Lines

An RP23-422n18 BAC clone containing the mouse *Ctsk* gene was purchased from Invitrogen (Carlsbad, CA). The *FRT-Kan^r/Neo^r-FRT* and *nlsCre* fragments were obtained from plasmids pSK2/3-*FRT-Neo* and pIC-*Cre*. Two homologous arms of 500 bp from the *Ctsk* gene were inserted into both sides of the *nlsCre-FRT-Kan^r/Neo^r-FRT* cassette in the pSK2/3-*FRT-Neo* plasmid. The *nlsCre-FRT-Kan^r/Neo^r-FRT* cassette was introduced into the endogenous ATG start site of the *Ctsk* gene by recombineering approaches (Copeland et al., 2001). Targeted BAC was reduced in size from 189 kb to 26 kb and subcloned into the pMC1-DTpA vector by the gap-repair method. The targeted TT2 ES clones were selected after positive-negative selection with G418 and DT-A with Southern analysis, then aggregated with single eight-cell embryos from CD-1 mice (Yoshizawa et al., 1997). Chimeric mice were then crossed with a general deleter mouse line, *ACTB-Flpe* (Jackson Laboratory), to remove the *Kan^r/Neo^r* cassette. The *Ctsk-Cre* mice (*Ctsk$^{Cre/+}$*), originally on a hybrid C57BL/6 and CBA genetic background, were backcrossed for four generations into a C57BL/6J background. *FasL$^{gld/gld}$* mice were also purchased from Jackson Laboratory.

Analysis of Cre Recombinase Activities

Expression of the Cre transcript was detected by RT-PCR. Southern analysis using a *Cre* cDNA probe was performed with total RNA extracted from 12-week-old mice. To evaluate the specificity and efficiency of Cre-mediated recombination, we mated the *Ctsk$^{Cre/+}$* mice to *CAG-CAT-Z* reporter mice (kindly provided by J. Miyazaki) (Sakai and Miyazaki, 1997) and genotyped their offspring with *Cre*-specific primers. β-galactosidase activity of the expressed *LacZ* gene driven by the *CAG* promoter was expected to be detected in the given cells expressing functional Cre recombinase.

In Vitro Osteoclastogenesis and Ligand Application

Bone-marrow cells derived from 8-week-old mice were plated in culture dishes containing α-MEM (GIBCO-BRL) with 10% FBS (JRH) and 10 ng/ml M-CSF (Genzyme). After incubation for 48 hr, adherent cells were used as osteoclast precursor cells after washing out the nonadherent cells. Cells were cultured in the presence of 10 ng/ml M-CSF and 100 ng/ml RANKL (Peprotech) to generate osteoclast-like cells (Koga et al., 2004) for 3 days, so the total culture time was 5 days. Three days after RANKL stimulation, primary cultured osteoclasts were treated with 10^{-8} M of 17β-estradiol (E2) (Sigma-Aldrich Co.) or 10^{-6} M 4-hydroxytamoxifen (Tam) (Sigma-Aldrich Co.) in phenol-red free medium.

Generation of Osteoclast-Specific ERα KO Mice

The ERα conditional (*ERα$^{flox/flox}$*) (Dupont et al., 2000) and null alleles with a C57BL/6J background have been previously described. *ERα$^{flox/flox}$* mice were crossed with *Ctsk$^{Cre/+}$* mice to generate *Ctsk$^{Cre/+}$; ERα$^{flox/+}$* mice. *Ctsk$^{Cre/+}$; ERα$^{+/+}$* (*ERα$^{+/+}$*) and *Ctsk$^{Cre/+}$; ERα$^{flox/flox}$* (*ERα$^{\Delta Oc/\Delta Oc}$*) mice were obtained by crossing *Ctsk$^{Cre/+}$; ERα$^{flox/+}$* with *ERα$^{flox/+}$* mouse lines.

Radiological Analysis

Bone radiographs of the femurs of 12-week-old *Ctsk$^{Cre/+}$; ERα$^{flox/flox}$* (*ERα$^{\Delta Oc/\Delta Oc}$*) and *Ctsk$^{Cre/+}$; ERα$^{+/+}$* (*ERα$^{+/+}$*) littermates were visualized with a soft X-ray apparatus (TRS-1005: SOFTRON). BMD was measured by DXA using a bone mineral analyzer (DCS-600EX: ALOKA). Micro Computed Tomography scanning of the femurs was performed using a composite X-ray analyzer (NX-CP-C80H-IL: Nittetsu ELEX Co.) (Kawano et al., 2003). Tomograms were obtained with a slice thickness of 10 μm and reconstructed at 12 × 12 pixels into a 3D image by the volume-rending method (VIP-Station; Teijin System Technology) using a computer.

Analysis of Skeletal Morphology

Twelve-week-old *Ctsk$^{Cre/+}$; ERα$^{flox/flox}$* (*ERα$^{\Delta Oc/\Delta Oc}$*) and *Ctsk$^{Cre/+}$; ERα$^{+/+}$* (*ERα$^{+/+}$*) littermates were double labeled with subcutaneous injections of 16 mg/kg of calcein (Sigma) at 4 and 2 days before sacrifice. Tibiae were removed from each mouse and fixed with 70% ethanol. They were stained with Villanueva bone stain for 7 days and embedded in methyl-methacrylate (Wako) (Yoshizawa et al., 1997). Frontal plane sections (5-μm thick) of the proximal tibia were cut using a Microtome (LEICA). The cancellous bone was measured in the secondary spongiosa located 500 μm from the epiphyseal growth plate and 160 μm from the endocortical surface (Kawano et al., 2003; Nakamichi et al., 2003). Bone histomorphometric measurements of the tibia were made using a semiautomatic image analyzing system (System Supply) and a fluorescent microscope (Optiphot; Nikon). Similar measurements of the lumbar vertebral bodies were done as previously reported (Takeda et al., 2002). Standard bone histomorphometrical nomenclatures, symbols, and units were used as described in the report of the ASBMR Histomophometry Nomenclature Committee.

Ovariectomy and Hormone Replacement

Female *Ctsk$^{Cre/+}$; ERα$^{flox/flox}$* (*ERα$^{\Delta Oc/\Delta Oc}$*) and *Ctsk$^{Cre/+}$; ERα$^{+/+}$* (*ERα$^{+/+}$*) littermates were ovariectomized or sham operated at 8–12 weeks of age for 2 weeks for all experiments, and slow releasing pellets of E2 (0.83 μg/day) or placebo (Innovative Research, Sarasota, FL) were implanted subcutaneously in the scapular region behind the neck (Sato et al., 2004; Shiina et al., 2006).

Immunohistochemistry

Twelve-week-old *Ctsk$^{Cre/+}$; ERα$^{flox/flox}$* (*ERα$^{\Delta Oc/\Delta Oc}$*) and *Ctsk$^{Cre/+}$; ERα$^{+/+}$* (*ERα$^{+/+}$*) littermates were fixed with 4% PFA by perfusion. Serial sections of the brain (20 μm thick) were divided into two groups and used for single labeling for the ERα or thionin to allow determination of the areas to be measured. Tibiae and femurs were decalcified in 10% EDTA for 2–4 weeks after fixation and then embedded in paraffin sections. Sections were incubated in L.A.B. solution (Polysciences) for 30 min to retrieve antigen. The cooled sections were incubated in 1% H_2O_2 for 30 min to quench endogenous peroxidase and then washed with 1% Triton X-100 in PBS for 10 min. To block nonspecific antibody binding, sections were incubated in blocking solution (DAKO) for 5 min. Sections were then incubated with anti-ERα (Santa Cruz, CA) and anti-FasL (Santa Cruz, CA) in blocking solution overnight at 4°C. Staining was then performed using the EnVision+ HRP System (Dako) and 3, 3′-diaminobendizine tetrahydrochloride substrate (Sigma), counterstained with TRAP, dehydrated through an ethanol series and xylene, before mounting (Sato et al., 2004).

ERα Overexpression

Two days after RANKL stimulation, an expression vector of mouse ERα was tranfected into immature osteoclastic cells from *ERα$^{\Delta Oc/\Delta Oc}$* mice using Superfect (QIAGEN) as manufacture's instruction.

Real-Time RT-PCR

One microgram of total RNA from each sample was reverse transcribed into first-strand cDNA with random hexamers using Superscript III reverse transcriptase (Invitrogen). Primer sets for all genes were purchased from Takara Bio. Inc. (Tokyo, Japan). Real-time RT-PCR was performed using SYBR Premix Ex Taq (Takara) with the ABI PRISM 7900HT (Applied Biosystems) according to the manufacturer's instructions. Experimental samples were matched to a standard curve generated by amplifying serially diluted products using the same PCR protocol. To correct for variability in RNA recovery and efficiency of reverse transcription, *Gapdh* cDNA was amplified and quantified in each cDNA preparation. Normalization and calculation steps were performed as reported previously (Takezawa et al., 2007).

TUNEL/TRAP Staining

The TUNEL method was performed using the ApopTag Fluorescein In Situ Apoptosis Detection Kit (CHEMICON international) according to the manufacturer's instructions with a slight modification. This was followed by TRAP staining as previously reported (Kobayashi et al., 2000).

Cytokine Assays

Bone marrow and blood were collected at 2 weeks after sham operation or ovariectomy. Bone-marrow cells were cultured for 3 days in DMEM. The levels of TNFα, IL-1α, and IL-6 in the culture media and serum RANKL were determined by ELISA (R&D Systems).

Western Blot

Osteoclast precursor cells were treated with or without 100 ng/ml of soluble RANKL. After 15 minutes, cell extracts were harvested from the cells using lysis buffer containing 100 mM Tris-HCl (pH 7.8), 150 mM NaCl, 0.1% Triton X-100, 5% protease inhibitor cocktail (Sigma), and 5% phosphatase inhibitor cocktail (Sigma). An equivalent amount of protein from each of the cell extracts and proteins of femoral bone extracted using ISOGEN was loaded for SDS-PAGE and transferred to PVDF membranes (Amersham Biosciences). The membranes were developed with enhanced chemiluminescence reagent (Amersham Biosciences) (Ohtake et al., 2003). Phosphorylation of p38 MAPK and IκB were evaluated using antibodies purchased from Cell Signaling Technology (Koga et al., 2004) and anti-FasL antibody was purchased from Santa Cruz Biotechnology (sc-834).

Actin-Ring Formation

Cells were fixed for 15 min in warm 4% paraformaldehyde (PFA). After fixation, cells were washed three times with PBS with 0.1% Triton X-100 (PBST) and incubated with 0.2 U/ml rhodamine phalloidin (Molecular Probes) for 30 min and washed again three times in PBST.

Statistical Analysis

Data were analyzed by two-tailed student's t test. For all graphs, data are represented as mean ± SEM.

Supplemental Data

Supplemental Data include Supplemental Experimental Procedures and four figures and can be found with this article online at http://www.cell.com/cgi/content/full/130/5/811/DC1/.

ACKNOWLEDGMENTS

We thank Drs. S. Krum and M. Brown to share with their unpublished results; Drs. K. Yoshimura, Y. Nakamichi, T. Watanabe, J. Miyamoto, H. Shiina, T. Fukuda, Ms. Y. Sato, and S. Tanaka for generation of the KO mice; Drs. T. Koga, H. Takagi, E. Ochiai, and N. Moriyama for technical help; Dr. J. Miyazaki for *CAG-CAT-Z* reporter mice, and H. Higuchi and K. Hiraga for manuscript preparation. This work was supported in part by priority areas from the Ministry of Education, Culture, Sports, Science and Technology (to S.K.) and the Program for Promotion of Basic Research Activities for Innovative Biosciences (PROBRAIN).

Received: February 23, 2007
Revised: May 21, 2007
Accepted: July 17, 2007
Published: September 6, 2007

REFERENCES

Belandia, B., and Parker, M.G. (2003). Nuclear receptors: a rendezvous for chromatin remodeling factors. Cell *114*, 277–280.

Bland, R. (2000). Steroid hormone receptor expression and action in bone. Clin. Sci. (Lond.) *98*, 217–240.

Carroll, J.S., Liu, X.S., Brodsky, A.S., Li, W., Meyer, C.A., Szary, A.J., Eeckhoute, J., Shao, W., Hestermann, E.V., Geistlinger, T.R., et al. (2005). Chromosome-wide mapping of estrogen receptor binding reveals long-range regulation requiring the forkhead protein FoxA1. Cell *122*, 33–43.

Chien, K.R., and Karsenty, G. (2005). Longevity and lineages: toward the integrative biology of degenerative diseases in heart, muscle, and bone. Cell *120*, 533–544.

Copeland, N.G., Jenkins, N.A., and Court, D.L. (2001). Recombineering: a powerful new tool for mouse functional genomics. Nat. Rev. Genet. *2*, 769–779.

Couse, J.F., and Korach, K.S. (1999). Estrogen receptor null mice: what have we learned and where will they lead us? Endocr. Rev. *20*, 358–417.

Delmas, P.D. (2002). Treatment of postmenopausal osteoporosis. Lancet *359*, 2018–2026.

Dupont, S., Krust, A., Gansmuller, A., Dierich, A., Chambon, P., and Mark, M. (2000). Effect of single and compound knockouts of estrogen receptors alpha (ERalpha) and beta (ERbeta) on mouse reproductive phenotypes. Development *127*, 4277–4291.

Gowen, M., Lazner, F., Dodds, R., Kapadia, R., Feild, J., Tavaria, M., Bertoncello, I., Drake, F., Zavarselk, S., Tellis, I., et al. (1999). Cathepsin K knockout mice develop osteopetrosis due to a deficit in matrix degradation but not demineralization. J. Bone Miner. Res. *14*, 1654–1663.

Harada, S., and Rodan, G.A. (2003). Control of osteoblast function and regulation of bone mass. Nature *423*, 349–355.

Kameda, T., Mano, H., Yuasa, T., Mori, Y., Miyazawa, K., Shiokawa, M., Nakamaru, Y., Hiroi, E., Hiura, K., Kameda, A., et al. (1997). Estrogen inhibits bone resorption by directly inducing apoptosis of the bone-resorbing osteoclasts. J. Exp. Med. *186*, 489–495.

Karsenty, G. (2006). Convergence between bone and energy homeostases: leptin regulation of bone mass. Cell Metab. *4*, 341–348.

Karsenty, G., and Wagner, E.F. (2002). Reaching a genetic and molecular understanding of skeletal development. Dev. Cell *2*, 389–406.

Kato, S., Ito, S., Noguchi, T., and Naito, H. (1989). Effects of brefeldin A on the synthesis and secretion of egg white proteins in primary cultured oviduct cells of laying Japanese quail (Coturnix coturnix japonica). Biochim. Biophys. Acta *991*, 36–43.

Kawano, H., Sato, T., Yamada, T., Matsumoto, T., Sekine, K., Watanabe, T., Nakamura, T., Fukuda, T., Yoshimura, K., Yoshizawa, T., et al. (2003). Suppressive function of androgen receptor in bone resorption. Proc. Natl. Acad. Sci. USA *100*, 9416–9421.

Kimble, R.B., Matayoshi, A.B., Vannice, J.L., Kung, V.T., Williams, C., and Pacifici, R. (1995). Simultaneous block of interleukin-1 and tumor necrosis factor is required to completely prevent bone loss in the early postovariectomy period. Endocrinology *136*, 3054–3061.

Kobayashi, Y., Hashimoto, F., Miyamoto, H., Kanaoka, K., Miyazaki-Kawashita, Y., Nakashima, T., Shibata, M., Kobayashi, K., Kato, Y., and Sakai, H. (2000). Force-induced osteoclast apoptosis in vivo is accompanied by elevation in transforming growth factor beta and osteoprotegerin expression. J. Bone Miner. Res. *15*, 1924–1934.

Koga, T., Inui, M., Inoue, K., Kim, S., Suematsu, A., Kobayashi, E., Iwata, T., Ohnishi, H., Matozaki, T., Kodama, T., et al. (2004). Costimulatory signals mediated by the ITAM motif cooperate with RANKL for bone homeostasis. Nature *428*, 758–763.

Li, C.Y., Jepsen, K.J., Majeska, R.J., Zhang, J., Ni, R., Gelb, B.D., and Schaffler, M.B. (2006). Mice lacking Cathepsin K maintain bone remodeling but develop bone fragility despite high bone mass. J. Bone Miner. Res. *21*, 865–875.

Mangelsdorf, D.J., Thummel, C., Beato, M., Herrlich, P., Schutz, G., Umesono, K., Blumberg, B., Kastner, P., Mark, M., Chambon, P., and Evans, R.M. (1995). The nuclear receptor superfamily: the second decade. Cell *83*, 835–839.

Martin, T.J., and Sims, N.A. (2005). Osteoclast-derived activity in the coupling of bone formation to resorption. Trends Mol. Med. *11*, 76–81.

Mueller, S.O., and Korach, K.S. (2001). Estrogen receptors and endocrine diseases: lessons from estrogen receptor knockout mice. Curr. Opin. Pharmacol. *1*, 613–619.

Mundy, G.R., and Elefteriou, F. (2006). Boning up on ephrin signaling. Cell *126*, 441–443.

Nakamichi, Y., Shukunami, C., Yamada, T., Aihara, K., Kawano, H., Sato, T., Nishizaki, Y., Yamamoto, Y., Shindo, M., Yoshimura, K., et al. (2003). Chondromodulin I is a bone remodeling factor. Mol. Cell. Biol. *23*, 636–644.

Ohtake, F., Takeyama, K., Matsumoto, T., Kitagawa, H., Yamamoto, Y., Nohara, K., Tohyama, C., Krust, A., Mimura, J., Chambon, P., et al. (2003). Modulation of oestrogen receptor signalling by association with the activated dioxin receptor. Nature *423*, 545–550.

Raisz, L.G. (2005). Pathogenesis of osteoporosis: concepts, conflicts, and prospects. J. Clin. Invest. *115*, 3318–3325.

Riggs, B.L., and Hartmann, L.C. (2003). Selective estrogen-receptor modulators–mechanisms of action and application to clinical practice. N. Engl. J. Med. *348*, 618–629.

Rodan, G.A., and Martin, T.J. (2000). Therapeutic approaches to bone diseases. Science *289*, 1508–1514.

Saftig, P., Hunziker, E., Wehmeyer, O., Jones, S., Boyde, A., Rommerskirch, W., Moritz, J.D., Schu, P., and von Figura, K. (1998). Impaired osteoclastic bone resorption leads to osteopetrosis in Cathepsin-K-deficient mice. Proc. Natl. Acad. Sci. USA *95*, 13453–13458.

Sakai, K., and Miyazaki, J. (1997). A transgenic mouse line that retains Cre recombinase activity in mature oocytes irrespective of the cre transgene transmission. Biochem. Biophys. Res. Commun. *237*, 318–324.

Sato, T., Matsumoto, T., Kawano, H., Watanabe, T., Uematsu, Y., Sekine, K., Fukuda, T., Aihara, K., Krust, A., Yamada, T., et al. (2004). Brain masculinization requires androgen receptor function. Proc. Natl. Acad. Sci. USA *101*, 1673–1678.

Shang, Y., and Brown, M. (2002). Molecular determinants for the tissue specificity of SERMs. Science *295*, 2465–2468.

Shiina, H., Matsumoto, T., Sato, T., Igarashi, K., Miyamoto, J., Takemasa, S., Sakari, M., Takada, I., Nakamura, T., Metzger, D., et al. (2006). Premature ovarian failure in androgen receptor-deficient mice. Proc. Natl. Acad. Sci. USA *103*, 224–229.

Simpson, E.R., and Davis, S.R. (2001). Minireview: aromatase and the regulation of estrogen biosynthesis–some new perspectives. Endocrinology *142*, 4589–4594.

Sims, N.A., Clement-Lacroix, P., Minet, D., Fraslon-Vanhulle, C., Gaillard-Kelly, M., Resche-Rigon, M., and Baron, R. (2003). A functional androgen receptor is not sufficient to allow estradiol to protect bone after gonadectomy in estradiol receptor-deficient mice. J. Clin. Invest. *111*, 1319–1327.

Smith, E.P., Boyd, J., Frank, G.R., Takahashi, H., Cohen, R.M., Specker, B., Williams, T.C., Lubahn, D.B., and Korach, K.S. (1994). Estrogen resistance caused by a mutation in the estrogen-receptor gene in a man. N. Engl. J. Med. *331*, 1056–1061.

Sun, L., Peng, Y., Sharrow, A.C., Iqbal, J., Zhang, Z., Papachristou, D.J., Zaidi, S., Zhu, L.L., Yaroslavskiy, B.B., Zhou, H., et al. (2006). FSH directly regulates bone mass. Cell *125*, 247–260.

Suzawa, M., Takada, I., Yanagisawa, J., Ohtake, F., Ogawa, S., Yamauchi, T., Kadowaki, T., Takeuchi, Y., Shibuya, H., Gotoh, Y., et al. (2003). Cytokines suppress adipogenesis and PPAR-gamma function through the TAK1/TAB1/NIK cascade. Nat. Cell Biol. *5*, 224–230.

Syed, F., and Khosla, S. (2005). Mechanisms of sex steroid effects on bone. Biochem. Biophys. Res. Commun. *328*, 688–696.

Takeda, S., Elefteriou, F., Levasseur, R., Liu, X., Zhao, L., Parker, K.L., Armstrong, D., Ducy, P., and Karsenty, G. (2002). Leptin regulates bone formation via the sympathetic nervous system. Cell *111*, 305–317.

Takezawa, S., Yokoyama, A., Okada, M., Fujiki, R., Iriyama, A., Yanagi, Y., Ito, H., Takada, I., Kishimoto, M., Miyajima, A., et al. (2007). A cell cycle-dependent co-repressor mediates photoreceptor cell-specific nuclear receptor function. EMBO J. *26*, 764–774.

Teitelbaum, S.L. (2006). Osteoclasts; culprits in inflammatory osteolysis. Arthritis Res. Ther. *8*, 201.

Teitelbaum, S.L. (2007). Osteoclasts: what do they do and how do they do it? Am. J. Pathol. *170*, 427–435.

Teitelbaum, S.L., and Ross, F.P. (2003). Genetic regulation of osteoclast development and function. Nat. Rev. Genet. *4*, 638–649.

Tolar, J., Teitelbaum, S.L., and Orchard, P.J. (2004). Osteopetrosis. N. Engl. J. Med. *351*, 2839–2849.

Windahl, S.H., Andersson, G., and Gustafsson, J.A. (2002). Elucidation of estrogen receptor function in bone with the use of mouse models. Trends Endocrinol. Metab. *13*, 195–200.

Yoshizawa, T., Handa, Y., Uematsu, Y., Takeda, S., Sekine, K., Yoshihara, Y., Kawakami, T., Arioka, K., Sato, H., Uchiyama, Y., et al. (1997). Mice lacking the vitamin D receptor exhibit impaired bone formation, uterine hypoplasia and growth retardation after weaning. Nat. Genet. *16*, 391–396.

Zaman, G., Jessop, H.L., Muzylak, M., De Souza, R.L., Pitsillides, A.A., Price, J.S., and Lanyon, L.L. (2006). Osteocytes use estrogen receptor alpha to respond to strain but their ERalpha content is regulated by estrogen. J. Bone Miner. Res. *21*, 1297–1306.

Accession Numbers

Microarray can be seen in Gene Expression Omnibus under accession number GSE7798.

nature cell biology

DEAD-box RNA helicase subunits of the Drosha complex are required for processing of rRNA and a subset of microRNAs

Toru Fukuda[1,6], Kaoru Yamagata[1,2,6], Sally Fujiyama[1,2,6], Takahiro Matsumoto[1,2], Iori Koshida[1], Kimihiro Yoshimura[1], Masatomo Mihara[1], Masanori Naitou[3], Hideki Endoh[3], Takashi Nakamura[1,2], Chihiro Akimoto[1], Yoko Yamamoto[1], Takenobu Katagiri[4], Charles Foulds[5], Shinichiro Takezawa[1], Hirochika Kitagawa[1], Ken-ichi Takeyama[1], Bert W. O'Malley[5] and Shigeaki Kato[1,2,7]

MicroRNAs (miRNAs) control cell proliferation, differentiation and fate through modulation of gene expression by partially base-pairing with target mRNA sequences[1–6]. Drosha is an RNase III enzyme that is the catalytic subunit of a large complex that cleaves pri-miRNAs with distinct structures into pre-miRNAs[7]. Here, we show that both the p68 and p72 DEAD-box RNA helicase subunits[8–10] in the mouse Drosha complex are indispensable for survival in mice, and both are required for primary miRNA and rRNA processing. Gene disruption of either *p68* or *p72* in mice resulted in early lethality, and in both *p68*$^{-/-}$ and *p72*$^{-/-}$ embryos, expression levels of a set of, but not all, miRNAs and 5.8S rRNA were significantly lowered. In *p72*$^{-/-}$ MEF cells, expression of p72, but not a mutant lacking ATPase activity, restored the impaired expression of miRNAs and 5.8S rRNA. Furthermore, we purified the large complex of mouse Drosha and showed it could generate pre-miRNA and 5.8S rRNA *in vitro*. Thus, we suggest that DEAD-box RNA helicase subunits are required for recognition of a subset of primary miRNAs in mDrosha-mediated processing.

DEAD-box RNA helicases unwind RNA and alter RNA structures through ATP binding and hydrolysis[8–10]. Two members of the family, p68 and p72, have been implicated in many biological events[11–17]. p68 and p72 function may facilitate processing of RNA, particularly miRNA, as generation of miRNAs from primary miRNAs (pri-miRNA) with diverse structures seems to require many RNA-associated factors for RNase III-mediated processing. miRNAs control cell proliferation, differentiation and fate through modulation of gene expression by partially base-pairing with target mRNA sequences[1–6,18]. Mammalian miRNA genes are initially transcribed as mono- or polycistronic precursor pri-miRNAs. Pri-mRNAs are processed into 60–70 nucleotide hairpins with 3′-overhangs by nuclear RNase III endonuclease Drosha to form pre-miRNAs[1,4,7]. Pre-miRNAs translocate into the cytosol and are then processed by Dicer, another RNase III-related enzyme, to form mature 17–24 nucleotide miRNAs[1–7]. Recently, the functional unit of human Drosha (hDrosha) was biochemically identified[7], and it was revealed that hDrosha forms two types of complexes. The smaller di-subunit complex (Drosha plus DGCR8), Microprocessor, mediates genesis of 5.8S rRNA and pre-miRNA from pri-miRNA[7]. The other larger hDrosha complex comprises multiple classes of RNA associated proteins including DEAH-box RNA helicases, heterogeneous nuclear ribonucleoproteins (hnRNP) and several proteins with RNA binding or RRM motifs. p68–p72 ATP-dependent DEAD-box RNA helicases are also components of the larger hDrosha complex[7]. The precise role of the large complex components, particularly the RNA-associated proteins, in processing of pri-miRNA and rRNA remains to be investigated.

The genes for the *p68* and *p72* DEAD-box RNA helicases were disrupted in mice using a conventional method (see Supplementary Information, Fig. S1). The human homologues (DDX5 for p68, refs 8, 9; and DDX17 for p72, ref. 10) are the subunits for the large hDrosha complex[7]. Although no clear phenotypic abnormalities were detected in *p68*$^{+/-}$ and *p72*$^{+/-}$ mice (data not shown), embryonic lethality was observed in *p68*$^{-/-}$ embryos at ~E11.5, and neonatal death occured in *p72*$^{-/-}$ pups (Fig. 1a) at postnatal day 2 (P2) with smaller body size (see Supplementary Information, Fig. S1f). Double disruption of *p68* and *p72* seemed to lead to earlier lethality than *p68* inactivation alone in embryos (Fig. 1a). Ubiquitous expression of p68 and p72 was observed in developing embryos (Fig. 1b). Irrespective of early lethality of the

[1]Institute of Molecular and Cellular Biosciences, University of Tokyo, Yayoi 1-1-1, Bunkyo-ku, Tokyo 113-0032, Japan. [2]ERATO, Japan Science and Technology, Honcho 4-1-8, Kawaguchi, Saitama 332-0012, Japan. [3]Applied Genomics, Molecular Medicine Labs., Drug Discovery Research, Astellas Pharma Inc., 21,Miyukigaoka, Tsukuba-shi, Ibaraki 305-8585, Japan. [4]Research Center for Genomic Medicine, Saitama Medical School, Yamane 1397-1, Hidakashi, Saitama, 350-1242, Japan. [5]Department of Molecular and Cellular Biology, Baylor College of Medicine, One Baylor Plaza, Houston, TX 77030, USA.
[6]These authors contributed equally to this work.
[7]Correspondence should be addressed to S.K. (e-mail: uskato@mail.ecc.u-tokyo.ac.jp)

Received 26 February 2007; accepted 27 March 2007; published online 15 April 2007; DOI: 10.1038/ncb1577

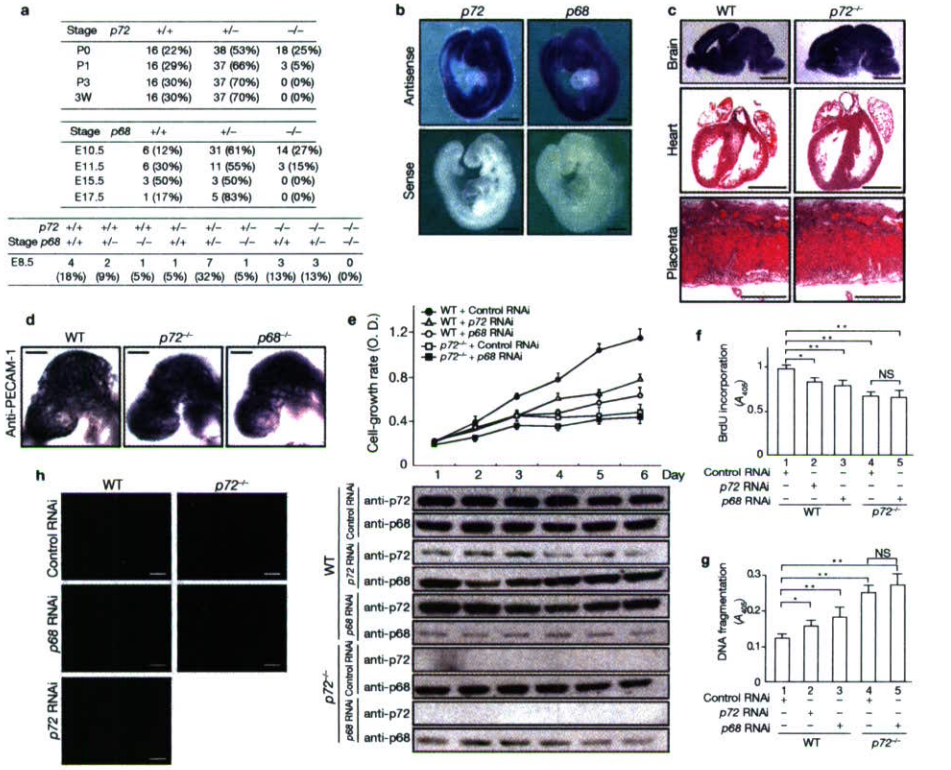

Figure 1 Embryonic and neonatal lethality of *p68* and *p72* knockout mice. (**a**) Genotype of F2 offspring from heterozygous and double (*p68* and *p72*) heterozygous matings. (**b**) Whole-mount *in situ* hybridization of *p72* and *p68* mRNA in wild-type (WT) embryos (E9.5). (**c**) Histological analysis of wild-type and *p72*$^{-/-}$ embryos (E18.5). Sections were stained with thionine (brain), and hematoxylin and eosin (heart and placenta). (**d**) Immunostaining with anti-PECAM-1 antibody. Wild-type, *p72*$^{-/-}$ and *p68*$^{-/-}$ mouse embryos were stage-matched to controls by somite count. (**e**) Analysis of cell-growth rate by modified MTT assay. Results are expressed as the mean ± s.d. of six independent experiments. Protein levels of p72 and p68 for 6 days were confirmed by western blotting. Uncropped images of the blots are shown in the Supplementary Information, Fig. S5a. (**f**) BrdU incorporation of wild-type and *p72*$^{-/-}$ MEFs with depletion of *p72* and *p68*. Results are expressed as the mean ± s.d. of six independent experiments. Significant differences when compared with the data for wild-type or *p72*$^{-/-}$ MEFs with control RNAi are shown (single asterisk indicate $P < 0.05$; double asterisks indicate $P < 0.01$ with one-way ANOVA). NS, not significant. (**g**) Apoptosis was measured by quantification of DNA fragmentation. Results are expressed as the mean ± s.d. of six independent experiments. Significant differences when compared with the data for wild-type or *p72*$^{-/-}$ MEFs with control RNAi are shown (single asterisk indicates $P < 0.05$; double asterisks indicate $P < 0.01$with one-way ANOVA). (**h**) TUNEL staining of wild-type and *p72*$^{-/-}$ MEFs with the indicated RNAi. The scale bars represent 250 μm in **b**, 1 mm in **c**, 150 μm in **d** and 200 μm in **h**.

homozygous mutants, no specific degeneration in organogenesis was detectable (Fig. 1c). Staining with a PECAM-1 antibody showed *p68–p72* homozygous-mutant embryos suffered malformation of blood vessels (Fig. 1d), as previously observed in mice with genetically reduced Dicer activity[19]. Assuming the putative role of the hDrosha complex is in processing of rRNA and miRNAs involved in cellular proliferation, differentiation and cell fate, we first examined cell-growth rates in mouse embryonic fibroblasts (MEFs) from *p72*$^{-/-}$ embryos. A severe reduction in cell-growth rate because of p72 deficiency was observed (Fig. 1e), and was confirmed by significantly impaired DNA synthesis in *p72*$^{-/-}$ MEFs, as measured by BrdU incorporation (Fig. 1f). In addition, a clear increase in cell death, as measured by TUNEL staining, was observed in *p72*$^{-/-}$ MEFs, which was further promoted by *p68* RNA interference (RNAi; Fig. 1g, h).

It has been suggested that the large hDrosha complex containing p68–p72 may, at least in part, excise pri-miRNAs into pre-miRNAs, and cleave preribosomal RNA[7,19–21]. As expression of mature miRNAs was shown to be reduced in human cultured cells deficient in Drosha[20], a global survey of miRNA microarray data was performed to assess expression of miRNAs (www.sanger.ac.uk/Software/Rfam/mirna/index.shtml) in *p72*$^{-/-}$ embryos at E18.5 (ref. 22). A particular set (94) of pri-miRNAs, but not all surveyed (266), were affected by p72 deficiency (more than 1.5

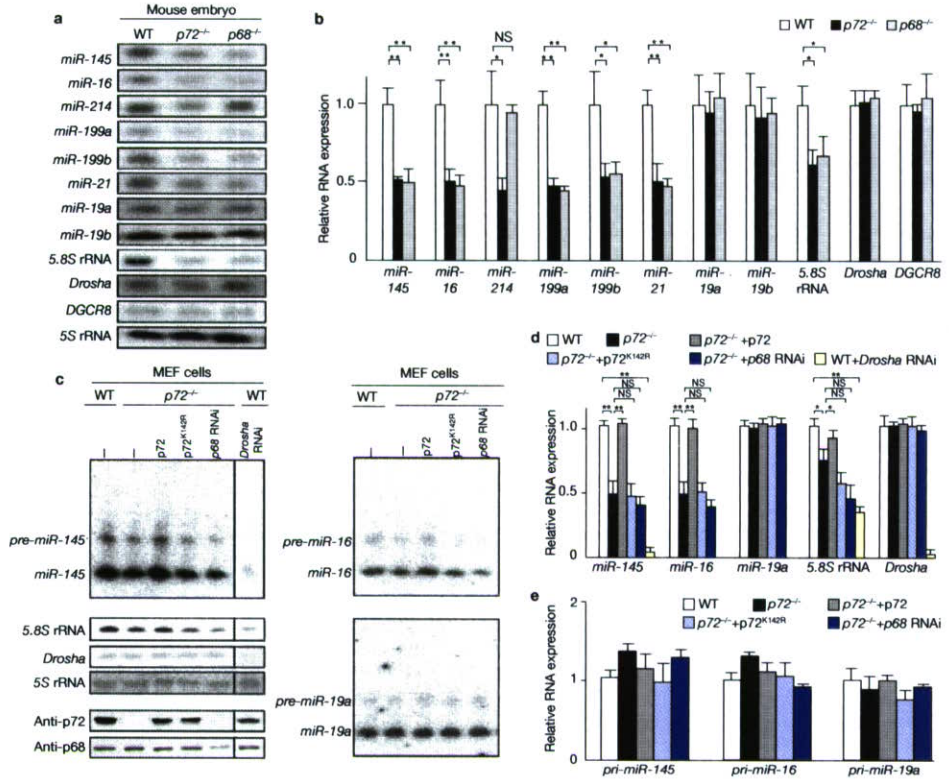

Figure 2 The role of RNA helicases p72 and p68 in miRNA or rRNA processing. (**a**) Northern blot analysis of miRNAs and 5.8S rRNA. Total RNA from wild-type, *p72*$^{-/-}$ and *p68*$^{-/-}$ mouse embryos (E9.5) were purified, and each RNAs were detected by specifc probes as miRNAs, *5.8S* rRNA, *Drosha*, *DGCR8* or *5S* rRNA. (**b**) Results from **a** are expressed as the mean ± s.d. of four independent experiments. Significant differences when compared with the data for wild-type and *p72*$^{-/-}$ or *p68*$^{-/-}$ are shown (single asterisks indicate $P < 0.05$; double asterisks indicate $P < 0.01$ with one-way ANOVA). (**c**) Northern blot analysis of *miRNA-145*, *miRNA-16*, *miRNA-19a*, *5.8S* rRNA, *Drosha* and *5S* rRNA. Total RNA from wild-type or *p72*$^{-/-}$ MEFs transfected with or without the indicated expression vectors were prepared, and each RNA was detected by specific probes as miRNAs, *5.8S* rRNA, *Drosha*, *DGCR8* or *5S* rRNA. The p72 and p68 expression levels in wild-type or *p72*$^{-/-}$ MEFs, with or without the indicated expression vectors, were detected by western blot analysis. Uncropped images of the blots are shown in the Supplementary Information, Fig. S5b. (**d**) Results from **c** are expressed as the mean ± s.d. of four independent experiments. Significant differences when compared with the data for wild-type or *p72*$^{-/-}$ MEFs are shown (single asterisks indicate $P < 0.05$, double asterisk indicates $P < 0.01$ with one-way ANOVA). (**e**) Quantitative RT–PCR analysis of *pri-miR-145*, *15* and *19a* expression in wild-type or *p72*$^{-/-}$ MEFs with indicated expression vectors. Results are expressed as the mean ± s.d. of six independent experiments.

times lowered; see Supplementary Information, Fig. S2). To search homologous motif in the regulated 94 miRNAs, a DNA clustering program (DIALIGN2.2.1, available at http://bibiserv.techfak.uni-bielefeld.de/dialign/) was used. Clustering analysis of the two data sets, revealed no continuous consensus sequence among the miRNAs examined. Expression of several of the miRNAs was detectable at significant levels by northern blot analysis. Deficiency of either p68 or p72 was found to reduce expression levels of *miR-145*, *miR-16*, *miR-199a*, *miR-199b* and *miR-21* to almost half of those in the wild-type littermate embryos (Fig. 2a, b). Likewise, expression levels of 5.8S rRNA were reduced in both homozygous embryos (Fig. 2a, b). However, unlike the miRNAs described above, the expression levels of *miR-19a*, *miR-19b* (Fig. 2a, b), and *miR-32*, *miR-128*, *miR-141* and *miR-146* (data not shown) seemed unaffected by p68–p72 deficiency, and *miR-214* expression was reduced only in *p72*$^{-/-}$, but not in *p68*$^{-/-}$ (Fig. 2a, b).

To verify the putative function of p68 and p72 in RNA processing in embryos, expression levels of these RNAs were then measured in MEF cells from *p72*$^{-/-}$ and wild-type littermate embryos. As expected, a significant reduction in the expression levels of the examined miRNAs and 5.8S rRNA because of p72 deficiency was detected (Fig. 2c, d). Knockdown of Drosha by RNAi (see Supplementary Information, Fig. S3c) caused a reduction in the miRNA expression level (Fig. 2c), as expected. However,

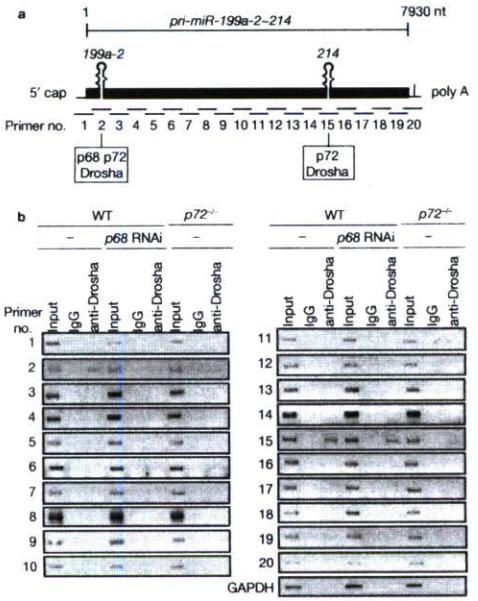

Figure 3 *In vivo* association of the Drosha complex with pri-miRNAs through p68–p72. (**a**) Schematic representation of *pri-miR-199a-2/-214* with the hairpin structure. The numbers (1–20) under the pri-miRNA indicate the amplified region by PCR with specific primer pairs used for RNA–ChIP analysis in **b**. Binding sites for p68–p72 and Drosha in *pri-miR-199a-2/-214* deduced from the RNA–ChIP analysis in **b** are also indicated. (**b**) RNA–ChIP analysis of p68–p72 and Drosha binding sites in *pri-miR-199a-2/-214*. ChIP samples were prepared from wild-type MEFs transfected with *p68* RNAi or not, and from *p72*$^{-/-}$ MEFs. RT–PCR was performed with either total input RNA, RNA precipitated with IgG (negative control) or anti-Drosha antibody.

pri-miRNA-145, *pri-miRNA-16* and *pri-miR-19a* gene expression seemed unaffected by *p72* deficiency plus *p68* RNAi knockdown (Fig. 2e), suggesting that the reduced miRNA levels were not caused by reduced gene expression. Ectopic expression of p72 in *p72*$^{-/-}$ MEFs was sufficient to restore expression levels of the RNAs, whereas such recovery was not induced by expression of a p72 mutant (p72^{K142R}; Fig. 2c, d). p72^{K142R} lacks the putative ATPase activity that is believed essential for RNA helicase activity[10,17]. Knockdown of *p68* and *p72* in the wild-type MEFs clearly lowered expression levels of the miRNAs and 5.8S rRNA, as expected (see Supplementary Information, Fig. S3a), and rRNA processing was significantly affected by *Drosha* RNAi (Fig. 2c). Interestingly, expression levels of *miR-19a* were again unaltered when expression levels of p68–p72 were modulated.

We then addressed the *in vivo* association of pri-miRNAs with p68–p72 in the Drosha complex using an RNA–chromatin immunoprecipiation (ChIP) assay with an mouse Drosha (mDrosha)-specific antibody[23] (Fig. 3b). Using several sets of primers, *in vivo* association of *pri-miR-214* and *pri-mR-16* with Drosha was detected, and the associating regions of pri-miRNAs were mapped (Fig. 3a, b for *pri-miR-214* and see Supplementary Information, Fig. S3b for *pri-miR-16*), although no clearly homologous RNA sequence was present in these regions. Such association was impaired, as expected, in *p72*$^{-/-}$ MEFs and wild-type MEFs with *p68* knocked down by RNAi (Fig. 3b).

To verify the role of the p68–p72 subunits in the mDrosha complex *in vitro*, the association of endogenous p68–p72 with endogenous mDrosha was confirmed by coimmunoprecipitation (Fig. 4a). DGCR8 coimmunoprecipitated with mDrosha as expected. Using a biochemical approach[24,25], the Drosha complex (Fig. 4b) was purified from nuclear extracts of MCT mouse kidney proximal tubule cells stably expressing Flag- and His-tandem tagged mDrosha at a similar expression level to that of endogenous mDrosha (see Supplementary Information, Fig. S2d). The purified mDrosha complex was present in a single complex with a relative molecular mass of over 670,000 when fractionated on a glycerol density gradient (Fig. 4b). Fractionation of total nuclear extracts with western blotting also showed comigration of endogenous Drosha with DGCR8 and p68–p72 at the similar molecular masses with the purified mDrosha complex (Fig. 4c). These findings are consistent with a previous report that the Drosha complex was biochemically isolated as one large complex from S2 insect cells[26]. However, the small complex corresponding to the human Microprocessor complex was undetectable. Even under more stringent conditions (such as at higher salt concentrations), the smaller mDrosha complex was biochemically undetectable in our hands (data not shown). Using mass spectrometric sequencing, p68–p72, several RNPs and mouse DGCR8 were identified (Fig. 4d), and all of the examined subunits were detected by western blotting analysis (Fig. 4b). Two-step column purification of mDrosha complex identified the same subunits (Fig. 4e), supporting previous reports that p68–p72 form a complex[7,27]. As the subunit composition of the purified mDrosha complex accurately reflects the reported composition of the large hDrosha complex components, we presumed that mDrosha forms one large complex similar to the large hDrosha complex.

We then examined whether this purified large complex mediates the processing of miRNA *in vitro*. The purified complex from fraction 7 (Fr. 7) on the glycerol density gradient (see Fig. 4b), as well as the immunoprecipitates of Drosha (Flag–His–mDrosha; Fig. 5a), were able to cleave *miR-16* and *miR-145* pri-miRNAs into pre-miRNAs (Fig. 5b), but not mRNAs (see Supplementary Information, Fig. S4a). Cleavage products of pre-miRNAs were of the expected size (70 nucleotides for *miR-145*, 93 nucleotides for *miR-16*) and 5.8S rRNA (157 nucleotides) was generated from 12S rRNA *in vitro* (Fig. 5b)[21]. However, conversion efficiency of this *in vitro* RNA processing was unexpectedly low, even for longer incubations (Fig. 5c), raising the possibility that a coregulatory subunit for the mDrosha complex may be lost during biochemical purification. Such *in vitro* RNA processing activity of the purified complex (Fr. 7) was significantly attenuated by specific antibodies for p68–p72, as well as mDrosha (Fig. 5d), and by the presence of an ATP analogue (see Supplementary Information, Fig. S4b, c), supporting ATP dependency (Fig. 5e). Furthermore, the complex deficient of either p68 or p72, purified from stable transformants knocked down with RNAi, was impaired in RNA processing (Fig. 5f). This confirms the significance of p68–p72 subunits within the mDrosha complex in RNA processing.

In this study, early lethality of *p68*$^{-/-}$ and *p72*$^{-/-}$ mice clearly establishes the physiological significance of DEAD-box RNA helicases in survival. The physiological impact of p68–p72 on cell differentiation, proliferation and cell fate was also observed in MEFs. Most importantly, the processing of a set of miRNAs and rRNA seemed to

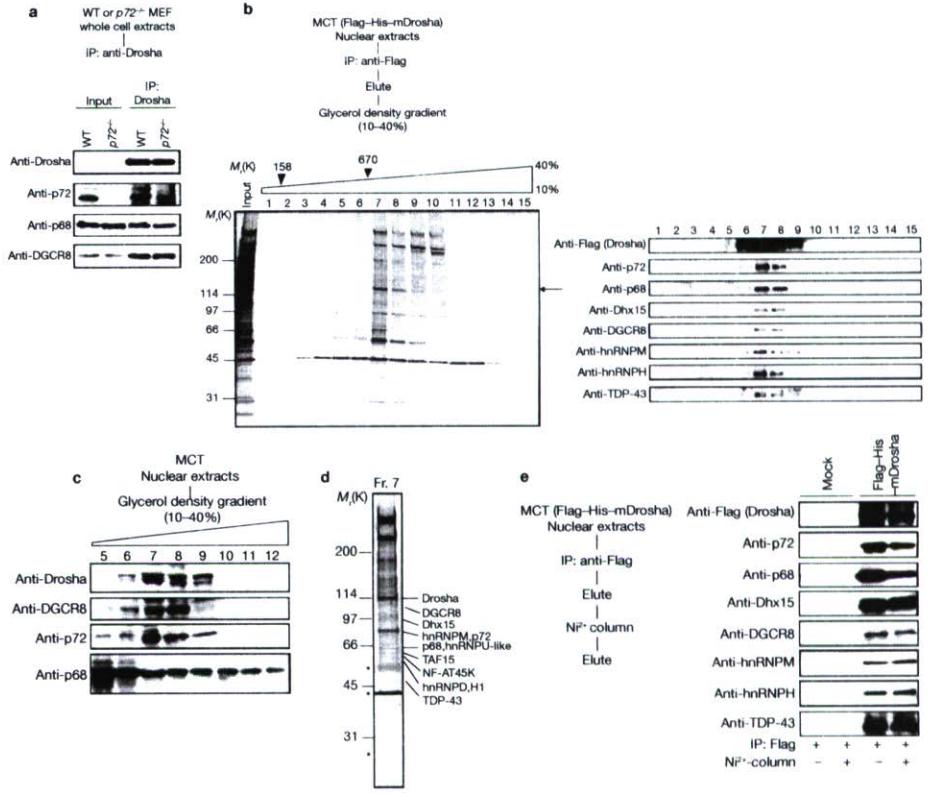

Figure 4 Biochemical isolation of mouse Drosha-containing complex. (**a**) Coimmunoprecipitation of p68–p72 with mDrosha. Whole-cell extracts from MEFs (wild-type and *p72*$^{-/-}$) were prepared for immunoprecipitation (IP) with endogenous mDrosha followed by western blotting (IB). Input, 5% of the cell extracts for immunprecipitiation. Uncropped images of the blots are shown in the Supplementary Information, Fig. S5c. (**b**) Biochemical isolation of mouse Drosha-containing complexes. Silver staining and western blot analysis of glycerol density-gradient fractions are displayed. Molecular masses of marker proteins and fraction numbers are indicated. Fraction 7 was used for mass spectrometric analysis and *in vitro* RNA processing. Input, 5% of the input for glycerol density gradient. The arrow indicates Flag–His–mDrosha. (**c**) Endogenous mDrosha, DGCR8, p72 and p68 cosediment at the same fractions with the Flag–His–mDrosha complex on glycerol density gradients. (**d**) Mass spectrometric identifications of the components in Fr. 7 Flag–His–mDrosha complex in **b**. Asterisks indicate background bands. (**e**) Identification of mDrosha complex components in the mDrosha immunoprecipitant. The Flag–His–mDrosha complex was collected from the nuclear extracts using an anti-Flag antibody column, then repurified by Ni^{2+} affinity chromatography. The complex components were analysed by western blot

be impaired in both of the homozygous mutants (Fig. 2a, b and see Supplementary Information, Fig. S2). Currently, it remains unclear whether the cellular function of affected miRNAs as a result of *p68–p72* knockout is related to early lethality observed in *p68*$^{-/-}$ and *p72*$^{-/-}$ mice. However, considering the previous report that mouse embryogenesis in the absence of Dicer ceases at an earlier stage (E7.5)[28], normal expression of miRNAs may be essential for survival. Furthermore, the purified mDrosha complex containing p68–p72 was capable of generating a set of processed pre-miRNAs and rRNA through p68 and p72 using an *in vitro* assay (Fig. 5b). Impaired miRNA processing was detected for several, but not all, of the examined miRNA species. Therefore, we speculate that p68–p72 DEAD-box RNA helicases serve as miRNA species-selective subunits in the conversion of pri-miRNA into pre-miRNA by specific recognition of a certain structure of pri-miRNA. This hypothesis is supported by a previous report that the double-stranded RNA-binding protein partner of Drosha (Pasha) is required for insect Drosha-mediated pri-miRNA processing[26]. In this respect, it would be interesting to know whether the cellular functions of the specific miRNAs species processed by p68–p72 correlate with the putative biological functions of p68–p72 (refs 11–17).

Different sets of RNA-associated protein subunits may be required for the processing of other miRNA species[29]. Notably, in the p68–p72 homozygous mutants, the expression levels of several miRNAs were reduced to only half of the wild-type littermates. Therefore, we

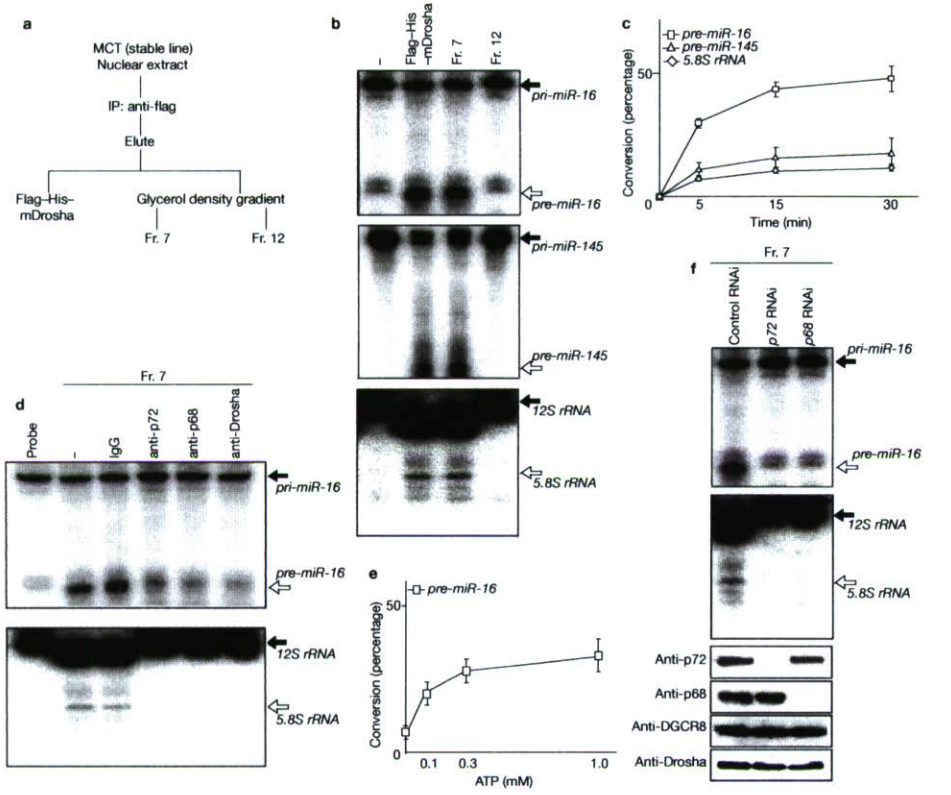

Figure 5 Purified mDrosha complex mediates processing of miRNA and rRNA *in vitro*. (**a**) Schematic representation of the preparation of the samples used in **b**. (**b**) *In vitro* processing analysis of *pri-miR-16*, *pri-miR-145* and *12S* rRNA with Flag–HIS–mDrosha immunocomplexes, fractionated mDrosha complex (Fr. 7), mDrosha-negative fraction (Fr. 12) or negative control (–). Closed arrows and opened arrows indicate the precursor RNA and processed RNA, respectively. (**c**) Time-course conversion rate of *pre-miR-16*, *pre-miR-145* and *5.8S* rRNA (diamond) by purified mDrosha complex (Fr. 7). Results are expressed as the mean ± s.d. of three independent experiments. (**d**) Specific antibodies for p68, p72 and mDrosha attenuated the *pri-miR-16* and *12S* rRNA cleavage by the purified mDrosha complex (Fr. 7). All studies were repeated three times. Probe, input of the substrate *pri-miR-16*; –, Fr. 7 only; IgG, negative control. Closed arrows and opened arrows indicate the precursor RNA and processed RNA, respectively. (**e**) ATP concentration-dependent effect on the *pri-miR-16* cleavage by purified mDrosha complex (Fr. 7). Results are expressed as the mean ± s.d. of three independent experiments. (**f**) *In vitro* processing analysis of *pri-miR-16* and *12S* rRNA with the purified mDrosha complexes prepared from Flag–His–mDrosha stable cells transfected with control RNAi, *p72* RNAi or *p68* RNAi. Western blotting indicates the presence of each complex component. Closed arrows and opened arrows indicate the precursor RNA and processed RNA, respectively. Uncropped images of the blots are shown in the Supplementary Information, Fig. S5d.

speculate that there is possible functional redundancy of p68–p72 with other RNA processing subunits. As it is known that nuclear complexes often form subclasses through association of core components with regulatory subunits[30,31], we cannot exclude the possibility that Drosha–DGCR8 exist as multiple complexes differentially combined with RNA-associated protein subunits in mammals. Furthermore, the subunit composition of the Drosha complex may be developmentally modulated, and thereby cell-type specific.

It remains unclear how the p68–p72 subunits support RNA processing activity of the complex. p68–p72 may function to specifically recognize and stably bind to certain structures of pri-miRNAs and 12S pre-rRNA, and to initiate cleavage at precise RNA sites by Drosha. As the p72 mutant lacking putative ATPase activity did not potentiate RNA processing (Fig. 2c, d), we suggest that ATPase activity of p68–p72 may be required. p68–p72 ATPase activity is dependent on RNA binding[10,32] and is likely to be critical for RNA-unwinding activity[3]. Therefore, we suggest that ATP-dependent p68–p72-mediated structural alteration of specifically associating protein subunits may lead to presentation of RNAs for cleavage by mammalian Drosha. DGCR8 has been reported to be a critical pri-miRNA-associated subunit for Drosha to precisely recognize miRNA stem-loop structures[7,33]. However, other RNA-associated subunits may recognize distinct cognate pri-miRNA tertiary structures by similar or different mechanisms, thus enabling the Drosha complex to process a number of pri-miRNAs. □

METHODS

Antibodies. The following antibodies were used: p68-ab10261 (Abcam, Cambridge, UK); p72 p72N (ref. 17); PECAM-1 MEC13.3 (BD Bioscience, San Jose, CA); Drosha 07017 (Upstate, Billerica, MA); Flag polyclonal (Sigma, St Louis, MO); TARDBP 2E2-D3 (Abnova, Taipei City, Taiwan); hnRNP H N16 (Santa Cruz Biotechnology, Santa Cruz, CA); DHX15 BL972 (Bethyl Laboratories, Montgomery, TX); hnRNP M1-M4 (Zymed, San Francisco, CA); Actin I19 (Santa Cruz). Anti-DGCR8 antibody was generated against a synthetic peptide corresponding to the carboxy-terminal 20 amino-acid sequence (Operon, Huntsville, AL). Appropriate anti-mouse, anti-rabbit and anti-goat secondary antibodies were obtained from Dako (Glostrup, Denmark).

Isolation of MEFs, MEF growth, BrdU incorporation, TUNEL assay and DNA fragmentation. MEFs were isolated from E13.5 embryos and cultured in DMEM with 10% FBS[34]. For MEF growth experiments, cells were seeded in 96-well plates and growth rates were measured by using Cell Counting Kit-8 (Dojindo Laboratories, Kumamoto, Japan). DNA synthesis was detected and measured in cultured cells by BrdU incorporation using 5′-bromo-2′-deoxy-uridine Labeling and Detection Kit III (Roche Applied Science, Basel, Switzerland). Apoptotic cells were assessed by the DNA terminal nick-end translation method (TUNEL assay) using the DeadEnd Fluorometric TUNEL System (Promega, Madison, WI). For apoptotic cell quantitation, DNA fragmentation was measured by using Cell Death Detection ELISA^{PLUS} (Roche Applied Science). These assays were performed following the manufacturer's instructions.

RNAi depletion of *p68*, *p72* and *Drosha*. Small interfering RNA (siRNA) oligonucleotides of *p68*, *p72* and *Drosha* were used for knockdown of endogenous protein expression using siGENOME (Dharmacon, Lafayette, CO). Four kinds of independent siRNA duplexes were mixed. Their sequences are: *p68* siRNA duplex, sense 5′-GAACUGAGUGCAAACCAUAUU-3′ and antisense 5′-PUAUGGUUUGCACUCAGUUCUU-3′: sense 5′-GCUUGUCGCUUGAAGUCUAUU-3′ and antisense 5′-PUAGACUUCAAGCGACAAGCUU-3′: sense 5′-UCAAUUAUGACUACCCUAAUU-3′ and antisense 5′-PUUAGGGUAGUCAUAAUUGAUU-3′;sense5′-GCGCACCGCACAAGAGGUAUU-3′ and antisense 5′-PUACCUCUUGUGCGGUGCGCUU-3′. *p72* siRNA duplex: sense 5′-GUACUUACCUUGUGUUGGAUU-3′ and antisense 5′-PUCCAACACAAGGUAAGUACUU-3′;sense5′-GAAAGAGAUUGGGUACUUAUU-3′ and antisense 5′-PUAAGUACCCAAUCUCUUUCUU-3′; sense 5′-GGAAGACAUUGGCGUAUUUUU-3′ and antisense 5′-PAAAUACGCCAAUGUCUUCCUU-3′;sense5′-GGGCUAGGUUUGUAUAGAUUU-3′ and antisense 5′-PAUCUAUACAAACCUAGCCCUU-3′. *Drosha* siRNA duplex: sense 5′-CGUGGAGGGUGUUAUAGUAUU-3′ and antisense 5′-PUACUAUAACACCCUCCACGUU-3′;sense5′-CAAUACGUGUCAUAGAAUGUU-3′ and antisense 5′-PCAUUCUAUGACACGUAUUGUU-3′: sense 5′-GAACCUACAUCGUGAGCGGUU-3′ and antisense 5′-PCCGCUCACGAUGUAGGUUCUU-3′;sense5′-GGGACUCUCUAGACUGUGAUU-3′and antisense 5′-PUCACAGUCUAGAGAGUCCCUU-3′. MEFs were transfected with each duplex (25 nM) using SuperFect transfection reagent (Qiagen, Hilden, Germany).

Northern blot analysis and quantitative RT–PCR. Total RNA from embryos or MEFs was prepared in TRIzol reagents (Invitrogen, Carlsbad, CA) in accordance with the manufacturer's instructions. Northern blot analysis was carried out as previously described[35]. *Drosha* cDNA and the following oligonucleotides were used as probes: *miR-145*, 5′-AAGGGATTCCTGGGAAAACTGGAC-3′; *miR-16*, 5′-CGCCAATATTTACGTGCTGCTA-3′; *miR-214*, 5′-CTGCCTGTCTGTGCCTGCTGT-3′; *miR-199a*, 5′-AACCAATGTGCAGACTACTGTA-3′; *miR-199b*, 5′-GAACAGGTAGTCTAAACACTGGG-3′; *miR-21*, 5′-TCAACATCAGTCTGATAAGCTA-3′; *miR-19a*, 5′-TCAGTTTTGCATAGATTTGCACA-3′; *miR-19b*, 5′-TCAGTTTTGCATGGATTTGCACA-3′; *5.8S* rRNA, 5′-TCAGACAGGCGTAGCCCCGGGAGGAACCCG-3′; and *5S* rRNA, 5′-CAGGCCCGACCCTGCTTAGCTTCCGAGATCAGACGAGAT-3′(5S rRNA). Real-time quantitative RT–PCR was performed on an ABI Prism 7900HT Sequence Detector (Applied Biosystems, Foster City, CA). The primers used were as follows: *pri-miR-16*, 5′-CCCTTGGAGTAAAGTAGCAGCA-3′ (forward) and 5′-GTCCTTGTATTTTGAGGCAGCA-3′ (reverse); *pri-miR-19*, 5′-ACTGCCCTAAGTGCTCCTTCTG-3′ (forward) and 5′-GAGGGCTGCAAACACAACTATG-3′(reverse); *pri-miR-145*, 5′-ATGCCGAGAGAACTGCTGGT-3′ (forward) and 5′-AAACTGGACCGTGAGGACAA-3′(reverse); *GAPDH*, 5′-AAATGGTGAAGGTCGGTGTG-3′(forward) and 5′-TGAAGGGGTCGTTGATGG-3′ (reverse). Expression levels were normalized for GAPDH expression.

Purification of Flag–His–mDrosha. Flag–His–mDrosha was transfected into MCT mouse kidney proximal tubule cells. Transfected cells were selected with G418 and individual colonies were isolated and analysed for Flag–His–mDrosha expression. To purify the mDrosha complex, nuclear extract was prepared as described previously[24,25] and applied to the anti-Flag M2 affinity resin (Sigma) column. After washes with buffer A (20 mM Tris–HCl at pH 7.9, 0.5 M KCl, 10% glycerol, 1 mM EDTA, 5 mM DTT, 0.5% NP-40, 0.2 mM PMSF), the affinity column was eluted with 400 μg ml^{-1} Flag peptide in buffer A. Eluted complex was analysed by 10–40% glycerol density gradient centrifugation. Fractions from the glycerol density gradient were concentrated by precipitation with trichloroacetic acid and analysed by SDS–PAGE followed by silver staining and western blotting[24,25]. For two-step purification, Flag-eluted complex was applied to HIS–Select nickel affinity gel (Sigma). After washes with 0.8× LEW buffer (40 mM NaH_2PO_4 at pH 8.0, 240 mM NaCl), the complex was eluted with elution buffer (50 mM NaH_2PO_4 at pH 8.0, 300 mM NaCl, 250 mM imidazole). For the large mDrosha complex deficient for p68 or p72, *p68* or *p72* was knocked down by RNAi in the stable transformants before the complex purification.

***In vitro* miRNA or rRNA processing analysis.** *In vitro* transcription was carried out using linearized pcDNA3 vector containing *pri-miR-16* or *12S* rRNA[24]. Briefly, the miRNA probes (*pri-miR-16* or *pri-miR-145*) were amplified from embryo RNA by RT–PCR with 5′-TTCAGGGATCCCATGCTAGCAAGAAGCACTTGGCCA-3′ as forward primer and 5′-AACAAGAATTCTGAAAAGGTGCAGGCCATACTGTGC-3′ as reverse primer or 5′-TTCAGGGATCCAAAAGCTATACAAAGGTCAGAAGAG-3′ as forward primer and 5′-AACAAGAATTCTTCCCAGAGCAGGACGCTGCATCCC-3′as reverse primer, respectively. The *12S* rRNA probes were also prepared with 5′-TCTATGGATCCGTCAGAAAGGGGGGACACGCGCCCAGCCGC-3′as forward primer and 5′-TCTATGAATTCCGACTCTTAGCGGTGGATCACTCGGCTCGTG-3′ as reverse primer. The processing reaction, containing the indicated amounts of Drosha complex (immunoprecipitation products or two-step purification products from MCT cells), 3 μl of solution containing 32 mM $MgCl_2$, 10 mM ATP, 2006mM creatine phosphate, 20 U μl^{-1} RNAase inhibitor (Toyobo, Osaka, Japan) and the α^{32}P-UTP-internal-labelled pri-miRNA and buffer (20 mM Tris–HCl at pH 7.9, 0.1 M KCl, 10% glycerol, 5 mM DTT, 0.2 mM PMSF), were added to a final volume of 30 μl, as previously described[7,20], in the absence or presence of hexokinase (Sigma). The reaction mixture was incubated at 37 °C for 90 min and extracted with phenol:chloroform mixture, then with chloroform and precipitated with 300 mM sodium acetate and ethanol. The precipitated RNA was loaded on 15% denaturing polyacrylamide gels, and then autoradiographed.

RNA–ChIP. RNA–ChIP was performed as previously described[23]. All the buffers used in this study contained 0.5 U μl RNase inhibitor. Nuclei from MEF cells (wild-type, *p68*-knocked down wild-type or *p72*$^{-/-}$) were first isolated from 1% formaldehyde-fixed cells and used for chromatin fragmentation. After immunoprecipiation with anti-Drosha antibody, washing and elution, the precipitated RNA–DNA pellets were resuspended in 70 μl nuclease-free water with 1 μl of 40 U μl^{-1} RNase inhibitor, 5 μl of 1 M Tris–HCl at pH 7.5, 20 μl of 50 mM $MgCl_2$, and 4 μl of 10 U μl DNase I. The mixture was incubated for 30 min at 37 °C and extracted once with phenol:chloroform (5:1). RNA was precipitated with ethanol and dissolved in 30 μl of nuclease-free water. Twenty-nine microliters of the RNA was used for a 60 μl cDNA synthesis reaction. The PCR reactions were performed at 33 cycles, which was within the linear range of the amplification. Of 50 μl of product, 6 μl was loaded onto a 1.5% agarose gel, stained with ethidium bromide, and photographed. The primer sequences used are given in the Supplementary Information.

Microarray data. The microarray data can be be seen in ArrayExpress (accession number, E-MEXP-1052; for further details see Supplementary Information, Methods).

Statistical analysis. Statistical differences were determined using one-way ANOVA followed by post-hoc comparison with the Fisher's protected least significant difference test. Statistical significance is displayed as $P < 0.05$ (one asterisk) or $P < 0.01$ (two asterisks).

Note: Supplementary Information is available on the Nature Cell Biology website.

ACKNOWLEDGEMENTS

We thank T. Watanabe, H. Shiina, J. Miyamoto, K. Sekine, R. Fujiki, Y. Imai and S. Tanaka for generation of knockout mice, and H. Higuchi for manuscript preparation. This work was supported in part by the Program for Promotion of Basic Research Activities for Innovative Biosciences (PROBRAIN) and priority areas from the Ministry of Education, Culture, Sports, Science and Technology (to S.K.).

AUTHOR CONTRIBUTIONS

The experimental concept was developed by S.K., B.W.O.M, S.T., K.T., H.E. and H.K. T.F., K.Y. and S.F. conducted most of experiments, and I.K., K.Y., M.M., M.N., T.N., C.A., Y.Y., T.K., C.F. and S.T. contributed materials and supported several experiments. S.K., T.F., K.Y. and S.F. wrote the manuscript.

COMPETING FINANCIAL INTERESTS

The authors declare that they have no competing financial interests.

Published online at http://www.nature.com/naturecellbiology/
Reprints and permissions information is available online at http://npg.nature.com/reprintsandpermissions/

1. Carthew, R. W. Gene regulation by microRNAs. *Curr. Opin. Genet. Dev.* **16,** 203–208 (2006).
2. Cullen, B. R. Transcription and processing of human microRNA precursors. *Mol. Cell* **16,** 861–865 (2004).
3. Filipowicz, W., Jaskiewicz, L., Kolb, F. A. & Pillai, R. S. Post-transcriptional gene silencing by siRNAs and miRNAs. *Curr. Opin. Struct. Biol.* **15,** 331–341 (2005).
4. Kim, V. N. MicroRNA biogenesis: coordinated cropping and dicing. *Nature Rev. Mol. Cell Biol.* **6,** 376–385 (2005).
5. Valencia-Sanchez, M. A., Liu, J., Hannon, G. J. & Parker, R. Control of translation and mRNA degradation by miRNAs and siRNAs. *Genes Dev.* **20,** 515–524 (2006).
6. Zamore, P. D. & Haley, B. Ribo-gnome: the big world of small RNAs. *Science* **309,** 1519–1524 (2005).
7. Gregory, R. I. *et al.* The Microprocessor complex mediates the genesis of microRNAs. *Nature* **432,** 235–240 (2004).
8. Hirling, H., Scheffner, M., Restle, T. & Stahl, H. RNA helicase activity associated with the human p68 protein. *Nature* **339,** 562–564 (1989).
9. Huang, Y. & Liu, Z. R. The ATPase, RNA unwinding, and RNA binding activities of recombinant p68 RNA helicase. *J. Biol. Chem.* **277,** 12810–12815 (2002).
10. Lamm, G. M., Nicol, S. M., Fuller-Pace, F. V. & Lamond, A. I. p72: a human nuclear DEAD box protein highly related to p68. *Nucleic Acids Res.* **24,** 3739–3747 (1996).
11. Auboeuf, D., Honig, A., Berget, S. M. & O'Malley, B. W. Coordinate regulation of transcription and splicing by steroid receptor coregulators. *Science* **298,** 416–419 (2002).
12. Bates, G. J. *et al.* The DEAD box protein p68: a novel transcriptional coactivator of the p53 tumour suppressor. *EMBO J.* **24,** 543–553 (2005).
13. Causevic, M. *et al.* Overexpression and poly-ubiquitylation of the DEAD-box RNA helicase p68 in colorectal tumours. *Oncogene* **20,** 7734–7743 (2001).
14. Dubey, P. *et al.* The immunodominant antigen of an ultraviolet-induced regressor tumor is generated by a somatic point mutation in the DEAD box helicase p68. *J. Exp. Med.* **185,** 695–705 (1997).
15. Endoh, H. *et al.* Purification and identification of p68 RNA helicase acting as a transcriptional coactivator specific for the activation function 1 of human estrogen receptor alpha. *Mol. Cell Biol.* **19,** 5363–5372 (1999).
16. Kircher, S. G., Kim, S. H., Fountoulakis, M. & Lubec, G. Reduced levels of DEAD-box proteins DBP-RB and p72 in fetal Down syndrome brains. *Neurochem. Res.* **27,** 1141–1146 (2002).
17. Watanabe, M. *et al.* A subfamily of RNA-binding DEAD-box proteins acts as an estrogen receptor alpha coactivator through the N-terminal activation domain (AF-1) with an RNA coactivator, SRA. *EMBO J.* **20,** 1341–1352 (2001).
18. Boehm, M. & Slack, F. A developmental timing microRNA and its target regulate life span in *C. elegans*. *Science* **310,** 1954–1957 (2005).
19. Yang, W. J. *et al.* Dicer is required for embryonic angiogenesis during mouse development. *J. Biol. Chem.* **280,** 9330–9335 (2005).
20. Lee, Y. *et al.* The nuclear RNase III Drosha initiates microRNA processing. *Nature* **425,** 415–419 (2003).
21. Wu, H., Xu, H., Miraglia, L. J. & Crooke, S. T. Human RNase III is a 160-kDa protein involved in preribosomal RNA processing. *J. Biol. Chem.* **275,** 36957–36965 (2000).
22. Han, J. *et al.* The Drosha–DGCR8 complex in primary microRNA processing. *Genes Dev.* **18,** 3016–3027 (2004).
23. Ni, J. Q., Liu, L. P., Hess, D., Rietdorf, J. & Sun, F. L. *Drosophila* ribosomal proteins are associated with linker histone H1 and suppress gene transcription. *Genes Dev.* **20,** 1959–1973 (2006).
24. Kitagawa, H. *et al.* The chromatin-remodeling complex WINAC targets a nuclear receptor to promoters and is impaired in Williams syndrome. *Cell* **113,** 905–917 (2003).
25. Yanagisawa, J. *et al.* Nuclear receptor function requires a TFTC-type histone acetyl transferase complex. *Mol. Cell* **9,** 553–562 (2002).
26. Denli, A. M., Tops, B. B., Plasterk, R. H., Ketting, R. F. & Hannon, G. J. Processing of primary microRNAs by the Microprocessor complex. *Nature* **432,** 231–235 (2004).
27. Ogilvie, V. C. *et al.* The highly related DEAD box RNA helicases p68 and p72 exist as heterodimers in cells. *Nucleic Acids Res.* **31,** 1470–1480 (2003).
28. Bernstein, E. *et al.* Dicer is essential for mouse development. *Nature Genet.* **35,** 215–217 (2003).
29. Lu, J. *et al.* MicroRNA expression profiles classify human cancers. *Nature* **435,** 834–838 (2005).
30. Otte, A. P. & Kwaks, T. H. Gene repression by Polycomb group protein complexes: a distinct complex for every occasion? *Curr. Opin. Genet. Dev.* **13,** 448–454 (2003).
31. Perissi, V. & Rosenfeld, M. G. Controlling nuclear receptors: the circular logic of cofactor cycles. *Nature Rev. Mol. Cell Biol.* **6,** 542–554 (2005).
32. Iggo, R. D. & Lane, D. P. Nuclear protein p68 is an RNA-dependent ATPase. *EMBO J.* **8,** 1827–1831 (1989).
33. Han, J. *et al.* Molecular basis for the recognition of primary microRNAs by the Drosha–DGCR8 complex. *Cell* **125,** 887–901 (2006).
34. Fujiki, R. *et al.* Ligand-induced transrepression by VDR through association of WSTF with acetylated histones. *EMBO J* **24,** 3881–3894 (2005).
35. Ohtake, F. *et al.* Modulation of oestrogen receptor signalling by association with the activated dioxin receptor. *Nature* **423,** 545–550 (2003).

nature cell biology

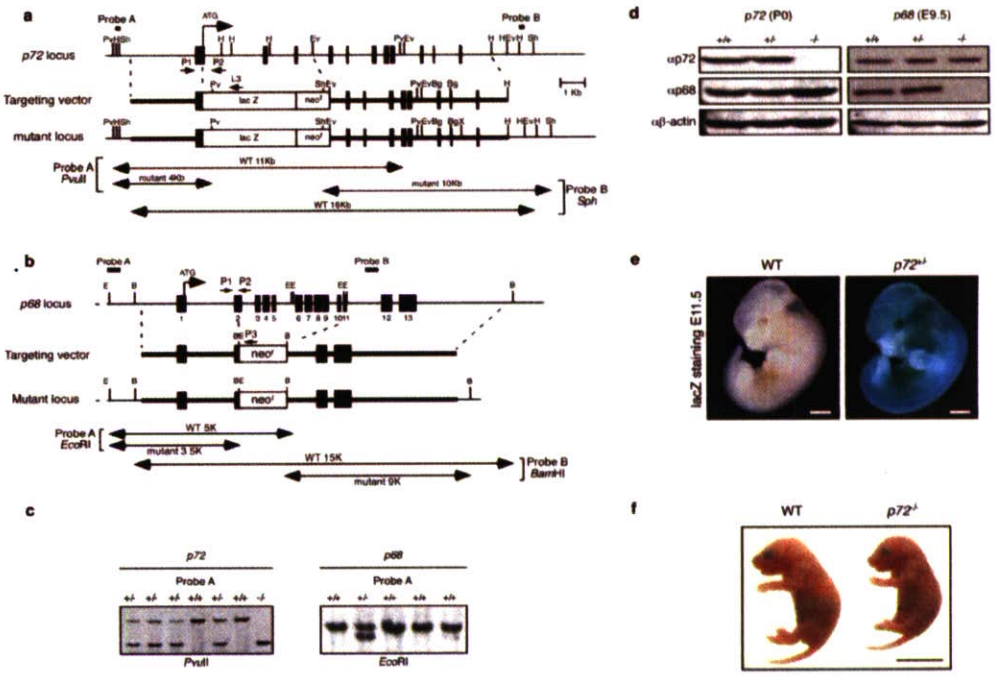

Figure S1 Targeted disruption of the *p68* and *p72* genes. **(a)** Scheme of the genomic structure of *p72* locus (top), targeting vector (middle) and predicted mutant locus (bottom). Southern blot probes and PCR primers (P1, P2 and L3) used for genotyping are indicated. Southern blot fragments detected by each probe are indicated by arrows. Restriction sites indicated are *Pvu*II (Pv), *Hind*III (H), *Sph*I (Sh), and *Eco*RV (Ev). **(b)** Scheme of the genomic structure of *p68* locus (top), targeting vector (middle) and predicted mutant locus (bottom). Filled boxes indicate exons. Southern blot probes (probe A, B) and PCR primers (P1, P2 and P3) used for genotyping are indicated. Southern blot fragments detected by each probe are indicated by arrows. Restriction sites indicated are *Eco*RI (E) and *Bam*HI (B). **(c)** Southern blot analysis of the offspring obtained by heterozygous cross. Genomic DNA from *p72* F2 tails was digested with *Pvu*II and detected by Probe A as described S1a (left). Genomic DNAs from *p68* F2 yolk sacs were digested with *Eco*RI and detected by Probe A as described S1b (right). **(d)** Both $p68^{-/-}$ and $p72^{-/-}$ mice were null in protein expression. Western blot analysis of p72 protein in P0 liver (left) and p68 protein in E9.5 embryos (right) of the indicated genotype. **(e)** Expression of lacZ driven by the p72 endogenous promoter. E11.5 embryo was visualized by whole-mount lacZ staining. The scale bars represent 1 mm. **(f)** Body size of $p72^{-/-}$ pups and WT littermates (P2). The scale bars represent 10 mm.

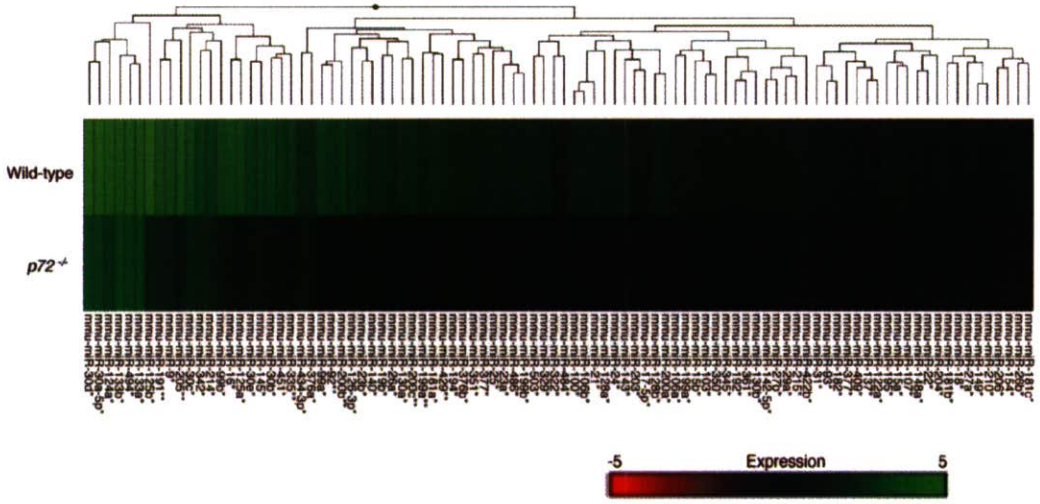

Figure S2 Microarray expression profile of 266 mouse miRNAs in *p72*$^{-/-}$ embryos (E18.5) compared with WT embryos (n=3 per genotype). Relative expression levels for the 94 miRNAs that changed significantly and more than 1.5 fold in three experiments are shown (*p < 0.05; **p < 0.01 with one-way ANOVA).

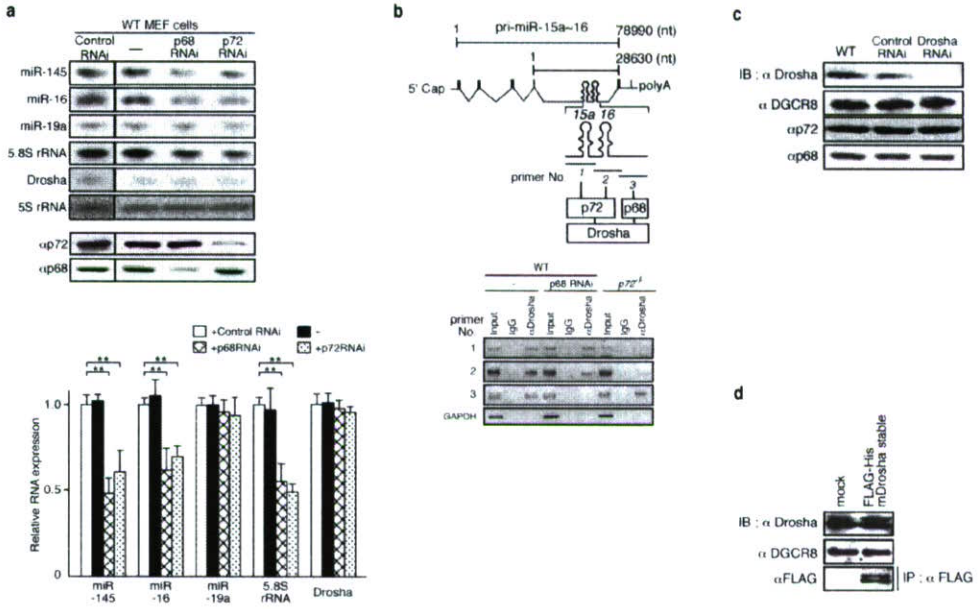

Figure S3 (a) Northern blot analysis of miRNAs and 5.8S rRNA of WT MEF cells transfected with control RNAi, p68 RNAi or p72 RNAi. Results are expressed as the mean ±SD of four independent experiments. Lower bar graph indicates the results from upper panel Northern blots, expressed as the mean ± SD of four independent experiments. Significant differences when compared with the data for WT MEF cells with control RNAi are shown (**p <0.01 with one-way ANOVA). **(b)** RNA-ChIP analysis was performed to estimate the p68, p72 and Drosha binding sites on pri-miR-15a and pri-miR-16. Schematic representation of the hairpin structure between pri-miR-15a and pri-miR-16 (upper). Ethidium bromide stained agarose gels of each RT-PCR products (lower). The numbers under the pri-miRNAs indicate the positions of primer pairs used for RNA-ChIP analysis. Indicated p68, p72 and Drosha binding sites in pri-miR-15a and pri-miR-16 were deduced from results shown lower panels. ChIP samples were prepared from WT MEF cells transfected with p68 RNAi or without, and *p72*$^{-/-}$ MEF cells. RT-PCR was carried out on total-input RNA and RNA precipitated with IgG (negative control) or anti-Drosha antibody. **(c)** Efficiency of Drosha knockdown by RNAi. WT MEF cells were transfected with or without indicated siRNA. Expression levels of Drosha, DGCR8, p72 and p68 were examined by Western blotting. **(d)** Comparison of mDrosha expression in the mock and FLAG-His-mDrosha stable transfected MCT cells. The expression levels of mDrosha and DGCR8 proteins were estimated by Western blotting.

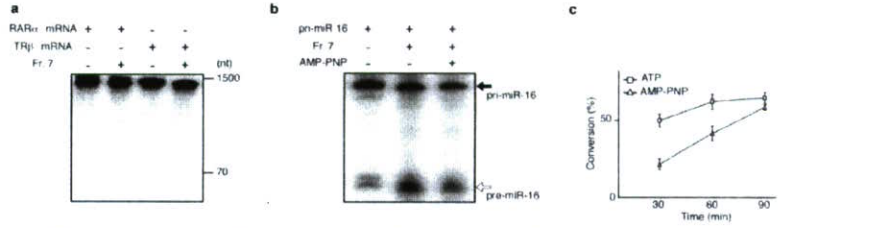

Figure S4 Selective and ATP-dependent processing of RNA processing by the purified mDrosha complex. **(a)** No cleavage of mRNAs by the purified mDrosha complex. *In vitro* transcribed mRNAs of human RARα and TRβ were applied for the *in vitro* processing assay by the purified complex, and no clear cleavage was detected. **(b)** ATP-dependent processing of pre-miRNA by the purified complex. The *in vitro* processing of pri-miR-16 was attenuated in the presence of an ATP analog, AMP-PNP; Adenosine 5'-triphosphate tetralithium salt hydrate (1 mM). **(c)** Time-course analysis of the ATP analog effect on pre-miRNA processing. Pri-miR-16 was incubated with 10 mM ATP (square) or 10 mM AMP-PNP (triangle) for indicated times.